

Tectonophysics

New insights on the fossil arc of the Tyrrhenian Back-Arc Basin(Mediterranean Sea)

--Manuscript Draft--

Manuscript Number:	TECTO15884R1
Article Type:	Research Paper
Keywords:	Back-Arc Basins, Tyrrhenian Sea, Volcanic Arc, Geodynamics
Corresponding Author:	Camilla Palmiotto, PhD National Research Council BOLOGNA, BOLOGNA ITALY
First Author:	Camilla Palmiotto, PhD
Order of Authors:	Camilla Palmiotto, PhD Maria Filomena Loreto, PhD Valentina Ferrante, PhD Roberto Braga Letizia Di Bella Laura Corda Filippo Muccini, PhD
Abstract:	<p>Geology, geophysics and geodynamics of the Tyrrhenian back-arc basin (BAB; central Mediterranean Sea) have been studied extensively during the last 50 years. However, some topics are still open: for example, the possible migration of the volcanic arc during the Ionian subduction of the past few Ma. We improved our knowledge of the geodynamics of the Tyrrhenian BAB in the area South of the Vavilov Volcano by analyzing multibeam bathymetry and unpublished single-channel reflection seismic and magnetic data. Furthermore, we studied the petrology of igneous rocks as well as facies and microfaunas of carbonates dredged from the Aurelia and the Augusto seamounts. The Aurelia basement is made of basalts with calc-alkaline affinity. Carbonates from the Aurelia and the Augusto seamounts consist of cemented Mg-calcite biomicrite crusts rich in planktonic foraminifera not older than Early Pleistocene. Based on our results, we interpret the Augusto and Aurelia seamounts as part of the active volcanic arc seaward of the Tyrrhenian BAB in Late Pliocene–Early Pleistocene.</p>



Consiglio Nazionale delle Ricerche
ISMAR - Istituto di Scienze Marine
Sede Secondaria di Bologna
Via P. Gobetti, 101 – 40129 Bologna, Italy
Tel +39 051 6398891 Fax +39 051 6398939
C.F. 80054330586 - P. IVA 02118311006
segreteria@bo.ismar.cnr.it - protocollo.ismar@pec.cnr.it
www.ismar.cnr.it

Dr. Ramon Carbonell
Editor, Tectonophysics

Manuscript TECTO-15884

Bologna, October 27, 2022

Dear **Dr. Ramon Carbonell**,

I am grateful for yours and your referees positive response to our manuscript “**New insights on the fossil arc of the Tyrrhenian Back-Arc Basin (Mediterranean Sea)**” (TECTO-15884).

The comments of your reviewers have been very useful and have helped us to improve the manuscript. We have revised the manuscript following their comments, as explained in the revision notes, where we addressed each of the points raised in your letter. All changes in the text are in red.

With many regards,
Camilla Palmiotto

Venezia

Tesa 104 - Arsenale,
Castello 2737/F
30122 - Venezia, IT
+39 041 2407911
protocollo.ismar@pec.cnr.it
www.ismar.cnr.it

Bologna

Area della Ricerca
di Bologna –
Via P. Gobetti 101
40129 - Bologna, IT
+39 051 639 8891

Lerici

Forte Santa Teresa,
Pozzuolo di Lerici
19032 - La Spezia, IT
+39 0187 1788900

Napoli

Calata Porta Di Massa
Porto Di Napoli 80
80133 - Napoli, IT
+39 081 5423802

Roma

Area della Ricerca
di Roma 2 - Tor Vergata
Via del Fosso del Cavaliere 100
00133 - Roma, IT
+39 06 45488634

Trieste

Area Science Park
Basovizza - Edificio Q2
Strada Statale 14, km 163.5
34149 - Trieste, IT
+39 040 3756872

1 **New insights on the fossil arc of the Tyrrhenian Back-Arc Basin**
2 **(Mediterranean Sea)**

3

4 Camilla Palmiotto^{1*}, Roberto Braga², Laura Corda³, Letizia Di Bella³, Valentina Ferrante¹,
5 Maria Filomena Loreto¹ and Filippo Muccini^{4,5}

6 ¹ *Consiglio Nazionale delle Ricerche, Istituto di Scienze Marine, via Gobetti 101, 40129, Bologna, Italy.*

7 ² *Dipartimento di Scienze Biologiche, Geologiche e Ambientali, Università di Bologna, Piazza di Porta San*
8 *Donato 1, 40126, Bologna, Italy.*

9 ³ *Dipartimento di Scienze della Terra, Università "La Sapienza", Piazzale Aldo Moro 5, 00185, Roma, Italy.*

10 ⁴ *Istituto Nazionale di Geofisica e Vulcanologia, via di Vigna Murata 605, 00143, Roma, Italy.*

11 ⁵ *Consiglio Nazionale delle Ricerche, Istituto di Geologia Ambientale e Geoingegneria, 00185, Roma, Italy.*

12

13 *Corresponding author. Tel: +39 051 6398900

14 E-mail address: camilla.palmiotto@bo.ismar.cnr.it

15 **Abstract**

16 Geology, geophysics and geodynamics of the Tyrrhenian back-arc basin (**BAB**; central
17 Mediterranean Sea) have been studied extensively during the last 50 years. However,
18 some topics are still open: for example, the possible migration of the volcanic arc during
19 the Ionian subduction of the past few Ma. We improved our knowledge of the geodynamics
20 of the Tyrrhenian **BAB** in the area South of the Vavilov Volcano **by analyzing** multibeam
21 bathymetry and **unpublished** single-channel reflection seismic and magnetic data.
22 Furthermore, we studied the petrology of igneous rocks as well as facies and microfaunas
23 of carbonates dredged from the Aurelia and the Augusto seamounts. The Aurelia
24 basement is made of basalts with calc-alkaline affinity. Carbonates from the Aurelia and
25 the Augusto seamounts consist of cemented Mg-calcite biomicrite crusts rich in planktonic
26 foraminifera not older than Early Pleistocene. Based on our results, we interpret the
27 Augusto and Aurelia seamounts as part of the **active** volcanic arc **seaward** of the
28 Tyrrhenian BAB in Late Pliocene–Early **Pleistocene**.



Consiglio Nazionale delle Ricerche
 ISMAR - Istituto di Scienze Marine
 Sede Secondaria di Bologna
 Via P. Gobetti, 101 – 40129 Bologna, Italy
 Tel +39 051 6398891 Fax +39 051 6398939
 C.F. 80054330586 - P. IVA 02118311006
segreteria@bo.ismar.cnr.it - protocollo.ismar@pec.cnr.it
www.ismar.cnr.it

Manuscript TECTO-15884 –

New insights on the fossil arc of the Tyrrhenian Back-Arc Basin (Mediterranean Sea)

Answers to the Reviewers comments

Response to Referee 1

General

We thank this Referee for his statements on our work. Most of the comments concern a recent publication of Corradino et al. (2022): “Arc and forearc rifting in the Tyrrhenian subduction system”. According to Corradino et al. (2022), the current back-arc extension in the Tyrrhenian basin is located between Vavilov and Marsili volcanoes; our study, based on geological, geochronological and petrological constrains, show that the Aurelia and the Augusto Seamounts, located between the Vavilov and the Marsili, were part of the active Tyrrhenian volcanic arc during the Late Pliocene-Early Pleistocene. Furthermore, Corradino et al. (2022) consider Marsili part of an old (Pliocene) volcanic arc; our new map of the reduced to the pole magnetic anomalies of the Southern Tyrrhenian (Figure 6b) reinforces the standard model, with the Marsili Seamount as the current back-arc spreading center of the Southern Tyrrhenian, and the Aeolian Islands as the current volcanic arc front of the system. We added the reference of Corradino et al. (2022) and we motivate in the “Discussion” section our results, based on multidisciplinary and unpublished data. We clarified some sentences of our manuscript following the Reviewer’s suggestions (see additional points); all changes in the text are in red.

Additional points

Line 38: As suggested by the Reviewer, we rewrote this sentence (lines from 35 to 41).

Line 47-49: We deleted this phrase, explaining the meaning of the Marsili Volcano in the Tyrrhenian geodynamic setting in a new sentence (lines from 71 to 75).

Venezia

Tesa 104 - Arsenale,
 Castello 2737/F
 30122 - Venezia, IT
 +39 041 2407911
protocollo.ismar@pec.cnr.it
www.ismar.cnr.it

Bologna

Area della Ricerca
 di Bologna –
 Via P. Gobetti 101
 40129 - Bologna, IT
 +39 051 639 8891

Lerici

Forte Santa Teresa,
 Pozzuolo di Lerici
 19032 - La Spezia, IT
 +39 0187 1788900

Napoli

Calata Porta Di Massa
 Porto Di Napoli 80
 80133 - Napoli, IT
 +39 081 5423802

Roma

Area della Ricerca
 di Roma 2 - Tor Vergata
 Via del Fosso del Cavaliere 100
 00133 - Roma, IT
 +39 06 45488634

Trieste

Area Science Park
 Basovizza - Edificio Q2
 Strada Statale 14, km 163.5
 34149 - Trieste, IT
 +39 040 3756872

Line 50: As suggested by the Reviewer, we added a short sentence in this paragraph (lines from 48 to 50).

Lines 72-74: We thank the Reviewer to let us know the recent paper “Arc and forearc rifting in the Tyrrhenian subduction system” (Corradino et al., 2022). In this paper, the authors, based on the interpretation of multi-channel seismic and numerical modelling, state that the current back-arc extension in the Tyrrhenian basin is located between the Vavilov and Marsili volcanoes, and that Marsili was part of an old (Pliocene) volcanic arc. Our paper, based on unpublished data, provides geological, geochronological and petrological constraints that the Late Pliocene - Early volcanic arc of the Tyrrhenian basin was located between the Vavilov and Marsili, in the area where the Aurelia and Augusto Seamounts are located. Our results reinforce the geological and geodynamic literature of the Tyrrhenian back-arc basin of the last 50 years, considering Marsili volcano as the modern spreading centre of the Marsili back-arc basin, as shown also in our map of the reduced to the pole magnetic anomalies in the Southern Tyrrhenian Sea (Figure 6b), where the Marsili Seamount is marked by the positive/normal magnetic anomaly C1n (0.780 to 0.00 Ma). As suggested by the Reviewer, we added other references in order to reinforce the well-established interpretation that the Marsili Volcano is the modern active back-arc spreading center related to the Tyrrhenian Basin (lines from 73 to 75). We also added the reference of Corradino et al. (2022) in the “Introduction” section and motivate the discrepancy between our and their idea in the “Discussion” section (lines from 484 to 490).

Line 137-142: We rewrote the beginning of the paragraph 3.1 (“Geophysics”), explaining the relationship between the colours and the seismic units of Figure 3.1. This point was also stressed by the second Reviewer.

Line 191: As the Reviewer noted, our interpretation about the nature of the Plinia Seamount is based on the morphological trend similar to that of the Vavilov Volcano, and in particular on the magneto-stratigraphy. We removed the interpretation in this section, that focuses on the results only. We rewrote the sentence (lines 190-191) and modified the Figure 3.

Figure 4: The resolution of the EDAS spectrum was very very low. We recreated part of Figure 4 in order to make the EDAS spectrum readable.

Line 330: We thank the Reviewer for this comment that helped us to better explain our reasoning. There is a vast literature that interpret Ti and Zr as immobile elements during rock-fluid interaction (Pearce, 2014 and reference therein). Thanks to their behavior, Ti and Zr (along with other immobile elements) are used to fingerprint the tectonic setting of igneous rock. A reasonable way to identify the “immobility” of the two elements is to assess whether Ti and Zr show a positive correlation on a binary diagram. The strong Ti and Zr positive correlation in fresh, altered or metamorphosed cogenetic primitive and moderately evolved lavas is known since decades ago (Cann, 1970) and is considered a test for Ti and Zr immobility. We tested the immobility of Ti and Zr in the altered T75 samples by plotting our data along with data of rocks and glass shards from the Marsili seamount (Fig.5b). The plot shows a positive correlation of Ti and Zr, with our data within the main trend. In addition, the sub N-MORB titanium content of our samples suggest that the parent lava of our rocks derives from a subduction zone setting (Pearce, 2014). We slightly modified the original text (lines from 328 to 331) and the Ti/Zr diagram in Figure 5b.

Line 418: We corrected this sentence adding the reference of Cande and Kent (1995) (line 419).

Line 426-431: In this sentence we do not talk about the Vavilov Volcano, but about the Vavilov Basin (line 427: “The end of extension in the Vavilov basin...”; line 435: “We assume that the extensional tectonics of the Vavilov plain...”).

Figure 6: We corrected the names of the chrones in Figure 6 as the reader can find in the paper (“Discussion” section).

Line 445: As suggested by the Reviewer, we added two references in this sentence (Bortoluzzi et al., 2010; Cocchi et al., 2017); see new line 455.

Line 457 and Line 491: Those two annotations concern the discrepancy between the results published by Corradino et al. (2022) and ours. We explained this point in the line 72-74 (see above). Furthermore, we added a short sentence in the “Discussion” section (lines from 484 and 490), where we complete the explanation of our cartoon on the formation and evolution of the volcanic arc related to the Tyrrhenian subduction during the last 3 Ma (Figure 7).

Line 448: Thanks to the Reviewer. This sentence is correct, and we added a phrase to show how the transfer zones could also be inherited from the upper plate along the convergent boundaries (from lines 499 to 502).

Response to Referee 2

We are grateful to this Reviewer for his/her helpful comments. Following the Reviewer's suggestion, we modified the Highlights, Figures 1a and 2a, and the Manuscript (see red lines in the new text).

Additional points

Line 23: This sentence has been corrected in the "Highlights" section.

Line 20: We introduced here the "Back-Arc Basin" acronym, as suggested by the Reviewer.

Line 25: We changed this sentence (lines 25 and 26) as suggest by the Reviewer 1.

Line 32: We introduced the "BAB" acronym in line 20 ("Abstract" section).

Line 85: As the Reviewer suggested, we added in this sentence the seamount names (Aurelia and Augusto).

Line 133: We modified Figure 1a as the Reviewer suggested, showing the parts of the seismic profiles interpreted in this work and adding a short sentence in the caption of Figure 1.

Line 138: We rewrote the beginning of the paragraph 3.1 ("Geophysics"), explaining the relationship between the colours and the seismic units of Figure 3.1. This point was also noted by the first Reviewer.

Line 221: According to the Reviewer, we modified Figure 2b showing in red the six peaks along the Augusto Seamount; furthermore, we added a short sentence in the caption of Figure 2.

Line 483: In this paper we identified the Vavilov-Marsili Transfer Zone interpreting: 1) the regional bathymetry map and the map of the reduced to the pole magnetic anomalies of the Southern Tyrrhenian (Figure 6a and b, respectively); 2) the Sparker profile PM12 (Figure 6c). As shown in Figure 1a, several seismic profile are available to interpret this area; however, this subject may be an interesting theme for another manuscript.

1 **New insights on the fossil arc of the Tyrrhenian Back-Arc Basin**
2 **(Mediterranean Sea)**

3
4 Camilla Palmiotto^{1*}, Roberto Braga², Laura Corda³, Letizia Di Bella³, Valentina Ferrante¹,
5 Maria Filomena Loreto¹ and Filippo Muccini^{4,5}

6 ¹ *Consiglio Nazionale delle Ricerche, Istituto di Scienze Marine, via Gobetti 101, 40129, Bologna, Italy.*

7 ² *Dipartimento di Scienze Biologiche, Geologiche e Ambientali, Università di Bologna, Piazza di Porta San*
8 *Donato 1, 40126, Bologna, Italy*

9 ³ *Dipartimento di Scienze della Terra, Università "La Sapienza", Piazzale Aldo Moro 5, 00185, Roma, Italy.*

10 ⁴ *Istituto Nazionale di Geofisica e Vulcanologia, via di Vigna Murata 605, 00143, Roma, Italy.*

11 ⁵ *Consiglio Nazionale delle Ricerche, Istituto di Geologia Ambientale e Geoingegneria, 00185, Roma, Italy.*

12
13 *Corresponding author. Tel: +39 051 6398900

14 E-mail address: camilla.palmiotto@bo.ismar.cnr.it

15
16 **Highlights**

- 17 • We studied the Augusto and Aurelia Seamounts, located South of the Vavilov
18 **Volcano**, in order to improve the geodynamics of the Tyrrhenian Sea.
- 19 • A morpho-structural study has been done creating local and regional
20 bathymetric maps and interpreting unpublished **Sparker** profiles.
- 21 • Facies, microfauna and petrography of samples of rocks dredged from the
22 Aurelia and Augusto seamounts have been analyzed.
- 23 • A new map of the **reduced** to pole magnetic anomalies of the Southern
24 Tyrrhenian has been created using unpublished magnetic data.
- 25 • Results reveal that the Augusto and Aurelia Seamounts were part of the
26 volcanic arc in the Tyrrhenian Back-Arc Basin during the Late Pliocene-Early
27 Pleistocene.

1 **New insights on the fossil arc of the Tyrrhenian Back-Arc Basin**
2 **(Mediterranean Sea)**

3
4
5 Camilla Palmiotto^{1*}, Roberto Braga², Laura Corda³, Letizia Di Bella³, Valentina Ferrante¹,
6 Maria Filomena Loreto¹ and Filippo Muccini^{4,5}

7 ¹ *Consiglio Nazionale delle Ricerche, Istituto di Scienze Marine, via Gobetti 101, 40129, Bologna, Italy.*

8 ² *Dipartimento di Scienze Biologiche, Geologiche e Ambientali, Università di Bologna, Piazza di Porta San*
9 *Donato 1, 40126, Bologna, Italy.*

10 ³ *Dipartimento di Scienze della Terra, Università "La Sapienza", Piazzale Aldo Moro 5, 00185, Roma, Italy.*

11 ⁴ *Istituto Nazionale di Geofisica e Vulcanologia, via di Vigna Murata 605, 00143, Roma, Italy.*

12 ⁵ *Consiglio Nazionale delle Ricerche, Istituto di Geologia Ambientale e Geoingegneria, 00185, Roma, Italy.*

13

14

15

16 *Corresponding author. Tel: +39 051 6398900

17 E-mail address: camilla.palmiotto@bo.ismar.cnr.it

18

19 **Abstract**

20 Geology, geophysics and geodynamics of the Tyrrhenian back-arc basin (**BAB**; central
21 Mediterranean Sea) have been studied extensively during the last 50 years. However,
22 some topics are still open: for example, the possible migration of the volcanic arc during
23 the Ionian subduction of the past few Ma. We improved our knowledge of the geodynamics
24 of the Tyrrhenian **BAB** in the area South of the Vavilov Volcano **by analyzing** multibeam
25 bathymetry and **unpublished** single-channel reflection seismic and magnetic data.
26 Furthermore, we studied the petrology of igneous rocks as well as facies and microfaunas
27 of carbonates dredged from the Aurelia and the Augusto seamounts. The Aurelia
28 basement is made of basalts with calc-alkaline affinity. Carbonates from the Aurelia and
29 the Augusto seamounts consist of cemented Mg-calcite biomicrite crusts rich in planktonic
30 foraminifera not older than Early Pleistocene. Based on our results, we interpret the
31 Augusto and Aurelia seamounts as part of the **active** volcanic arc **seaward** of the
32 Tyrrhenian BAB in Late Pliocene–Early **Pleistocene**.

33 1. Introduction

34 Back-arc basins (BABs) and volcanic arcs are two main features characterizing the
35 upper plates along convergent plate boundaries (Uyeda, 1979; Leat & Larter, 2003). The
36 relative kinematics, composition and thermal state of the upper **and lower** plates, **together**
37 **with the age of the subducting lithosphere and** the morpho-tectonic inheritance of the
38 upper plate, rule the extensional tectonics along the BABs and their progressive evolution
39 from a younger rifting stage to a mature spreading stage (**e.g.**, Parson and Wright, 1996;
40 Fujiwara et al., 2001; Martinez and Taylor, 2002; Sdrolias and Muller, 2006; Weins et al.,
41 2006; Schellart et al., 2007). BABs in a rifting stage do not show a BAB magmatism, as for
42 example the Havre Trough in the Southern Pacific, characterized by an oblique southward
43 propagating extension and by the absence of a clear spreading ridge (Caratori Tontini et
44 al., 2019); mature BABs show a back-arc spreading center (BASC), i.e. the Mariana
45 Spreading Center in the Pacific (Hynes and Mott, 1985), or the East Scotia Ridge in the
46 Southern Atlantic (Livermore et al., 1997; Fretzdorff et al., 2002).

47 **Here we focus on the** Tyrrhenian Sea (located in the central Mediterranean Sea,
48 between the Italian Peninsula and the Sardinia; Fig. 1), **a peculiar case of BAB associated**
49 **to compressional tectonics where the lower oceanic plate is subducting under continental**
50 **lithosphere.** The Tyrrhenian is a BAB formed by extensional tectonics due to the
51 progressive eastward/south-estward retreat of the Ionian subduction (**e.g.**, Malinverno and
52 Ryan, 1986; Doglioni et al., 1991; 1999; 2004; Faccenna et al., 1997; 2001; Carminati et
53 al., 1998; Sartori, 2003; Rosembaum et al., 2008; Conti et al., 2017; Loreto et al., 2020).
54 First studies on the regional geology and geodynamics of the Tyrrhenian **were** published
55 during 1970s and 1980s (**e.g.**, Barberi, 1973; 1978; Selli et al., 1977; Hsü et al., 1978;
56 Wezel, 1982; Della Vedova et al., 1984; Sartori, 1986; Rehault et al., 1987; Trincardi and

57 Zitellini, 1987; Savelli, 1988). An important contribution on the knowledge of the Tyrrhenian
58 basin occurred with the Deep Sea Drilling Project (DSDP) Leg 42, the Ocean Drilling
59 Program (ODP) Leg 107 (Kastens et al., 1988; Kastens and Mascle, 1990). A collection of
60 multidisciplinary papers on the geology and geodynamics of the Tyrrhenian Sea **was**
61 **shown by** Marani et al. (2004), after the deep seismic exploration of the central
62 Mediterranean and Italy (CROsta Profonda project; **Scrocca et al., 2003**; Finetti, 2005)
63 during the 1990s. Recently, seismic refraction data have been acquired during the
64 MEDOC Cruises in the 2010 (Ranero et al., 2012) in order to display the velocity structure
65 of the Tyrrhenian crust and uppermost mantle together with the Moho reflector geometry
66 (Prada et al., 2014; 2016; 2018).

67 The Tyrrhenian abyssal plain (TAP), marked by the isobaths of the 3000 m in
68 Fig.1a, is floored by basaltic and **ultramafic** rocks covered by Pliocene-Quaternary
69 sediments (Hsü et al., 1978; Kasten and Mascle, 1990). The TAP shows three huge
70 fissural volcanoes (the Magnaghi, the Vavilov and the Marsili) located in the center of three
71 different basins (Fig. 1a). **The Marsili and the Aeolian Islands represent respectively the**
72 **current magmatism in the back-arc basin and in the arc front (Fig.1; Kastens et al., 1988;**
73 **Kastens and Mascle, 1990; Marani and Trua, 2002; Trua et al., 2002; 2018; Rosenbaum**
74 **and Lister, 2004; Marani et al., 2004; Nicolosi et al., 2006; Cocchi et al., 2009; Ventura et**
75 **al., 2013).** The Magnaghi and the Vavilov can be considered segments of extinct back-arc
76 spreading centres evolved naturally **in a basin characterized by** frequent spreading jumps
77 (Magni et al., 2021; Schiffke et al., 2022). In this paper we focus on the region East of the
78 Magnaghi and South of the Vavilov volcanoes (Figure 1a). This area shows an alternation
79 of deep basins and high seamounts from which we have little understanding of their age
80 and composition, given the lack of data. Some information can be extracted from studies

81 of regional geology (Marani et al., 2004; Marani and Gamberi, 2004; Rovere and Wurtz,
82 2015; Palmiotto and Loreto, 2019; Pensa et al., 2019), the lithological and stratigraphic
83 map of the Italian Seas (Colantoni et al., 1981), multichannel seismic reflection profiles
84 (Finetti and Del Ben, 1986; [Corradino et al., 2022](#)) and the distribution of the regional
85 magnetic data (Cella et al., 1998; [Florio et al., 2022](#)). In particular, we study two different
86 seamounts ([Aurelia and Augusto](#)) in order to investigate their origin and to improve the
87 geology and geodynamics of the central Tyrrhenian BAB.

88 We carried out a geophysical study based on: 1) multibeam bathymetry data
89 downloaded from the European Marine Observation and Data Network (EMODnet;
90 <http://doi.org/10.12770/c7b53704-999d-4721-b1a3-4ec60c87238>); 2) single-channel
91 reflection seismics collected by the Institute of Marine Sciences (ISMAR) of the National
92 Research Council (CNR) of Bologna in the 1970s (Fabbri et al., 1981; see Fig.1a and
93 methods); 3) magnetic data collected by the Institute of Marine Sciences (ISMAR) of the
94 National Research Council (CNR) of Bologna in the 1990s (Bortoluzzi et al., 1999; see
95 Fig.1b and methods). We created regional bathymetry maps and an updated map of the
96 reduced to pole magnetic anomalies of the central / Southern Tyrrhenian using magnetic
97 data. Furthermore, we analyzed [for the first](#) time the petrology of igneous rocks and re-
98 analysed facies and microfauna of carbonates dredged [at](#) two seamounts South of the
99 Vavilov Volcano. Results reveal new insights on the geodynamics of the Tyrrhenian BAB
100 during the Late Pliocene-Early Pleistocene.

101 **2. Material and Methods**

102 2.1.1 Bathymetry

103 Middle resolution bathymetric data (200 m-cell grid size) used in this paper have
104 been downloaded from the European Marine Observation and Data Network (EMODnet;

105 <http://doi.org/10.12770/c7b53704-999d-4721-b1a3-4ec60c87238>). Spatial analysis and
106 mapping of ASCII data used **the** open source software GMT (Wessel and Smith, 1998)
107 with the nearest neighbour algorithm. Datum and projection used are, respectively,
108 WGS84 and Mercator. The Global Mapper Software has been used to create 2D digital
109 elevation images.

110 2.1.2 Magnetic data

111 Magnetic data **were** collected by the CNR-ISMAR during the TIR-96 cruise onboard
112 the R/V Gelendzhik in the 1996 and the TIR-99 cruise onboard the R/V A.N. Strakhov in
113 the 1999 (Bortoluzzi et al., 1999). In total, more than 25000 magnetic measurements along
114 1400 km of lines NNE-SSW oriented were used to create a new regional map (**Fig.1b**).
115 Raw data were corrected for spikes and diurnal variations using the reference station of
116 L'Aquila (Central Italy). Magnetic anomalies were calculated by subtracting the IGRF
117 (International Geomagnetic Reference field) model and then reducing the data to the North
118 Pole by phase shifting them using the regional inclination and declination values of the
119 IGRF.

120 2.1.3 Seismics

121 Seismic profiles used in this paper are part of **an old** large (about 46000 km)
122 dataset, available as profiles printed on paper, collected during several cruises carried out
123 **by CNR-ISMAR** of Bologna between the 1970s and the 1980s (Fabbri et al., 1981).
124 Seismic data have been shot using a Sparker 30 KJ and recorded with a trace length of 8
125 s (TWT). A new digital seismic database is under construction at the CNR-ISMAR of
126 Bologna in order to preserve **these data**, inspired by FAIR (findable, accessible,
127 interoperable and reusable) principles (Wilkinson et al, 2016). Seismic lines were
128 scanned from paper to high resolution raster image (TIFF); they will then be converted into
129 georeferenced SEG-Y format using the free Matlab program IMAGE2SEGY (Farran, 2008)

130 distributed by the Department of Marine Geosciences of The Spanish National Research
131 Council (<http://www.icm.csic.es/gma/en/content/image2segy/>).

132 Here we present parts of five profiles acquired during oceanographic cruises T71,
133 T73 and T75 (yellow, green and pink lines respectively and shown in Fig. 1a) onboard of
134 the N/O Bannock carried out by the “Bacini Sedimentari” Group on behalf of the “Progetto
135 Finalizzato Oceanografia e Fondi Marini” of the Italian CNR in the Tyrrhenian Basin
136 (Fabbri et al., 1981).

137 2.2 Samples

138 Analyzed rocks **were** dredged by the CNR-ISMAR of Bologna during cruise T75 in
139 the Tyrrhenian Sea. Samples labels refer to cruise, dredge station and rock samples
140 numbers; for example, 75-30-3 refers to rock sample number 3, dredge station 30, carried
141 out during the oceanographic expedition T75.

142 Samples dredged from site 75-30 (orange dot in Fig.2a) are carbonates and
143 volcanic rocks: volcanic samples have been re-analyzed; carbonates have been analyzed
144 for the first time. Samples dredged from sites 75-35 (yellow dot in Fig.2a) and 75-36
145 (green dot in Fig.2a), composed only of limestones, have been re-analysed in order to
146 determine the micropaleontological identifications and carbonate facies. Results of past
147 samples analysis are shown in the lithological and stratigraphic map of the Italian Seas
148 (Colantoni et al., 1981).

149 Rock samples underwent macroscopic and thin section examination under the
150 petrographic and binocular microscopes. Bulk-rock abundances of major and minor
151 elements were determined by X-ray fluorescence (XRF). Micropaleontological
152 identifications were based on a bio and chronostratigraphical scheme for the
153 Mediterranean of Iaccarino et al. (2007). Digital photographs and Energy Dispersive
154 Spectroscopy (EDS) for elemental composition were obtained with a scanning electron

155 microscope (FEI QUANTA 400) at the SEM Laboratory of Earth Sciences Department –
156 Sapienza University of Rome (Italy). For the identification of crystalline material X-ray
157 diffraction on sample powder were also carried out by a Phillips PANalytical X'Pert PRO
158 diffractometer using CuK α radiation ($n=1.5418 \text{ \AA}$), operating at 40kV and 40mA at a step
159 size of 0.0260° at the Department of Earth Science, Sapienza University of Rome (Italy).
160 The program used for qualitative analyses is WinPLOTR Programme (CDIFX UMR6226
161 Rennes/ILL Grenoble).

162 **3. Results**

163 3.1 Geophysics

164 Bathymetry and the reduced to the pole magnetic anomalies of the Southern
165 Vavilov region maps are shown in Fig. 2. Part of sparker profiles here interpreted, with
166 their values of magnetic anomalies associated, are shown in Fig. 3. **Based on** Loreto et al.
167 (2020), three main seismic units have been identified: 1) a well-stratified unit (**green color**
168 **in Figs. 3 and 6**), **interpreted** as Pliocene-Quaternary (PQ) deposits, based on
169 lithostratigraphic information (Kastens et al., 1988); 2) a poorly-stratified and transparent
170 unit (**violet in color in Figs. 3 and 6**), **interpreted as coexisting** sediments and volcanic
171 layers; 3) a more chaotic and less reflective **unit, interpreted** as the basement (**brown color**
172 **in Figs. 3 and 6**). **Because of** the low resolution of the Sparker profiles and their smaller
173 size in Figure 3, we created supplementary figures in order to zoom them and increase
174 their resolution.

175 The Seamounts D'Ancona I and II, Plinia, Vavilov and Tibullo are located in the
176 Northern part of the region, from West to East (Fig. 2). The D'Ancona is formed by two
177 different seamounts located in the Eastern Magnaghi Abyssal Plain (EMAP; Fig. 2a). The
178 D'Ancona I, a NNW-SSE oriented ridge, is located between 3485 m and 2696 m of depth;
179 it is 19 km long and 12 km wide, with a steep western flank (20°) and an eastern flank 10°

180 steep (Fig. 2b). The D’Ancona II is a 13 km long and 11 km wide seamount, E-W oriented,
181 with a depth ranges from 3476 m to 2900 m (Fig. 2a). The northern flank is 12° steep; the
182 southern is 7° (Fig. 2b). From a magnetic viewpoint, the D’Ancona I shows a negative
183 magnetic anomaly (from 0 to -50 nT), whereas the D’Ancona II a positive magnetic
184 anomaly (> 100 nT). East of the D’Ancona II, there is a NNE-SSW oriented topographic
185 ridge 17 km long and 6.5 km wide; it is unnamed in literature and here we called it “Plinia”.
186 This seamount ranges between 3150 m and 2647 m of depth (Fig. 2a), and it is
187 characterized by a western flank steeper than the eastern side (20° and 15° respectively;
188 Fig. 2b); the magnetic anomaly is negative and it ranges from 0 to -150 nT. The Southern
189 part of the Plinia can be shown in the in the PM3E sparker profile of Fig. 3 (Box A and A’)
190 and Supp. Fig. 1, between the Fix 26 and 28, covered by a thin PQ unit. Plinia is located
191 near Vavilov: they show a similar trend and value of magnetic anomaly (Fig. 2).

192 The Vavilov Seamount is located east of the Plinia Seamount. This huge submarine
193 volcano rises from the abyssal plain at a depth of 3500 and arrives at only 793 m below
194 sea level. The Vavilov shows an asymmetric perpendicular profile, with the western flank
195 steeper than the eastern side (23° and 14° respectively; see the slope shader map of Fig.
196 2b). The depth of the volcano ranges from 3600 m to 823 m. The Vavilov shows a very
197 strong negative magnetic anomaly (from 0 to -681 nT), although a small portion of its
198 eastern flank shows a positive anomaly (from 0 to 150 nT). To the east of Vavilov, there is
199 Tibullo Seamount, an elongated narrow NNE-SSW ridge, only 400 m high, characterized
200 by a symmetric profile (flanks ~ 13° steep); the magnetic anomaly is positive (between 0
201 and 50 nT) on the northern part, and negative on the southern part (between 0 and -50
202 nT).

203 The Southern Vavilov Abyssal Plain (SVAP; mean depth ~ 3600 m) is filled by >
204 500 m of sediments (PQ unit along the PM3E profile; Fig. 3 and Supp. Fig. 1). East of the

205 SVAP, there is a seamount unnamed in literature, here called “Aurelia” (Fig. 2). The
206 Aurelia is a WNW/ESE-oriented seamount between 3500 m and 2750 m deep,
207 characterized by a strongly asymmetrical perpendicular profile, with the northern flank
208 steeper than the southern flank (25° and 12° respectively; Fig. 2b). The magnetic anomaly
209 ranges from 0 to 50 nT in the western part and from 0 to -50 nT in the eastern part of this
210 seamount. The profile PM4 (Fig. 3, Box B and B’ and Supp. Fig. 2) crosses
211 perpendicularly the Aurelia, showing between Fix 75 and 76 a sub-vertical discontinuity
212 that connects laterally the basement with the PQ unit. The Aurelia is crossed also by
213 Profile PM11 (Fig. 3, Box C and C’ and Supp. Fig. 3): also here the asymmetry of the
214 seamount, with a sub-vertical fault affecting the northern flank, is clearly visible. South of
215 the Aurelia, the NNE-SSW oriented ridge Virgilio is formed by two different highs: the
216 northern high (~ 2800 m of depth) with a shallow negative magnetic anomaly (from 0 to -
217 50 nT); in contrast, the southern high (~ 2700 m of depth) with very strong positive values
218 (> 100 nT).

219 The southern part of this region is characterized by two arc-shaped seamounts.
220 One of those, the Augusto, a ~ 55 km-long seamount ranging from 3100 m to 1950 m of
221 depth (Fig. 2a), is characterized by six peaks located between 2400 and 1950 m of depth
222 (Fig. 2b). It shows a very strong positive magnetic anomaly, particularly in its central part
223 (> 200 nT). The Augusto is separated from an unnamed seamount, here we call “Emilia”
224 (minor depth 2200 m) from a NNW-SSE oriented basin. West of the Emilia, we have a
225 deep (> -3500 m) and almost circular basin.

226 The NNE-SSW segment of the PM11 profile (Fig. 3, Box C and C’ and Supp. Fig. 3)
227 crosses the Aurelia, a small basin filled by PQ sediments and Augusto. PQ sediments in
228 the small basins are well-stratified and undeformed in the shallow part, while gently
229 deformed in the deeper part. This intra-Pliocene unconformity corresponding probably to

230 the “X Unconformity” (Zitellini et al., 1986) is marked with a violet horizon. Several NE- and
231 SW-dipping normal faults control the formation of small basins (see at Fix 13 and 2 in the
232 box C’ of Fig. 3).

233 The SW-NE- oriented segment of the profile PM10E (Fig. 3, Box D and D’ and
234 Supp. Fig. 4) crosses the Emilia, Augusto and Virgilio Seamounts. Emilia and Virgilio are
235 bounded by several SW- and NE-dipping normal faults, as suggested by the abrupt lateral
236 interruption and dislocation of well-stratified PQ unit (marked in green). These normal
237 faults dislocate also the basement and an intermediate unit (VIOLET) with a transitional
238 seismo-stratigraphic character. The PQ unit covers part of these two seamounts, part of
239 the intermediate unit and forms thick and narrow basins (see at Fix 17 of box D’ in Fig. 3).
240 The Augusto seamount, with a chaotic seismo-stratigraphic character, does not show any
241 sedimentary cover nor faults dislocations.

242 3.2 Facies and microfaunal associations

243 The sample dredged from site 75-30-3 (Aurelia Seamount; Fig. 2a) shows the direct
244 contact between a few centimeters thick completely lithified limestone, and a greenish
245 volcanic rock (Fig.4a). The upper surface of the volcanic rock appears to be irregular and
246 affected by frequent fractures filled by carbonate mud. A thin non-continuous brownish-to-
247 black film marks the contact magmatic rock/limestone and locally also the neptunian-dykes
248 walls. The carbonate crust overlying the volcanic rock appears to be completely lithified; its
249 upper surface, exposed to seawater, is coated by a thin black film and is strongly
250 colonized by serpulids that are, in turn, covered by a black film. Frequent microhollows
251 representing the moulds of eroded and/or dissolved tests are recognizable.

252 Samples dredged from sites 75-35-(5-7-9) and 75-36-7 (Augusto Seamount; Fig.2a)
253 consist of 2-3 cm of light brownish consolidated limestones. No direct contact with volcanic
254 rocks has been observed here. The limestone upper surface is coated by a black film

255 strongly colonized by serpulids, which are in turn mineralized. In site 75-35 the carbonate
256 crust is totally colonized by corals and serpulids. Most of the recovered corals are solitary
257 cold-water species as *Desmophyllum* with characteristic cup-shaped morphology and
258 marked septa (Fig.4b). Their size varies from a few up to 6-7 centimeters; the younger
259 individuals, growing on top of the older ones, simulate pseudo-colonies. The corals
260 represent fossil occurrences; no living corals have been recovered. The corals surface
261 appears to be almost completely covered by a very thin film, black in color.

262 All the carbonates consist of crusts cemented throughout their total thickness
263 without textural evolution from chalk to limestones. Just in one sample (75-36-7a) a small
264 cavity is filled by a not completely lithified planktonic-rich mud.

265 Microfaunal analysis of the carbonate crusts reveals coral fragments, gasteropods,
266 pteropods, sponge spicules and foraminifera. The foraminiferal content is represented by
267 planktonic taxa widely distributed in the hazel-brown micritic carbonate with mudstone
268 texture or gathered inside bioturbation pockets, bioerosive structures and neptunian dykes
269 within the volcanic substratum. Mn-Fe-oxides films (or permeation or crusts) always outline
270 the bioerosion structures. The most frequent taxa are: *Pulleniatina obliquiloculata*,
271 *Globorotalia inflata*, *Globorotalia scitula*, *Orbulina universa* and globigerinids (e.g. *G.*
272 *bulloides*). Genus *Globigerinoides* is less abundant and it is mainly represented by *G.*
273 *trilobus*. *Globorotalia truncatulinoides* (in the 75-30-3) and of *Pulleniatina obliquiloculata*
274 were also observed (Fig.4d).

275 X-ray diffraction on the carbonate crusts showed Mg-calcite and calcite as the most
276 abundant phases with a subordinate silicate fraction with mica, chlorite, quartz, and
277 probably montmorillonite. Also SEM analysis, coupled with EDS, showed predominance of
278 carbonate composition with a very subordinate clay-sized silicate fraction (Fig. 4a).

279 Isolated volcanic minerals (quartz and feldspar) and volcanic fragments have been found
280 within the carbonate crust from site 75-36-7 (Fig.4c).

281 The thin brownish-to-black film marking the contact magmatic rock/limestone and
282 the neptunian-dykes walls is of Mn-Fe oxides (Fig. 4a) and shows a thin layered structure.
283 All limestone surfaces, borings (Fig.4e) and/or skeletons exposed to sea-water are coated
284 by a Mn and Fe-oxy-hydroxides thin black-brownish botryoidal film with a laminated
285 texture. The major mineral phase is todorokite, with subordinate amounts of phosphates
286 and montmorillonite (X-ray diffraction data).

287 Based on thin section and SEM-EDS observations, the limestones exhibit a
288 complex diagenetic history. Sometimes the carbonate crusts are characterized by a first
289 thin portion of an early consolidated limestone with bioclastic fragments and diffuse
290 serpulids separated, by means of a thin film of Mn-Fe-oxides, from a portion richer in
291 planktonic foraminifera. The lower portion may display borings and/or fractures, coated by
292 a Mn-Fe oxides film, filled by carbonate pelagic sediments that, in turn underwent a new
293 early lithification and mineralization. All these features indicate at least two phases of early
294 diagenesis accompanied by Mn-Fe mineralization. Both the mineralogical composition and
295 the planktonic associations of the two portions do not show significant differences.

296 3.3 Petrography

297 Samples were chosen for petrographic analyses to verify or discard their igneous
298 nature. In particular, we selected samples with phyrlic-like texture, i.e. large minerals in an
299 aphanitic ground mass. Sample T75-30-3 (Aurelia Seamount; Fig.2a) shows white to light-
300 brown grains up to two mm across set in a gray-greenish matrix (Fig. 5a1). A vein of 10
301 mm maximum apparent thickness cuts the sample. The vein is filled by very fine-grained
302 material and the contact with the host rock is sharp. Sample T75-30-5 displays phyrlic
303 texture made of vitreous grains (average 1 mm across) in a relatively soft light-gray matrix

304 (Fig. 5a2). Inspection under a polarizing optical microscope (Fig. 5a3,4) reveals a texture
305 with euhedral to anhedral grains set in a chlorite- and opaque-rich matrix. Matrix minerals
306 are locally aligned to form a fluidal texture. Two types of grains are recognized: (1)
307 euhedral to subhedral grains with pseudo-hexagonal and prismatic shapes (Fig.5a4,5) and
308 (2) rounded fractured grains with clear appearance under plane polarized light (Fig. 5a3).
309 The euhedral to subhedral grains may be former phenocrysts now completely replaced by
310 secondary chlorite and carbonates, mainly dolomite and minor Mg-calcite, as determined
311 by energy-dispersive spectrometry in a SEM. These phenocrysts occur as single grains or
312 as clusters that locally gives the rock a glomeroporphyritic texture. The rounded fractured
313 grains are made of quartz (sample T75-30-3). The matrix is composed of euhedral to
314 subhedral microlites, now completely replaced by secondary low-Fe chlorite, and rounded
315 Ti-rich minerals. High-Fe chlorite fills the interstices among microlites. Sample T75-30-5 is
316 cut by at least two sets of veins. Earlier veins, maximum thickness 0.25 mm, are filled by
317 coarse grained Fe-bearing dolomite with irregular shapes. Late veins are wider, and are
318 filled by euhedral dolomite. Finally, sample T75-30-5 contains amygdale showing a
319 zonation, from rim to core of the amygdala, chlorite, opaque material and dolomite (Fig.
320 5a6).

321 **4. Discussion**

322 4.1 Environmental significance of the Aurelia and Augusto rocks and carbonate facies

323 Samples of rock analyzed from the Aurelia seamount preserve a porphyritic texture with
324 different types of phenocrysts set in a matrix with microlites that locally define a flow
325 texture. These features are compatible with an igneous nature of the samples. Their
326 primary mineralogy is now replaced by secondary phases such as low-Fe chlorite and
327 dolomite. Similarly, the matrix contains microlites now replaced mainly by low-Fe chlorite,
328 and Ti-rich phases that possibly represent remnants of primary Fe-Ti oxides that

329 underwent iron loss during low-temperature rock-water interaction. Plotting our data of Ti
330 and Zr, two elements usually interpreted as relatively immobile during low-T alteration
331 (Pearce, 2014), the rocks of the Aurelia Seamount fall in the calc-alkaline field (Fig. 5b).

332 From a carbonate/biostratigraphic viewpoint, samples from the Aurelia and Augusto
333 Seamounts consist of crusts cemented throughout their total thickness without textural
334 evolution from chalk to limestones. The crusts, with thickness between 15 to 30 mm, are
335 made of Mg-calcite biomicrite rich in planktonic foraminifera with a very subordinate
336 silicate component. The occurrence of *Globorotalia truncatulinoides* on the Aurelia
337 Seamount suggests for this sample an age not older than Early Pleistocene (Iaccarino et
338 al., 2007). This is also confirmed by the presence of *Pulleniatina obliquiloculata*, a warm
339 tropical-subtropical species, that although it occurred in the Atlantic basin in Early Pliocene
340 (Zankl, 1969; Bolli and Sanders, 1985; Iaccarino et al., 2007), it is never recorded in
341 Pliocene Mediterranean deposits. Moreover, according to Bolli and Sanders (1985), *P.*
342 *obliquiloculata* shows major frequency peaks during the Pleistocene–Holocene time
343 interval. This taxon would have entered the Mediterranean during the Pleistocene warmer
344 climatic stages (Conti et al., 2013) probably from the Atlantic occurring exclusively in the
345 western sector of the Mediterranean basin. An interesting feature is the occurrence within
346 the carbonate crust from the Augusto Seamount of isolated volcanic minerals (quartz and
347 feldspar) and of volcanic fragments, probably indicating a coeval magmatic activity or
348 alternatively a supply of volcanic material eroded from a nearby seamount.

349 The occurrence in many areas of the Mediterranean of Quaternary deep-water
350 cemented limestones with different grades of consolidation, from brittle to consolidated
351 chalk to cemented limestones, has been reported in literature (Alloué, 1990). The study of
352 the carbonate crusts and their relationships with the volcanic substrate, are important for
353 understanding the rapid formation of hardgrounds in ancient sedimentary sequences.

354 A number of studies have focused on the driving mechanisms for the early
355 lithification of the Quaternary deep-sea crusts (Emelyanov & Shimkus, 1986; McKenzie
356 and Bernoulli, 1982; Alloué 1987, 1990; Remia et al., 2004). Early lithification, occurring at
357 or below the seafloor, takes place under varying conditions: it may occur in sediment-
358 starved environments, it may depend on ascending interstitial carbonate-rich waters, or on
359 microbiological precipitation or it may be physiochemically controlled and related to inward
360 diffusion of sea-water solutions. Concerning the degree of saturation relative to calcite,
361 Mediterranean waters remained saturated at all depths also during the Pleistocene cold
362 phases (Alloué, 1987). Another significant factor controlling carbonate precipitation or
363 dissolution is the concentration of dissolved phosphates and organic matter (Morse, 1986).

364 The carbonate crusts taken into consideration in this study are predominantly made
365 of Mg-calcite with a very subordinate silicate fraction, mostly represented by mica, quartz
366 chlorite and montmorillonite, probably deriving from the weathered volcanic substrate. One
367 of the factors controlling early lithification is the purity of lime mud; less than 2% of
368 insoluble residue (especially clay minerals) favors cementation and recrystallization (Zankl,
369 1969). Nevertheless an excess of hydrothermal metals (i.e. Mn-Fe-oxyhydroxides) may
370 “fertilize” areas of normal biological productivity, resulting in massive phytoplankton
371 blooms (Coale et al., 1996; Larson and Erba, 1999; Corda and Palmiotto, 2015). The
372 microorganisms activity may have a significant influence in precipitating hydrothermal Mn-
373 Fe-oxyhydroxide (Dekov and Savelli, 2004); in addition, Mutti and Bernoulli (2003) stress
374 the relationship between phosphate mineralization, trophic resources and microbial micrite
375 precipitation. Based on our observations, we assume a significant role of the
376 microbiological precipitation of calcite in facilitating the early lithification of planktonic ooze.

377 Sources of magnesium are usually seawater and sometimes, fresh waters but could
378 also derive from weathered magmatic Fe-Mg rich rocks. When magnesium is delivered to

379 seawater, Mg-calcite can precipitate (Mackenzie and Andersson, 2013; Morse and
380 Mackenzie, 1990).

381 The limited thickness of the carbonate crusts points to very slow rates of
382 sedimentation and /or accumulation probably related to high hydrodynamics. The very thin
383 brownish film of Mn-Fe oxides, even if non-continuous, covering the volcanic substrate
384 hints at a period of water-rock exposure before the carbonate planktonic-rich mud began
385 to deposit. During this period the volcanic substrate underwent a phase of extensional
386 tectonics promoting intense fracturing, as testified by neptunian dykes partially mineralized
387 and successively filled by pelagic sediments. This substrate should be firstly colonized by
388 small rapidly-growing opportunistic organisms such as serpulids, favored by strong storm
389 activity, and covered by few millimeters of carbonate mud cemented early. Above this first
390 phase of sedimentation, accompanied by early diagenesis, bioturbation processes and
391 Mn-Fe mineralization, a new phase of sedimentation of carbonate planktonic-rich ooze
392 began, that was rapidly lithified and mineralized.

393 Ultimately our findings suggest that the pelagic sediments settled on the magmatic
394 substrates underwent an early lithification process induced by precipitation of Mg-calcite
395 within the pelagic carbonate matrix in areas of very slow sedimentation rates. The volcanic
396 substrates underwent a tectonic instability, testified by fractures and neptunian dykes
397 infilled by planktonic mudstones. Their morphostructural configuration as isolated highs,
398 suffering high hydrodynamic conditions, is here interpreted as responsible for low
399 sedimentation/accumulation rates, clustering of planktonic foraminifera and skeletal
400 fragmentation. The slow rates of deposition favored prolonged conditions of exposure at
401 the seawater-sediment interface of the pelagic and skeletal carbonates, enhancing the
402 diffusion of seawater-ions throughout the sediments and promoting chemical precipitation
403 and the consequent development of hardgrounds prone to be colonized by corals and

404 serpulids. In addition, the presence of phosphorous as evidenced by the SEM-EDS
405 analysis, suggests that the pelagic carbonates underwent early diagenetic lithification
406 phases under high-fertility conditions which, favoring an increase of microbiota
407 communities, promoted an increase of microbiological micrite precipitation. The
408 widespread Mn-Fe mineralizations covering both the carbonate deposits and the
409 encrusting/colonizing biota on the base of crust morphologies, textural evidence and
410 tectonic setting, can be related to hydrothermal processes.

411 4.2 Geodynamic significance of the Aurelia and Augusto Seamounts

412 We discuss here the significance of the Aurelia and Augusto seamounts in the
413 geodynamics of the central Tyrrhenian Back-Arc Basin, based on our results, on data from
414 literature, on the regional bathymetry map and the map of the distribution of the reduced to
415 the pole magnetic anomalies of the Southern Tyrrhenian (Figure 6a and b, respectively).

416 The Magnaghi basin (Fig. 6a) starts opening during the Tortonian/Messinian (Loreto
417 et al., 2020). Volcanism of the Magnaghi Volcano is characterized by basalts with an Na-
418 alkaline affinity, dated from 3.1 to 2.7 Ma (Late Pliocene; Serri et al., 2001), in line with the
419 **subchron C2An.1n** (3.040 to 2.581 Ma; **Cande and Kent, 1995**) shown in Fig. 6b.

420 The Vavilov basin (Fig. 6a) opened between the Late Miocene and the Early
421 Pliocene (the older basalts from the ODP 373 are 7.5 Ma old; Hsü et al., 1978) when their
422 composition is similar to mid-ocean ridges (MORB), as shown by the basalts sampled from
423 the ODP 655 on the Gortani Ridge (Fig. 6a), dated ~4 Ma (Kastens et al., 1988). The
424 beginning of the Vavilov Volcano activity is placed at 3 Ma, at the same time of the
425 spreading of the basin (Robin et al., 1987). The Vavilov lavas, very similar to those of the
426 Magnaghi Volcano, are formed by basalts ranging from tholeiitic to Na-alkaline (Peccerillo,
427 2017). The end of extension in the Vavilov basin allows the growth of the volcano, which
428 shows in Figure 6b a negative magnetic anomaly (C2r.2r; 2.581 to 2.150 Ma; Savelli and

429 Ligi, 2017). According to Parson et al. (1990), the change in chemical composition from
430 MORB to calc-alkaline marks the evolution of a back-arc basin from an early stage, where
431 a pure extensional tectonics produced an oceanic crust with MORB affinity, to a mature
432 stage of back arc spreading, where the oceanic crust has a calc-alkaline affinity. Based on
433 the age of the boundary between the older sediments and calc-alkaline rocks sampled in
434 the ODP 651 (Northern Vavilov basin; Kastens et al., 1988; Bonatti et al., 1990), we
435 assume that the extensional tectonics of the Vavilov plain continued until 2.6 Ma.

436 The Marsili basin (Fig. 6a) starts opening in the Early Pleistocene (basalts dated ~ 2
437 Ma from the OPD 650; Kastens et al., 1988); it shows a negative/inverse magnetic
438 anomaly falling in the chron C1r.2r (1.770 to 1.070 Ma; Fig. 6b). The Marsili volcano is
439 located in the center of the basin, formed by calc-alkaline rocks (Trua et al., 2002) not
440 older than 1.07 Ma (Cocchi et al., 2009), corresponding with the positive/normal magnetic
441 anomaly C1n (0.780 to 0.00 Ma; Cocchi et al., 2009; see Fig. 6b). The Marsili is
442 surrounded by several volcanic islands and seamounts (Fig. 6a): the Palinuro Volcanic
443 Complex, a E-W oriented volcanic structure formed by basaltic-andesite compositions
444 lavas dated 0.8-0.3 Ma (e.g., Colantoni et al., 1981; Cocchi et al., 2017); the Alcione, and
445 Lametini 1 and 2 seamounts, related to the geodynamic environment to the Aeolian arc
446 and younger than 1 Ma (Barberi et al., 1974; Beccaluva et al., 1985; Lupton et al., 2011);
447 the Aeolian Islands, consisting of calc-alkaline to shoshonitic lavas and pyro-clastics, with
448 minor potassic alkaline rocks (Peccerillo, 2005), originated by volcanism due to the “wet”
449 melting of a suprasubduction mantle wedge (Lupton et al., 2011); the Enarete, Eolo, Sisifo
450 and Tiro Seamounts, the oldest volcanoes of the Aeolian Islands Arc (Beccaluva 1982;
451 1985). All these volcanoes and seamounts show a normal/positive magnetic anomaly (i.e.
452 Bortoluzzi et al., 2010; Cocchi et al., 2017) that, as in Marsili, can be attributed to the C1n
453 (0.780 to 0.00 Ma), although some of them show a volcanism > 0.780 Ma, before the

454 formation of the Marsili volcano. For example, the Tiro and Sisifo Seamounts are formed
455 by calc-alkaline and high K₂O calcalkaline rocks dated ~1.5 Ma and from 1.3 Ma to 0.9,
456 respectively (Beccaluva et al., 1985); Enarete and Eolo, formed by basalts, dacites and
457 rhyolites, have been dated between 0.85-0.77 Ma (Beccaluva et al., 1982, 1985; Trua et
458 al., 2004).

459 Based on the geodynamic models of Carminati et al. (2010), we reconstructed a
460 cartoon showing the migration of the volcanic arc associated to the Ionian slab during the
461 last 3 Ma (Figure 7). In this cartoon, at 3 Ma, when the Magnaghi and Vavilov volcanoes
462 were active, we assume that Aurelia, Virgilio and the western part of Augusto seamount
463 were part of the active volcanic arc. We based on: 1) the calc-alkaline basement rocks of
464 the Aurelia (Ti/Z diagram data of Fig.5b), indicating a subduction-related volcanism; 2) the
465 calc-alkaline basement rocks of the western part of the Augusto (Colantoni et al.,1981),
466 testified also by the occurrence of volcanic fragments in our carbonate samples, and on
467 the strong positive magnetic anomaly (Fig. 6b and Cella, 1998); 3) the volcanic nature of
468 the Virgilio, considered a NNE-SSW oriented composite volcanic structure made by a
469 coalescence of a series of centres (Finetti et al., 1986); 4) the recognized planktonic
470 foraminifera assemblages of the Aurelia and Augusto carbonates, cannot be older than
471 Early Pleistocene, indicating a volcanic activity before 2.58 Ma.

472 Based on the bathymetry maps (Figs. 2 and 6a), the Augusto Seamount is
473 composed by several peaks forming a curved arc, located between 2400 and 1900 m
474 below sea level. This curved morphology resembles more the fossil Aeolian volcanic arc,
475 South of the Marsili, formed by the Seamounts Sisifo and Tiro, active between 1.5 and 1
476 Ma (Fig.7 - 1 Ma; Beccaluva et al.,1985), than the morphology of the modern Aeolian
477 volcanic arc (Fig.7 - 0 Ma). Considering the location of the Augusto, between the Aurelia
478 and the Augusto, and the Sisifo and Tiro, and based on the age of their volcanism, we

479 assume the Augusto Seamount as part of the Early/Middle Pleistocene Tyrrhenian
480 volcanic arc (Fig.7 - 2 Ma). The different trend of the Tyrrhenian volcanic arc between the
481 Late Pliocene (Fig. 7 - 3 Ma) and the Early Pleistocene (Fig. 7 – from 2 to 0 Ma) could
482 testify the change from eastward to southeastward of the Ionian slab retreat, due to
483 collision with the Apulia platform to the north and the Hyblean platform to the south, during
484 the Pliocene (Van Dijk et al., 2000). The geodynamic model by Corradino et al. (2022)
485 considers the area between Vavilov and Marsili as the present place of back-arc
486 extension, and the Marsili as part of a Pliocene volcanic arc. In contrast, our geological,
487 geochronological and petrological results show that the Aurelia and the Augusto
488 Seamounts were part of the active Tyrrhenian volcanic arc during the Late Pliocene-Early
489 Pleistocene, and that the Marsili is the present back-arc spreading center (positive/normal
490 magnetic anomaly C1n - 0.780 to 0.00 Ma; Fig. 6b).

491

492 4.3 The Vavilov-Marsili Transfer Zone

493 According to Macdonald et al. (1988) and Pagli et al. (2019), along the back-arc
494 basins, seafloor spreading is offset by transfer zones where strike-slip tectonics transfers
495 displacement between two similar non-coplanar structures. Transfer zones are striking
496 parallel to the regional direction of extension. They are local and passive fracture formed in
497 response to active faulting on faults which link with the transfer; an example is transfer
498 zone is the Central Lau Spreading Centre (CLSC) and the Eastern Lau Spreading Centre
499 (ELSC) in the Lau Back-arc Basin (SW Pacific Ocean; Parson and Wright, 1996). Also,
500 transfer zones could also be inherited from the overriding plate, as in the Northern Lau
501 Basin, where the upper plate is affected by strike-slip tectonics along older tectonic
502 lineaments (Palmiotto et al., 2022).

503 The central region of the Tyrrhenian Back-Arc Basin is characterized by a WNW-
504 ESE oriented basin, located between the Vavilov and the Marsili basins, perpendicular to
505 the NNE-SSW trend of the Vavilov and Marsili volcanoes (Fig. 6a). This basin shows low
506 values of magnetic anomalies (Fig. 6b) and, based on seismic refraction data (Recq et al.,
507 1984), it is characterized by a minimum value of crustal thickness (the velocity is 6 km/s at
508 only 5 km of depth). We show here part of a sparker profile (PM12; Fig. 6c and Supp. Fig.
509 5), acquired during the oceanographic expedition T71 (see the Fig.1a and the methods).
510 The profile PM12 is NE-SW oriented and crosses perpendicular the basin between Vavilov
511 and Marsili. An interpretation of the profile shows that the basin is covered by PQ
512 sediments and it shows in its center, from fix 32 to 37 (Fig. 6c and Supp. Fig. 5), a feature
513 we interpreted as a positive flower structure. This feature can be attributed to a
514 transcurrent fault that in the bathymetry map (Fig. 6a) can be followed from the Southern
515 Vavilov basin, where affects the Aurelia basement (see the sub-vertical fault in the profiles
516 PM4 and PM11 of Fig. 3 and Supp. Figs.3,4), to the Western Marsili basin. Furthermore,
517 based on the maps of the distribution of the reduced to the pole magnetic anomalies (Figs.
518 2c,d and 6b), the upper part of the Vavilov volcano and a small part of its eastern flank
519 show a positive magnetic anomaly which could be attributed to a recent volcanic event,
520 considering that the summit lavas have been dated between 0.37 and 0.09 Ma (C1n;
521 Robin et al., 1987; Savelli and Ligi, 2017). Based on those considerations, we interpreted
522 the Tyrrhenian as a BAB where two different segment of spreadings are active at the same
523 time and, the basin between the Vavilov and the Marsili, their “Transfer Zone” (Figs. 6 and
524 7).

525

526 **5. Conclusions**

527 We analyzed geophysical and geological data of two seamounts (Augusto and
528 Aurelia) located South of the Vavilov volcano. The Augusto is characterized by an arc-
529 shaped morphology, with several peaks located between 1950 and 2400 m below sea
530 level; the Aurelia shows an asymmetric perpendicular profile due sub-vertical faults
531 affecting its northern side, visible both from bathymetry and from the sparker profiles. The
532 distribution of the reduced to the pole magnetic anomalies shows positive values on the
533 Augusto, and low negative values on the Aurelia. Samples of rocks dredges from the
534 Seamounts show a magmatic nature of their basement (basalts with a calc-alkaline
535 affinity). Carbonate samples consist of thin crusts cemented early made of Mg-calcite
536 biomicrite rich in planktonic foraminifera, dated not older than Early Pleistocene. Based on
537 our results, we interpret the Augusto and Aurelia as part of the volcanic arc of the
538 Tyrrhenian BAB during the Late Pliocene–Early Pleistocene time.

539 **Acknowledgements**

540 Work supported by the Italian National Research Council (Consiglio Nazionale Ricerche).

541 We thank Enrico Bonatti for the revision of the English; Marco Ligi for constructive

542 comments that helped us to improve the manuscript; **Marzia Rovere and Maria Filomena**

543 **Loreto for starting the creation of a digital seismic database of the old Sparker data at the**

544 **CNR-ISMAR of Bologna. We are also grateful to the Editor and to the Reviewers for their**

545 **constructive comments that helped improve the manuscript.**

546

547 **References**

- 548 Allouc, J., 1987. Les paléocommunautés profondes sur fond rocheux du Pléistocène
549 méditerranéen. Description et essai d'interprétation paléogéologique. *Géobios* 20
550 (2), 241–263.
- 551 Allouc, J., 1990. Quaternary crusts on slopes of the Mediterranean Sea: A tentative
552 explanation for their genesis. *Mar. Geol.* 94, 205–238.
- 553 Barberi, F., Gasparini, P., Innocenti, F., Villari, L., 1973. Volcanism of the southern
554 Tyrrhenian Sea and its geodynamic implications. *J. Geophys. Res.* 78(23), 5221–5232.
- 555 Barberi, F., Bizouard, H., Capaldi, G., Ferrara, G., Gasparini, P., Innocenti, F., Joron, J.L.,
556 Lambret, B., Treuil, M., Allegre, C., 1978. Age and nature of basalts from the
557 Tyrrhenian Abyssal Plain. From Hsü, K., et al., 1978. Site 373: Tyrrhenian Basin. Initial
558 reports of the Deep Sea Drilling Project, 42(part 1), pp. 151–174, Washington, D.C.,
559 U.S. Government Printing Office.
- 560 Beccaluva, L., Gabbianelli, G., Lucchini, F., Rossi, P.L., Savelli, C., 1985. Petrology and
561 K/Ar ages of volcanics dredged from the Eolian seamounts: implications for
562 geodynamic evolution of the southern Tyrrhenian basin. *Earth Planet. Sci. Lett.* 74(2-
563 3), 187–208.
- 564 Beccaluva, L., Rossi, P.L., Serri, G., 1982. Neogene to Recent volcanism of the southern
565 Tyrrhenian-Sicilian area: Implications for the geodynamic evolution of the Calabrian
566 arc. *Earth Evol. Sci* 3, 222–238.
- 567 Bolli, H.M., Saunders, J.B., 1985. Oligocene to Holocene low latitude planktic foraminifera.
568 In: Bolli, H.M., Saunders, J.B., Perch-Nilsen, K. (Eds.), *Plankton Stratigraphy*.
569 Cambridge University Press, Cambridge, pp. 155–262.
- 570 Bonatti E., Seyler, M., Channell, J., Giraudeau, J., Mascle, G., 1990. Peridotites Drilled
571 From The Tyrrhenian Sea, Odp Leg 1071. In: Kastens, K.A., Mascle, J. et al.,

572 Proceedings of the Ocean Drilling Program, Scientific Results, Vol. 107, College
573 station, Texas.

574 Bortoluzzi, G., Carrara, G., Fabretti, P., Gamberi, F., Marani, M., Penitenti, D., Stanghellini,
575 G., Tonani, M., Zitellini, N., Bonazzi, C., Lippolis, S., Musacchio, M., Daviddi, A.,
576 Diroma, G., Ferrarini, A., Leotta, A., Gilod, D., Nikaronenkov, B., Efimov, V., Erofeev,
577 S., 1999. Swath bathymetry and geophysical survey of the Tyrrhenian sea report on
578 bathymetric, magnetic and gravimetric investigations during cruises TIR96 and TIR99.
579 IGM TECHNICAL REPORT N. 52, Bologna.
580 http://ricerca.ismar.cnr.it/CRUISE_REPORTS/1990-1999/GELENDZHIK_TIR96_99_REP

581 Bortoluzzi, G., Ligi, M., Romagnoli, C., Cocchi, L., Casalbore, D., Sgroi, T., Cuffaro, M.,
582 Caratori Tontini, F., D'Orlando, F., Ferrante, V., Remia, A., and Riminucci, F., 2010,
583 Interactions between volcanism and tectonics in the western Aeolian sector,
584 southern Tyrrhenian Sea. *Geophys. J. Int.* 183, 64-78.

585 Cande, S.C., and Kent, D.V., 1995. Revised Calibration of the Geomagnetic Polarity
586 Timescale for the Late Cretaceous and Cenozoic. *J. Geophys. Res. Solid Earth*,
587 100, 6093-6095.

588 Cann, J.R., 1970. Rb, Sr, Y, Zr and Nb in some ocean floor basaltic rocks. *Earth Planet.*
589 *Sci. Lett.* 10, 7-11.

590 Caratori Tontini, F., Bassett, D., De Ronde, C.E.J., Timm, C., Wysoczanski, R., 2019.
591 Early evolution of a young back-arc basin in the Havre Trough. *Nat. Geosci.*, 12,
592 856-862.

593 Carminati, E., Lustrino, M., Cuffaro, M., Doglioni, C., 2010. Tectonics, magmatism and
594 geodynamics of Italy: What we know and what we imagine. In: M. Beltrando, A.
595 Peccerillo, M. Mattei, S. Conticelli, and C. Doglioni (Eds.), *The Geology of Italy*, J.
596 Virtual Explor., ISSN 1441-8142, Vol. 36.

597 Carminati, E., Wortel, M.J.R., Meijer, P.T., Sabadini, R., 1998. The two-stage opening of
598 the western–central Mediterranean basins: a forward modeling test to a new
599 evolutionary model. *Earth Planet. Sci. Lett* 160(3-4), 667–679

600 Cella, F., Fedi, M., Florio, G., Rapolla, A., 1998. Boundaries of magnetic anomaly sources
601 in the Tyrrhenian region. *Ann. Geophys.* 51(1), 1–23.

602 Coale, K.H., Fitzwater, S.E., Gordon, R.M., Johnson, K.S., Barber, R.T., 1996. Control of
603 community growth and export production by upwelled iron in the equatorial Pacific
604 Ocean. *Nature* 379, 621–624.

605 Cocchi, L., Passaro, S., Caratori Tontini, F., and Ventura, G., 2017, *Volcanism in slab tear*
606 *faults is larger than in island-arcs and back-arcs*, *Nature Communications* 8, 1451.

607 Cocchi, L., Caratori Tontini, F., Muccini, F., Marani, M. P., Bortoluzzi, G., Carmisciano, C.,
608 2009. Chronology of the transition from a spreading ridge to an accretional
609 seamount in the Marsili backarc basin (Tyrrhenian Sea). *Terra Nova* 21, 369 – 374.

610 Colantoni, P., Fabbri, A., Gallignani, P., Sartori, R., Rehault, J.P., 1981. Carta litologica e
611 stratigrafica dei mari italiani. Scale 1:500.000. Litografica Artistica Cartografica,
612 Firenze.

613 Conti, A., Bigi, S., Cuffaro, M., Doglioni, C., Scrocca, D., Muccini, F., Cocchi, L., Ligi, M.,
614 Bortoluzzi, G., 2017. Transfer zones in an oblique back-arc basin setting: Insights from
615 the Latium-Campania segmented margin (Tyrrhenian Sea). *Tectonics* 36(1), 78–107.

616 Conti, M.A., Girasoli, D.E., Frezza, V., Conte, A.M., Martorelli, E., Matteucci, R., Chiocci,
617 F.L., 2013. Repeated events of hardground formation and colonisation by endo-
618 epilithozoans on the sediment-starved Pontine continental slope (Tyrrhenian Sea,
619 Italy). *Mar. Geol.* 336, 184–197.

620 Corda, L., Palmiotto, C., 2015. Rhodalgal–foramol facies in equatorial carbonates: Insights
621 from Miocene tectonic islands of the central Atlantic. *Palaeogeogr. Palaeoclimatol.*
622 *Palaeoecol.* 428, 21–30.

623 Corradino, M., Balasz, A., Faccenna, C., and Pepe, F., 2022. Arc and forearc rifting in the
624 Tyrrhenian subduction system. *Scientific Reports* 12, 4728.

625 Della Vedova, B., Pellis, G., Foucher, J.P. Rehault, J.-P, 1984. Geothermal structure of the
626 Tyrrhenian Sea. *Mar. Geol.* 55, 271–289.

627 Dekov, V.M., Savelli, C., 2004. Hydrothermal activity in the SE Tyrrhenian Sea: an
628 overview of 30 years of research. *Mar. Geol.* 204, 161–185.

629 Doglioni, C., 1991. A proposal for the kinematic modelling of W-dipping subductions-
630 possible applications to the Tyrrhenian-Apennines system. *Terra Nova* 3, 423–434.

631 Doglioni, C., E. Gueguen, P. Harabaglia, Mongelli, F., 1999. On the origin of W-directed
632 subduction zones and applications to the western Mediterranean. *Geol. Soc. Spec.*
633 *Publ.* 156, 541–561.

634 Doglioni, C., Innocenti, F., Morellato, C., Procaccianti, D., Scrocca, D., 2004. On the
635 Tyrrhenian sea opening. *Mem. Descr. Carta Geol. d'It.* 44, 147–164.

636 Emelyanov, E.M., Shimkus, K.M., 1986. Geochemistry and Sedimentology of the
637 Mediterranean sea. *Sedimentology and Petroleum Geology.* Reidel, Dordrecht, 553.

638 Fabbri, A., Gallignani, P., Zitellini, N., 1981. Geologic evolution of the peri-Tyrrhenian
639 sedimentary basins. In: Wezel, F.C, “Sedimentary basins of Mediterranean
640 margins”, 101-26, C.R.N., Italian Project of Oceanography, Tecnoprint, Bologna,
641 1981.

642 Faccenna, C., Mattei, M., Funicello, R., Jolivet, L., 1997. Styles of back-arc extension in
643 the central Mediterranean. *Terra Nova* 9(3), 126–130.

644 Faccenna, C., Becker, T.W., Lucente, F.P., Jolivet, L., Rossetti, F., 2001. History of
645 subduction and back arc extension in the Central Mediterranean. *Geophys. J. Int.*
646 145(3), 809–820.

647 Faggion, O., Pinna, E., Savelli, C., Schreider, A.A., 1999. Geomagnetism and age study of
648 Tyrrhenian Seamounts. *Geophys. J. Int.* 123, 915–930.

649 Farran, M., 2008: IMAGE2SEGY: Una aplicación informática para la conversión de
650 imágenes de perfiles sísmicos a ficheros en formato SEG Y. *Geo- Temas* 10,
651 1215–1218.

652 Finetti, I.R., Del Ben, A., 1986. Geophysical study of the Tyrrhenian opening. *Boll. di*
653 *Geofis. Teor. ed Appl.* 28, 75–155.

654 Finetti, I. R., 2005. CROP project: deep seismic exploration of the central Mediterranean
655 and Italy. (Eds. By Finetti, I. R.), Elsevier, Vol. 1.

656 Florio, G., Passaro, S., de Alteriis, G., Cella, F., 2022. Magnetic Anomalies of the
657 Tyrrhenian Sea Revisited: A Processing Workflow for Enhancing the Resolution of
658 Aeromagnetic Data. *Geosciences* 2022, 12, 377.

659 Fretzdorff, S., Livermore, R. A., Devey, C. W., Leat, P. T., Stoffers, P., 2002. Petrogenesis
660 of Back-Arc East Scotia Ridge, South Atlantic Ocean. *Journal of Petrology*, 43, 1435 –
661 1467.

662 Fujiwara, T., Yamazaki, T., Joshima M., 2001. Bathymetry and magnetic anomalies in the
663 Havre Trough and southern Lau Basin: from rifting to spreading in back-arc basins.
664 *Earth Planet. Sci. Rev.*, 185, 253-264.

665 Hofmann, A.W., 1988. Chemical Differentiation of the Earth: The Relationship between
666 Mantle, Continental Crust, Oceanic Crust. *Earth Planet. Sci. Lett.* 90, 297-314.

667 Hsü, K., Montadert, L., Bernoulli, D., Bizon, G., Cita, M.B., Erickson, A., Fabrcius, F.,
668 Garrison, R.E., Kidd, R.B., Mèlerés, F., Müller, C., Wright, C.R., 1978. Site 373:

669 Tyrrhenian Basin. Initial reports of the Deep Sea Drilling Project 42(part 1), pp. 151-
670 174, Washington, D.C., U.S. Government Printing Office.

671 Hynes, A., Mott, J., 1985. On the causes of back-arc spreading. *Geology* 13, 387–389.

672 Iaccarino, S., Premoli Silva, I., Biolzi, M., Foresi, L.M., Lirer, F., Turco, E., Petrizzo, M.R.,
673 2007. Practical manual of Neogene Planktonic Foraminifera. International School on
674 Planktonic Foraminifera, 6th course, Perugia 19-23 February 2007, University of
675 Perugia, 1–181.

676 Kastens, K., Mascle, J., Auroux, C., Bonatti, E., Broglia, C., Channell, J., Curzi, P., Emeis,
677 K.-C., Glaçon, G., Hasegawa, S., Hieke, W., Mascle, G., Mccoy, F., Mckenzie, J.,
678 Mendelson, J., Müller, C., Réhault, J.P., Robertson, A., Sartori, R., Sprovieri, R.,
679 Torii, M., 1988. ODP Leg 107 in the Tyrrhenian Sea: Insights into passive margin
680 and back-arc basin evolution. *Geol. Soc. Am. Bull.* 100(7), 1140–1156.

681 Kastens, K. A., Mascle, J., 1990. The geological evolution of the Tyrrhenian Sea: An
682 introduction to the scientific results of ODP Leg 107. In: *Proceedings of the Ocean*
683 *Drilling Program, Scientific Results, Vol. 107*, (Ed. by K. A. Kastens & J. Mascle, et
684 al.), pp. 3–26. Ocean Drilling Program, College station, Texas.

685 Larson, R.L., Erba, E., 1999. Onset of the mid-Cretaceous greenhouse in the Barremian–
686 Aptian: igneous events and the biological, sedimentary, and geochemical
687 responses. *Paleoceanography* 14, 663–678.

688 Leat, P.T., Larter, R.D., 2003. Intra-oceanic subduction systems: introduction. *Geological*
689 *Society, London, Special Publications*, 219, 1-17.

690 Livermore, R., Cunningham, A., Vanneste, L., Larter, R., 1997. Subduction influence on
691 magma supply at the East Scotia Ridge. *Earth Planet. Sci. Lett.* 1997, 150, 261-
692 275.

693 Loreto, M.F., Zitellini, N., Ranero, C., Palmiotto, C., Manel, P., 2020. Extensional tectonics
694 during the Tyrrhenian back-arc basin formation and a new morpho-tectonic map.
695 Basin Research 33, 138–158.

696 Lupton, J., De Ronde, C., Sprovieri, M., Baker, E.T., Bruno, P.P., Italiano, F., Walker, S.,
697 Faure, K., Leybourne, M., Britten, K., Greene, R., 2011. Active hydrothermal
698 discharge on the submarine Aeolian Arc. J. Geophys. Res. 116, 1–22.

699 Macdonald, K.C., Fox, P.J., Perram, L.J., Eisen, M.F., Haymon, R.M., Miller, S.P.,
700 Carbotte, S.M., Cormier, M.H., and Shor, A.N., 1988. A new view of the mid-ocean
701 ridge from the behaviour of ridge-axis discontinuities. Nature 335, 217–225.

702 Magni, V., J., Naliboff, M., Prada, C., Gaina, 2021. Ridge Jumps and Mantle Exhumation
703 in Back-Arc Basins. Geosciences 11, 475.

704 Malinverno, A., Ryan, W.B., 1986. Extension in the Tyrrhenian Sea and shortening in the
705 Apennines as result of arc migration driven by sinking of the lithosphere. Tectonics
706 5(2), 227–245.

707 Marani, M., Bonatti, E., Gamberi, F., 2004. From seafloor to deep mantle: architecture of
708 the Tyrrhenian back-arc basin. Mem. Descr. Carta Geol. D'It. 64, 1–194.

709 Marani, M., Gamberi, F., 2004. Structural framework of the Tyrrhenian Sea unveiled by
710 seafloor morphology. Mem. Descr. Carta Geol. d'It. 44, 97–108.

711 Martinez, F., Taylor, B., 2002. Mantle wedge control on back-arc crustal accretion. Nature
712 416, 417–420.

713 McKenzie, F.T., Bernoulli, D., 1982. Geochemical variations in Quaternary hardgrounds
714 from the Hellenic trench region and possible relationship to their tectonic setting.
715 Tectonophysics 86, 149-157.

716 Mackenzie, F.T., Andersson, A.J., 2013. The marine carbon system and ocean
717 acidification during Phanerozoic time. Geochem. Perspect. 2(1), 1–227.

718 Morse, J.W. 1986. The surface chemistry of calcium carbonate minerals in natural waters:
719 an overview. *Mar. Chem.* 20., 91–112.

720 Morse, J.W, McKenzie, FT., 1990. *Geochemistry of sedimentary carbonates.*
721 *Developments in Sedimentology* 48, Elsevier, 696.

722 Mutti M., Bernoulli D., 2003. Early marine lithification and hardground development on a
723 Miocene ramp (Maiella, Italy) key surfaces to track changes in trophic resources in
724 nontropical carbonate settings. *J. Sediment. Res.* 73, 296–308.

725 Pagli, C., Sang-Ho, Y., Ebinger, C., Keir, D., Wang, H., 2019. Strike-slip tectonics during
726 rift linkage. *Geology* 47, 31–34.

727 **Palmiotto, C., Ficini, E., Loreto, M.F., Muccini, F., Cuffaro, M., 2022. Back-Arc Spreading**
728 **Centers and Superfast Subduction: The Case of the Northern Lau Basin (SW**
729 **Pacific Ocean). *Geosciences* 12, 50.**

730 Palmiotto, C., Loreto, M.F., 2019. Regional scale morphological pattern of the Tyrrhenian
731 Sea: New insights from EMODnet bathymetry. *Geomorphology* 332, 88–99.

732 Parson, L.M., Pearce, J.A., Murton, B.J., Hodkinson, R.A., and the RRS Charles Darwin
733 Scientific Party, 1990. Role of ridge jumps and ridge propagation in the tectonic
734 evolution of the Lau back-arc basin, southwest Pacific. *Geology* 18, 470–473.

735 Parson, L.M., Wright, I.C., 1996. The Lau-Havre-Taupo back-arc basin: A southward-
736 propagating, multi-stage evolution from rifting to spreading. *Tectonophysics* 263, 1–
737 22.

738 **Pearce, J.A., 2014. Immobile Element Fingerprinting of Ophiolites. *Elements* 10, 101-108.**

739 Pearce, J., Cann, J., 1973. Tectonic Setting of Basic Volcanic Rocks determined using
740 Trace Element Analyses. *Earth Planet. Sci. Lett.* 19, 290–300.

741 Peccerillo, A., 2005. *Plio-quadernary volcanism in Italy*, vol. 365. Springer Verlag Berlin
742 Heidelberg.

743 Pensa, A., Pinton, A., Vita, L., Bonamico, A., De Benedetti, A.A., Giordano, G., 2019.
744 ATLAS of Italian Submarine Volcanic Structures. Mem. Descr. Carta Geol. d'It. 104,
745 77–183.

746 Prada, M., Sallarès, V., Ranero, C. R., Vendrell, M. G., Grevemeyer, I., Zitellini, N., De
747 Franco, R., 2014. Seismic structure of the Central Tyrrhenian basin: Geophysical
748 constraints on the nature of the main crustal domains. *J. Geophys. Res. Solid Earth*,
749 119(1), 52–70.

750 Prada, M., Ranero, C. R., Sallarès, V., Zitellini, N., & Grevemeyer, I., 2016. Mantle
751 exhumation and sequence of magmatic events in the Magnaghi-Vavilov Basin (Central
752 Tyrrhenian, Italy): New constraints from geological and geophysical observations.
753 *Tectonophysics* 689, 133–142.

754 Prada, M., Sallares, V., Ranero, C. R., Vendrell, M. G., Grevemeyer, I., Zitellini, N., De
755 Franco, R., 2018b. Spatial variations of magmatic crustal accretion during the opening
756 of the Tyrrhenian back-arc from wide-angle seismic velocity models and seismic
757 reflection images. *Basin Research* 30, 124–141.

758 Ranero, C.R., Sallarés, V., Zitellini, N., Grevemeyer, I., Guzman, M., Prada, M., Moeller,
759 S., De Franco, R., & The Medoc Cruise Party, 2012. The tectonic structure of the
760 Tyrrhenian Basin, a complex interaction among faulting and magmatism. *Rend. Online*
761 *Soc. Geol. It.* 21, 251–252.

762 Recq, M., Rehault J.P., Steinmetz L., Fabbri A., 1984. Amincissement de la crouete et
763 accretion au centre du bassin Tyrrhenien d'après la sismique refraction. *Mar. Geol.* 55,
764 411–428.

765 Rehault, J.P., Moussat, E., Fabbri, A., 1987. Structural evolution of the Tyrrhenian back-
766 arc basin. *Mar. Geol.* 74 (1-2), 123–150.

767 Remia A., Montagna P., Taviani M., 2004. Submarine diagenetic products on the
768 sediment-starved Gorgona slope, Tuscan Archipelago (Tyrrhenian Sea). *Chem.*
769 *Ecol.* 20 (1), 131–153.

770 Robin, C., Colantoni, P., Gennesseaux, M., Reehault, J.P., 1987. Vavilov seamount: a mild
771 alkaline Quaternary volcano in the Tyrrhenian basin. *Mar. Geol.* 78, 125–136.

772 Rosenbaum, G., Gasparon, M., Lucente, F.P., Peccerillo, A., Miller, M.S., 2008.
773 Kinematics of slab tear faults during subduction segmentation and implications for
774 Italian magmatism. *Tectonics* 27(2).

775 Rovere, M., Wurtz, M., 2015. Atlas of the Mediterranean seamounts and seamount-like
776 structures. IUCN, Gland, Switzerland and Málaga, Spain.

777 Sartori, R., 1986. Notes on the geology of the acoustic basement in the Tyrrhenian Sea.
778 *Mem. Soc. Geol. It.* 36, 99–108.

779 Sartori, R., 2003. The Tyrrhenian back-arc basin and subduction of the Ionian lithosphere.
780 *Episodes* 26(3), 217–221.

781 Savelli, C., 1988. Late Oligocene to Recent episodes of magmatism in and around the
782 Tyrrhenian Sea: implications for the processes of opening in a young inter-arc basin of
783 intra-orogenic (Mediterranean) type. *Tectonophysics* 146, 163–181.

784 Savelli, C., Ligi, M., 2017. An updated reconstruction of basaltic crust emplacement in
785 Tyrrhenian sea, Italy. *Scientific Reports* 7(1), 1–12.

786 Schellart, W. P., Freeman, J., Stegman, D. R., Moresi, L., May, D., 2007. Evolution and
787 diversity of subduction zones controlled by slab width. *Nature Letters*, 446, 308–311.

788 Schliffke, N., Van Hunen, J., Allen, M.B., Magni, V., Gueydan, F., 2022. Episodic back-arc
789 spreading centre jumps controlled by transform fault to overriding plate strength ratio.
790 *Nature Communications*, 13, 582.

791 Sdrolias, M., Muller, R.D., 2006. Controls on back-arc basin formation. *Geochem.*
792 *Geophys. Geosystems* 7 (4), 1–40.

793 Selli, R., Lucchini, F., Rossi, P.L., Savelli, C., Del Monte, M., 1977. Dati geologici,
794 petrochimici e radiometrici sui vulcani centro-tirrenici. *Giorn. Geol.* 42, 221–246.

795 Serri, G., Innocenti, F., Manetti, P., 2001. Magmatism from Mesozoic to Present:
796 Petrogenesis, time-space distribution and geodynamic implications. In: Vai, G.B.,
797 Martini, P.I., eds., *Anatomy of a Mountain: the Appenines and the Adjacent*
798 *Mediterranean Basins*, Dordrecht, the Netherland, Kluwer Academic Publishers,
799 pp.77–104.

800 Scrocca, D., Doglioni, C., Innocenti, F., Manetti, P., D'Offizi, S., 2003. CROP Atlas:
801 seismic reflection profiles of the Italian crust. *Mem. Descrit. Carta Geolo. d'It.* 62, 1–
802 193.

803 Trincardi, F., Zitellini, N., 1987. The rifting of the Tyrrhenian Basin. *Geo-Mar. Lett.* 7(1), 1–
804 6.

805 Trua, T., Serri, G., Marani, M., Renzulli, A., Gamberi, F., 2002. Volcanological and
806 petrological evolution of Marsili Seamount (southern Tyrrhenian Sea). *J. Volcanol.*
807 *Geotherm. Res.* 114 (3-4), 441–464.

808 Trua, T., Serri, G., Rossi, P.L., 2004. Coexistence of IAB-type and OIB-type magmas in
809 the southern Tyrrhenian back-arc basin: evidence from recent seafloor sampling and
810 geodynamic implications. *Mem. Descrit. Carta Geolo. d'It.* 44, 83–96.

811 Trua, T., Marani, M., Gamberi, F., 2018. Magma Plumbing System at a Young Back-Arc
812 Spreading Center: The Marsili Volcano, Southern Tyrrhenian Sea. *Geochem.*
813 *Geophys. Geosystems*, 19.

814 Uyeda, S., Kanamori, H., 1979. Back-arc opening and the mode of subduction. *J. Geophys.*
815 *Res.*, 84, 1049–1061.

- 816 Van Van Dijk, J.P., Bello, M., Brancaleoni, G.P., Toscano, C., 2000. A regional structural
817 model for the northern sector of the Calabrian Arc (southern Italy). *Tectonophysics* 324
818 (4), 267–320.
- 819 Ventura, G., Milano, G., Passaro, S., Sprovieri, M., 2013. The Marsili Ridge (Southern
820 Tyrrhenian Sea, Italy): An island-arc volcanic complex emplaced on a 'relict' back-arc
821 basin. *Earth Sci. Rev.*, 116, 85-94.
- 822 Weins, D. A., Kelley, K.A., Plank, T., 2006. Mantle temperature variations beneath back-
823 arc spreading centers inferred from seismology, petrology, and bathymetry. *Earth*
824 *Planet. Science Lett.*, 248, 30-42.
- 825 Wessel, P., Smith, W.H.F., 1998. New improved version of the Generic Mapping Tools
826 released. *EOS, Transaction of American Geophysical Union* 79, 579.
- 827 Wezel, F.C., 1982. The Tyrrhenian Sea: a Rifted Krikogenic-Swell Basin. *Mem. Soc. Geol.*
828 *It.* 24, 531–568.
- 829 Wilkinson, M.D., Dumontier, M., Aalbersberg, I.J., Appleton, G., 2016. The FAIR
830 Guiding Principles for scientific data management and stewardship. *Scientific*
831 *Data* 3, 160018.
- 832 Zankl, H., 1969. Structural and Textural evidence of early lithification in fine grained
833 carbonate rocks. *Sedimentology* 12, 241–256.
- 834 Zitellini, N., Trincardi, F., Marani, M., Fabbri, A., 1986. Neogenic tectonic of the Northern
835 Tyrrhenian Sea. *Giornale di Geologia* 48, 25–40.

836 **Captions of the Figures**

837 **Figure 1.** Geographic setting of the Mediterranean Sea (white star). A) Base colored
838 bathymetry map of the Tyrrhenian Back-Arc Basin (BAB). Black square is the area
839 shown in Fig. 2; black lines are isobaths (interval of 1000 m); the Tyrrhenian
840 Abyssal Plain (TAP), deeper than 3000 m, has been evidenced with the white area;
841 yellow, green and pink lines are the location of sparker lines acquired in the 1971,
842 1973 and 1975, respectively. **Thicked lines indicate parts of the seismic profiles**
843 **interpreted in this paper.** B) Base shaded bathymetry map of the Tyrrhenian BAB.
844 Black square is the area shown in Fig. 6; black line is the coast line; red lines are
845 the location of the magnetic lines acquired in the 1996 and 1999. Bathymetry has
846 been downloaded EMODnet portal ([http://portal.emodnet-bathymetry.eu/gebco-](http://portal.emodnet-bathymetry.eu/gebco-bathymetry-basemap)
847 [bathymetry-basemap](http://portal.emodnet-bathymetry.eu/gebco-bathymetry-basemap)) and gridded using GMT open software; bathymetric data
848 have been used to create 2D digital elevation model image using Global Mapper
849 Software.

850 **Figure 2.** Maps of the bathymetry and of the reduced to the pole magnetic anomalies of
851 the Southern Vavilov region. A) Shaded relief image of the bathymetry. Sun angle:
852 70°; Azimuth: 330°. Vertical Exaggeration: 10. Contour black lines are isobaths
853 every 100 m; green and pink lines indicate the location of the sparker lines shown in
854 Fig. 3; orange, yellow and green dots are the points of the dredges (75-30, 75-35
855 and 75-36, respectively). B) Slope shader relief map of the bathymetry (isobath
856 interval of 500 m). **Red areas show the six peaks along the summit of the Augusto**
857 **Seamount.** Sun angle: 70°; Azimuth: 330°. Vertical Exaggeration: 10. C) Shaded
858 relief image of the distribution of the reduced to the pole magnetic anomalies where
859 contour black lines indicate the lines with the same anomaly value (interval of 50
860 nT). D) Shaded relief image of the distribution of the reduced to the pole magnetic

861 anomalies where contour black lines are isobaths (interval of 100 m). 1. D'Ancona I
862 Seamount; 2. D'Ancona II Seamount; 3. Plinia Seamount; 4. Vavilov Seamount; 5.
863 Tibullo Seamount; 6. Aurelia Seamount; 7. Virgilio Seamount; 8. Augusto
864 Seamount; 9. Emilia Seamount.

865 **Figure 3.** Sparker profiles with their relative interpretation, maps of magnetic anomaly and
866 magnetic profiles extracted along the profiles. (A-A') Sparker Line PM3E; (B-B')
867 Sparker Line PM4; (C-C') Sparker Line PM11; (D-D') Sparker Line PM10E.

868 **Figure 4.** (a) Sample from dredge 75-30-3 (Aurelia Seamount). Macroscopic view of the
869 direct contact between the volcanic substrate and the overlying carbonate crust.
870 Neptunian dykes filled by carbonate mud are also visible; SEM photomicrograph of
871 the sample: the related EDAS spectrum B evidenced a predominantly carbonate
872 composition of the crust with a very subordinate clay-sized silicate fraction; the
873 black film marking the contact with the volcanic substrate is represented by Mn-Fe
874 oxides (spectrum A). (b) Black-coated corals (*Desmophyllum*) from dredge 75-35-5
875 (western Augusto Seamount), scale bar 2cm. (c) Thin section photomicrographs
876 from dredge 75-36-7A sample (eastern Augusto Seamount) showing isolated
877 volcanic minerals scattered within the planktonic-rich carbonate mud; quartz grains
878 are also evidenced by the SEM photomicrograph of the sample and the related
879 EDAS spectrum. (d) Thin section photomicrographs of the carbonate crusts: 1-2)
880 geopetal structures in pteropod-foraminifer wackestone, pteropod sections are
881 partially filled by foraminifer micrite and microspar at the top; 3) planktonic
882 foraminifera: *Pulleniatina obliquiloculata*, globigerinids, *Globorotalia truncatulinoides*
883 (dredge 75-30-3 sample), scale bar 500 μm ; 4) planktonic foraminifera: *Pulleniatina*
884 *obliquiloculata*, globigerinids (dredge 75-30-3 sample), scale bar 500 μm ; 5)

885 planktonic foraminifera: *Pulleniatina obliquiloculata*, globigerinids, *Globorotalia*
886 *inflata*, *Globigerinoides* spp. (dredge 75-36-7A sample), scale bar 1mm; 6) cloud of
887 planktonic foraminifera, pteropods shell, bioturbation evidences (dredge 75-36-7A
888 sample), scale bar 1mm. (e) Sample from dredge 75-36-7A. Thin section
889 photomicrograph showing a boring structure filled by planktonic-foraminifer mud;
890 SEM photomicrograph of the sample and the related EDAS spectra evidencing the
891 same composition of the carbonate mud outside and inside the cavity (A and B
892 spectra) and the Mn-Fe oxides-rich film coating the boring.

893 **Figure 5.** (a) 1-2) Low-magnification overview of the chosen samples. (3-4)
894 Photomicrographs (plane polarized light) showing altered phenocryst with euhedral
895 to subhedral shape. (5-6) Backscattered electron images with phase labelling based
896 on EDS microanalysis. Early igneous phenocrysts are now replaced by secondary
897 phases, mostly chlorite and dolomite. (b) Ti-Zr discrimination diagram (Cann, 1970;
898 Pearce and Cann, 1973) where the data of this study are compared to available
899 data from the Marsili Volcano (Pearce, 2014).

900 **Figure 6.** A) Shaded relief bathymetric image of the Southern Tyrrhenian Sea. Bathymetry
901 has been downloaded EMODnet portal ([http://portal.emodnet-bathymetry.eu/gebco-](http://portal.emodnet-bathymetry.eu/gebco-bathymetry-basemap)
902 [bathymetry-basemap](http://portal.emodnet-bathymetry.eu/gebco-bathymetry-basemap)) and gridded using GMT open software; bathymetric data
903 have been used to create 2D digital elevation model image using Global Mapper
904 Software. Sun angle: 70°; Azimuth: 330°. Vertical Exaggeration: 10. B) Map of the
905 distribution of the reduced to the pole magnetic anomalies in the Southern
906 Tyrrhenian Sea. Black contour lines are isobaths every 500 m. C) Sparker Profile
907 PM12 with interpretation.

908 **Figure 7.** Cartoon showing the formation and evolution of the volcanic arc related to the
909 Ionian subduction during the last 3 Ma. Geodynamic reconstruction is based on

910 the model published by Carminati et al. (2010). 3 Ma) Active volcanism of the
911 Magnaghi and Vavilov volcanoes; the active arc is formed by the Aurelia, the Virgilio
912 and the Western part of the Augusto Seamount. 2 Ma) Active volcanism of the
913 Magnaghi and Vavilov volcanoes; the active arc is formed by the Augusto
914 Seamount. 1 Ma) Active volcanism of the Marsili volcano; the active arc is formed
915 by the Sisifo and Tiro Seamounts. 0 Ma) Active volcanism of the Vavilov and Marsili
916 volcanoes; the active arc is formed by the Aeolian Islands and Seamounts.

917 **Supplementary Figure 1.** Seismic Sparker Profile PM3E not interpreted.

918 **Supplementary Figure 2.** Seismic Sparker Profile PM4 not interpreted.

919 **Supplementary Figure 3.** Seismic Sparker Profile PM11 not interpreted.

920 **Supplementary Figure 4.** Seismic Sparker Profile PM10E not interpreted.

921 **Supplementary Figure 5.** Seismic Sparker Profile PM12 not interpreted.

1 **New insights on the fossil arc of the Tyrrhenian Back-Arc Basin**
2 **(Mediterranean Sea)**

3
4
5 Camilla Palmiotto^{1*}, Roberto Braga², Laura Corda³, Letizia Di Bella³, Valentina Ferrante¹,
6 Maria Filomena Loreto¹ and Filippo Muccini^{4,5}

7 ¹ *Consiglio Nazionale delle Ricerche, Istituto di Scienze Marine, via Gobetti 101, 40129, Bologna, Italy.*

8 ² *Dipartimento di Scienze Biologiche, Geologiche e Ambientali, Università di Bologna, Piazza di Porta San*
9 *Donato 1, 40126, Bologna, Italy.*

10 ³ *Dipartimento di Scienze della Terra, Università “La Sapienza”, Piazzale Aldo Moro 5, 00185, Roma, Italy.*

11 ⁴ *Istituto Nazionale di Geofisica e Vulcanologia, via di Vigna Murata 605, 00143, Roma, Italy.*

12 ⁵ *Consiglio Nazionale delle Ricerche, Istituto di Geologia Ambientale e Geoingegneria, 00185, Roma, Italy.*

13

14

15

16 *Corresponding author. Tel: +39 051 6398900

17 E-mail address: camilla.palmiotto@bo.ismar.cnr.it

18

19 **Abstract**

20 Geology, geophysics and geodynamics of the Tyrrhenian back-arc basin (BAB; central
21 Mediterranean Sea) have been studied extensively during the last 50 years. However,
22 some topics are still open: for example, the possible migration of the volcanic arc during
23 the Ionian subduction of the past few Ma. We improved our knowledge of the geodynamics
24 of the Tyrrhenian BAB in the area South of the Vavilov Volcano by analyzing multibeam
25 bathymetry and unpublished single-channel reflection seismic and magnetic data.
26 Furthermore, we studied the petrology of igneous rocks as well as facies and microfaunas
27 of carbonates dredged from the Aurelia and the Augusto seamounts. The Aurelia
28 basement is made of basalts with calc-alkaline affinity. Carbonates from the Aurelia and
29 the Augusto seamounts consist of cemented Mg-calcite biomicrite crusts rich in planktonic
30 foraminifera not older than Early Pleistocene. Based on our results, we interpret the
31 Augusto and Aurelia seamounts as part of the active volcanic arc seaward of the
32 Tyrrhenian BAB in Late Pliocene–Early Pleistocene.

33 **1. Introduction**

34 Back-arc basins (BABs) and volcanic arcs are two main features characterizing the
35 upper plates along convergent plate boundaries (Uyeda, 1979; Leat & Larter, 2003). The
36 relative kinematics, composition and thermal state of the upper and lower plates, together
37 with the age of the subducting lithosphere and the morpho-tectonic inheritance of the
38 upper plate, rule the extensional tectonics along the BABs and their progressive evolution
39 from a younger rifting stage to a mature spreading stage (e.g., Parson and Wright, 1996;
40 Fujiwara et al., 2001; Martinez and Taylor, 2002; Sdrolias and Muller, 2006; Weins et al.,
41 2006; Schellart et al., 2007). BABs in a rifting stage do not show a BAB magmatism, as for
42 example the Havre Trough in the Southern Pacific, characterized by an oblique southward
43 propagating extension and by the absence of a clear spreading ridge (Caratori Tontini et
44 al., 2019); mature BABs show a back-arc spreading center (BASC), i.e. the Mariana
45 Spreading Center in the Pacific (Hynes and Mott, 1985), or the East Scotia Ridge in the
46 Southern Atlantic (Livermore et al., 1997; Fretzdorff et al., 2002).

47 Here we focus on the Tyrrhenian Sea (located in the central Mediterranean Sea,
48 between the Italian Peninsula and the Sardinia; Fig. 1), a peculiar case of BAB associated
49 to compressional tectonics where the lower oceanic plate is subducting under continental
50 lithosphere. The Tyrrhenian is a BAB formed by extensional tectonics due to the
51 progressive eastward/south-eastward retreat of the Ionian subduction (e.g., Malinverno and
52 Ryan, 1986; Doglioni et al., 1991; 1999; 2004; Faccenna et al., 1997; 2001; Carminati et
53 al., 1998; Sartori, 2003; Rosembaum et al., 2008; Conti et al., 2017; Loreto et al., 2020).
54 First studies on the regional geology and geodynamics of the Tyrrhenian were published
55 during 1970s and 1980s (e.g., Barberi, 1973; 1978; Selli et al., 1977; Hsü et al., 1978;
56 Wezel, 1982; Della Vedova et al., 1984; Sartori, 1986; Rehault et al., 1987; Trincardi and

57 Zitellini, 1987; Savelli, 1988). An important contribution on the knowledge of the Tyrrhenian
58 basin occurred with the Deep Sea Drilling Project (DSDP) Leg 42, the Ocean Drilling
59 Program (ODP) Leg 107 (Kastens et al., 1988; Kastens and Mascle, 1990). A collection of
60 multidisciplinary papers on the geology and geodynamics of the Tyrrhenian Sea was
61 shown by Marani et al. (2004), after the deep seismic exploration of the central
62 Mediterranean and Italy (CROsta Profonda project; Scrocca et al., 2003; Finetti, 2005)
63 during the 1990s. Recently, seismic refraction data have been acquired during the
64 MEDOC Cruises in the 2010 (Ranero et al., 2012) in order to display the velocity structure
65 of the Tyrrhenian crust and uppermost mantle together with the Moho reflector geometry
66 (Prada et al., 2014; 2016; 2018).

67 The Tyrrhenian abyssal plain (TAP), marked by the isobaths of the 3000 m in
68 Fig.1a, is floored by basaltic and ultramafic rocks covered by Pliocene-Quaternary
69 sediments (Hsü et al., 1978; Kasten and Mascle, 1990). The TAP shows three huge
70 fissural volcanoes (the Magnaghi, the Vavilov and the Marsili) located in the center of three
71 different basins (Fig. 1a). The Marsili and the Aeolian Islands represent respectively the
72 current magmatism in the back-arc basin and in the arc front (Fig.1; Kastens et al., 1988;
73 Kastens and Mascle, 1990; Marani and Trua, 2002; Trua et al., 2002; 2018; Rosenbaum
74 and Lister, 2004; Marani et al., 2004; Nicolosi et al., 2006; Cocchi et al., 2009; Ventura et
75 al., 2013). The Magnaghi and the Vavilov can be considered segments of extinct back-arc
76 spreading centres evolved naturally in a basin characterized by frequent spreading jumps
77 (Magni et al., 2021; Schiffke et al., 2022). In this paper we focus on the region East of the
78 Magnaghi and South of the Vavilov volcanoes (Figure 1a). This area shows an alternation
79 of deep basins and high seamounts from which we have little understanding of their age
80 and composition, given the lack of data. Some information can be extracted from studies

81 of regional geology (Marani et al., 2004; Marani and Gamberi, 2004; Rovere and Wurtz,
82 2015; Palmiotto and Loreto, 2019; Pensa et al., 2019), the lithological and stratigraphic
83 map of the Italian Seas (Colantoni et al., 1981), multichannel seismic reflection profiles
84 (Finetti and Del Ben, 1986; Corradino et al., 2022) and the distribution of the regional
85 magnetic data (Cella et al., 1998; Florio et al., 2022). In particular, we study two different
86 seamounts (Aurelia and Augusto) in order to investigate their origin and to improve the
87 geology and geodynamics of the central Tyrrhenian BAB.

88 We carried out a geophysical study based on: 1) multibeam bathymetry data
89 downloaded from the European Marine Observation and Data Network (EMODnet;
90 <http://doi.org/10.12770/c7b53704-999d-4721-b1a3-4ec60c87238>); 2) single-channel
91 reflection seismics collected by the Institute of Marine Sciences (ISMAR) of the National
92 Research Council (CNR) of Bologna in the 1970s (Fabbri et al., 1981; see Fig.1a and
93 methods); 3) magnetic data collected by the Institute of Marine Sciences (ISMAR) of the
94 National Research Council (CNR) of Bologna in the 1990s (Bortoluzzi et al., 1999; see
95 Fig.1b and methods). We created regional bathymetry maps and an updated map of the
96 reduced to pole magnetic anomalies of the central / Southern Tyrrhenian using magnetic
97 data. Furthermore, we analyzed for the first time the petrology of igneous rocks and re-
98 analysed facies and microfauna of carbonates dredged at two seamounts South of the
99 Vavilov Volcano. Results reveal new insights on the geodynamics of the Tyrrhenian BAB
100 during the Late Pliocene-Early Pleistocene.

101 **2. Material and Methods**

102 2.1.1 Bathymetry

103 Middle resolution bathymetric data (200 m-cell grid size) used in this paper have
104 been downloaded from the European Marine Observation and Data Network (EMODnet;

105 <http://doi.org/10.12770/c7b53704-999d-4721-b1a3-4ec60c87238>). Spatial analysis and
106 mapping of ASCII data used the open source software GMT (Wessel and Smith, 1998)
107 with the nearest neighbour algorithm. Datum and projection used are, respectively,
108 WGS84 and Mercator. The Global Mapper Software has been used to create 2D digital
109 elevation images.

110 2.1.2 Magnetic data

111 Magnetic data were collected by the CNR-ISMAR during the TIR-96 cruise onboard
112 the R/V Gelendzhik in the 1996 and the TIR-99 cruise onboard the R/V A.N. Strakhov in
113 the 1999 (Bortoluzzi et al., 1999). In total, more than 25000 magnetic measurements along
114 1400 km of lines NNE-SSW oriented were used to create a new regional map (Fig.1b).
115 Raw data were corrected for spikes and diurnal variations using the reference station of
116 L'Aquila (Central Italy). Magnetic anomalies were calculated by subtracting the IGRF
117 (International Geomagnetic Reference field) model and then reducing the data to the North
118 Pole by phase shifting them using the regional inclination and declination values of the
119 IGRF.

120 2.1.3 Seismics

121 Seismic profiles used in this paper are part of an old large (about 46000 km)
122 dataset, available as profiles printed on paper, collected during several cruises carried out
123 by CNR-ISMAR of Bologna between the 1970s and the 1980s (Fabbri et al., 1981).
124 Seismic data have been shot using a Sparker 30 KJ and recorded with a trace length of 8
125 s (TWT). A new digital seismic database is under construction at the CNR-ISMAR of
126 Bologna in order to preserve these data, inspired by FAIR (findable, accessible,
127 interoperable and reusable) principles (Wilkinson et al, 2016). Seismic lines were
128 scanned from paper to high resolution raster image (TIFF); they will then be converted into
129 georeferenced SEG-Y format using the free Matlab program IMAGE2SEGY (Farran, 2008)

130 distributed by the Department of Marine Geosciences of The Spanish National Research
131 Council (<http://www.icm.csic.es/gma/en/content/image2segy/>).

132 Here we present parts of five profiles acquired during oceanographic cruises T71,
133 T73 and T75 (yellow, green and pink lines respectively and shown in Fig. 1a) onboard of
134 the N/O Bannock carried out by the “Bacini Sedimentari” Group on behalf of the “Progetto
135 Finalizzato Oceanografia e Fondi Marini” of the Italian CNR in the Tyrrhenian Basin
136 (Fabbri et al., 1981).

137 2.2 Samples

138 Analyzed rocks were dredged by the CNR-ISMAR of Bologna during cruise T75 in
139 the Tyrrhenian Sea. Samples labels refer to cruise, dredge station and rock samples
140 numbers; for example, 75-30-3 refers to rock sample number 3, dredge station 30, carried
141 out during the oceanographic expedition T75.

142 Samples dredged from site 75-30 (orange dot in Fig.2a) are carbonates and
143 volcanic rocks: volcanic samples have been re-analyzed; carbonates have been analyzed
144 for the first time. Samples dredged from sites 75-35 (yellow dot in Fig.2a) and 75-36
145 (green dot in Fig.2a), composed only of limestones, have been re-analysed in order to
146 determine the micropaleontological identifications and carbonate facies. Results of past
147 samples analysis are shown in the lithological and stratigraphic map of the Italian Seas
148 (Colantoni et al., 1981).

149 Rock samples underwent macroscopic and thin section examination under the
150 petrographic and binocular microscopes. Bulk-rock abundances of major and minor
151 elements were determined by X-ray fluorescence (XRF). Micropaleontological
152 identifications were based on a bio and chronostratigraphical scheme for the
153 Mediterranean of Iaccarino et al. (2007). Digital photographs and Energy Dispersive
154 Spectroscopy (EDS) for elemental composition were obtained with a scanning electron

155 microscope (FEI QUANTA 400) at the SEM Laboratory of Earth Sciences Department –
156 Sapienza University of Rome (Italy). For the identification of crystalline material X-ray
157 diffraction on sample powder were also carried out by a Phillips PANalytical X'Pert PRO
158 diffractometer using CuK α radiation ($n=1.5418 \text{ \AA}$), operating at 40kV and 40mA at a step
159 size of 0.0260° at the Department of Earth Science, Sapienza University of Rome (Italy).
160 The program used for qualitative analyses is WinPLOTR Programme (CDIFX UMR6226
161 Rennes/ILL Grenoble).

162 **3. Results**

163 3.1 Geophysics

164 Bathymetry and the reduced to the pole magnetic anomalies of the Southern
165 Vavilov region maps are shown in Fig. 2. Part of sparker profiles here interpreted, with
166 their values of magnetic anomalies associated, are shown in Fig. 3. Based on Loreto et al.
167 (2020), three main seismic units have been identified: 1) a well-stratified unit (green color
168 in Figs. 3 and 6), interpreted as Pliocene-Quaternary (PQ) deposits, based on
169 lithostratigraphic information (Kastens et al., 1988); 2) a poorly-stratified and transparent
170 unit (violet in color in Figs. 3 and 6), interpreted as coexisting sediments and volcanic
171 layers; 3) a more chaotic and less reflective unit, interpreted as the basement (brown color
172 in Figs. 3 and 6). Because of the low resolution of the Sparker profiles and their smaller
173 size in Figure 3, we created supplementary figures in order to zoom them and increase
174 their resolution.

175 The Seamounts D'Ancona I and II, Plinia, Vavilov and Tibullo are located in the
176 Northern part of the region, from West to East (Fig. 2). The D'Ancona is formed by two
177 different seamounts located in the Eastern Magnaghi Abyssal Plain (EMAP; Fig. 2a). The
178 D'Ancona I, a NNW-SSE oriented ridge, is located between 3485 m and 2696 m of depth;
179 it is 19 km long and 12 km wide, with a steep western flank (20°) and an eastern flank 10°

180 steep (Fig. 2b). The D’Ancona II is a 13 km long and 11 km wide seamount, E-W oriented,
181 with a depth ranges from 3476 m to 2900 m (Fig. 2a). The northern flank is 12° steep; the
182 southern is 7° (Fig. 2b). From a magnetic viewpoint, the D’Ancona I shows a negative
183 magnetic anomaly (from 0 to -50 nT), whereas the D’Ancona II a positive magnetic
184 anomaly (> 100 nT). East of the D’Ancona II, there is a NNE-SSW oriented topographic
185 ridge 17 km long and 6.5 km wide; it is unnamed in literature and here we called it “Plinia”.
186 This seamount ranges between 3150 m and 2647 m of depth (Fig. 2a), and it is
187 characterized by a western flank steeper than the eastern side (20° and 15° respectively;
188 Fig. 2b); the magnetic anomaly is negative and it ranges from 0 to -150 nT. The Southern
189 part of the Plinia can be shown in the in the PM3E sparker profile of Fig. 3 (Box A and A’)
190 and Supp. Fig. 1, between the Fix 26 and 28, covered by a thin PQ unit. Plinia is located
191 near Vavilov: they show a similar trend and value of magnetic anomaly (Fig. 2).

192 The Vavilov Seamount is located east of the Plinia Seamount. This huge submarine
193 volcano rises from the abyssal plain at a depth of 3500 and arrives at only 793 m below
194 sea level. The Vavilov shows an asymmetric perpendicular profile, with the western flank
195 steeper than the eastern side (23° and 14° respectively; see the slope shader map of Fig.
196 2b). The depth of the volcano ranges from 3600 m to 823 m. The Vavilov shows a very
197 strong negative magnetic anomaly (from 0 to -681 nT), although a small portion of its
198 eastern flank shows a positive anomaly (from 0 to 150 nT). To the east of Vavilov, there is
199 Tibullo Seamount, an elongated narrow NNE-SSW ridge, only 400 m high, characterized
200 by a symmetric profile (flanks ~ 13° steep); the magnetic anomaly is positive (between 0
201 and 50 nT) on the northern part, and negative on the southern part (between 0 and -50
202 nT).

203 The Southern Vavilov Abyssal Plain (SVAP; mean depth ~ 3600 m) is filled by >
204 500 m of sediments (PQ unit along the PM3E profile; Fig. 3 and Supp. Fig. 1). East of the

205 SVAP, there is a seamount unnamed in literature, here called “Aurelia” (Fig. 2). The
206 Aurelia is a WNW/ESE-oriented seamount between 3500 m and 2750 m deep,
207 characterized by a strongly asymmetrical perpendicular profile, with the northern flank
208 steeper than the southern flank (25° and 12° respectively; Fig. 2b). The magnetic anomaly
209 ranges from 0 to 50 nT in the western part and from 0 to -50 nT in the eastern part of this
210 seamount. The profile PM4 (Fig. 3, Box B and B’ and Supp. Fig. 2) crosses
211 perpendicularly the Aurelia, showing between Fix 75 and 76 a sub-vertical discontinuity
212 that connects laterally the basement with the PQ unit. The Aurelia is crossed also by
213 Profile PM11 (Fig. 3, Box C and C’ and Supp. Fig. 3): also here the asymmetry of the
214 seamount, with a sub-vertical fault affecting the northern flank, is clearly visible. South of
215 the Aurelia, the NNE-SSW oriented ridge Virgilio is formed by two different highs: the
216 northern high (~ 2800 m of depth) with a shallow negative magnetic anomaly (from 0 to -
217 50 nT); in contrast, the southern high (~ 2700 m of depth) with very strong positive values
218 (> 100 nT).

219 The southern part of this region is characterized by two arc-shaped seamounts.
220 One of those, the Augusto, a ~ 55 km-long seamount ranging from 3100 m to 1950 m of
221 depth (Fig. 2a), is characterized by six peaks located between 2400 and 1950 m of depth
222 (Fig. 2b). It shows a very strong positive magnetic anomaly, particularly in its central part
223 (> 200 nT). The Augusto is separated from an unnamed seamount, here we call “Emilia”
224 (minor depth 2200 m) from a NNW-SSE oriented basin. West of the Emilia, we have a
225 deep (> -3500 m) and almost circular basin.

226 The NNE-SSW segment of the PM11 profile (Fig. 3, Box C and C’ and Supp. Fig. 3)
227 crosses the Aurelia, a small basin filled by PQ sediments and Augusto. PQ sediments in
228 the small basins are well-stratified and undeformed in the shallow part, while gently
229 deformed in the deeper part. This intra-Pliocene unconformity corresponding probably to

230 the “X Unconformity” (Zitellini et al., 1986) is marked with a violet horizon. Several NE- and
231 SW-dipping normal faults control the formation of small basins (see at Fix 13 and 2 in the
232 box C’ of Fig. 3).

233 The SW-NE- oriented segment of the profile PM10E (Fig. 3, Box D and D’ and
234 Supp. Fig. 4) crosses the Emilia, Augusto and Virgilio Seamounts. Emilia and Virgilio are
235 bounded by several SW- and NE-dipping normal faults, as suggested by the abrupt lateral
236 interruption and dislocation of well-stratified PQ unit (marked in green). These normal
237 faults dislocate also the basement and an intermediate unit (VIOLET) with a transitional
238 seismo-stratigraphic character. The PQ unit covers part of these two seamounts, part of
239 the intermediate unit and forms thick and narrow basins (see at Fix 17 of box D’ in Fig. 3).
240 The Augusto seamount, with a chaotic seismo-stratigraphic character, does not show any
241 sedimentary cover nor faults dislocations.

242 3.2 Facies and microfaunal associations

243 The sample dredged from site 75-30-3 (Aurelia Seamount; Fig. 2a) shows the direct
244 contact between a few centimeters thick completely lithified limestone, and a greenish
245 volcanic rock (Fig.4a). The upper surface of the volcanic rock appears to be irregular and
246 affected by frequent fractures filled by carbonate mud. A thin non-continuous brownish-to-
247 black film marks the contact magmatic rock/limestone and locally also the neptunian-dykes
248 walls. The carbonate crust overlying the volcanic rock appears to be completely lithified; its
249 upper surface, exposed to seawater, is coated by a thin black film and is strongly
250 colonized by serpulids that are, in turn, covered by a black film. Frequent microhollows
251 representing the moulds of eroded and/or dissolved tests are recognizable.

252 Samples dredged from sites 75-35-(5-7-9) and 75-36-7 (Augusto Seamount; Fig.2a)
253 consist of 2-3 cm of light brownish consolidated limestones. No direct contact with volcanic
254 rocks has been observed here. The limestone upper surface is coated by a black film

255 strongly colonized by serpulids, which are in turn mineralized. In site 75-35 the carbonate
256 crust is totally colonized by corals and serpulids. Most of the recovered corals are solitary
257 cold-water species as *Desmophyllum* with characteristic cup-shaped morphology and
258 marked septa (Fig.4b). Their size varies from a few up to 6-7 centimeters; the younger
259 individuals, growing on top of the older ones, simulate pseudo-colonies. The corals
260 represent fossil occurrences; no living corals have been recovered. The corals surface
261 appears to be almost completely covered by a very thin film, black in color.

262 All the carbonates consist of crusts cemented throughout their total thickness
263 without textural evolution from chalk to limestones. Just in one sample (75-36-7a) a small
264 cavity is filled by a not completely lithified planktonic-rich mud.

265 Microfaunal analysis of the carbonate crusts reveals coral fragments, gasteropods,
266 pteropods, sponge spicules and foraminifera. The foraminiferal content is represented by
267 planktonic taxa widely distributed in the hazel-brown micritic carbonate with mudstone
268 texture or gathered inside bioturbation pockets, bioerosive structures and neptunian dykes
269 within the volcanic substratum. Mn-Fe-oxides films (or permeation or crusts) always outline
270 the bioerosion structures. The most frequent taxa are: *Pulleniatina obliquiloculata*,
271 *Globorotalia inflata*, *Globorotalia scitula*, *Orbulina universa* and globigerinids (e.g. *G.*
272 *bulloides*). Genus *Globigerinoides* is less abundant and it is mainly represented by *G.*
273 *trilobus*. *Globorotalia truncatulinoides* (in the 75-30-3) and of *Pulleniatina obliquiloculata*
274 were also observed (Fig.4d).

275 X-ray diffraction on the carbonate crusts showed Mg-calcite and calcite as the most
276 abundant phases with a subordinate silicate fraction with mica, chlorite, quartz, and
277 probably montmorillonite. Also SEM analysis, coupled with EDS, showed predominance of
278 carbonate composition with a very subordinate clay-sized silicate fraction (Fig. 4a).

279 Isolated volcanic minerals (quartz and feldspar) and volcanic fragments have been found
280 within the carbonate crust from site 75-36-7 (Fig.4c).

281 The thin brownish-to-black film marking the contact magmatic rock/limestone and
282 the neptunian-dykes walls is of Mn-Fe oxides (Fig. 4a) and shows a thin layered structure.
283 All limestone surfaces, borings (Fig.4e) and/or skeletons exposed to sea-water are coated
284 by a Mn and Fe-oxy-hydroxides thin black-brownish botryoidal film with a laminated
285 texture. The major mineral phase is todorokite, with subordinate amounts of phosphates
286 and montmorillonite (X-ray diffraction data).

287 Based on thin section and SEM-EDS observations, the limestones exhibit a
288 complex diagenetic history. Sometimes the carbonate crusts are characterized by a first
289 thin portion of an early consolidated limestone with bioclastic fragments and diffuse
290 serpulids separated, by means of a thin film of Mn-Fe-oxides, from a portion richer in
291 planktonic foraminifera. The lower portion may display borings and/or fractures, coated by
292 a Mn-Fe oxides film, filled by carbonate pelagic sediments that, in turn underwent a new
293 early lithification and mineralization. All these features indicate at least two phases of early
294 diagenesis accompanied by Mn-Fe mineralization. Both the mineralogical composition and
295 the planktonic associations of the two portions do not show significant differences.

296 3.3 Petrography

297 Samples were chosen for petrographic analyses to verify or discard their igneous
298 nature. In particular, we selected samples with phyrlic-like texture, i.e. large minerals in an
299 aphanitic ground mass. Sample T75-30-3 (Aurelia Seamount; Fig.2a) shows white to light-
300 brown grains up to two mm across set in a gray-greenish matrix (Fig. 5a1). A vein of 10
301 mm maximum apparent thickness cuts the sample. The vein is filled by very fine-grained
302 material and the contact with the host rock is sharp. Sample T75-30-5 displays phyrlic
303 texture made of vitreous grains (average 1 mm across) in a relatively soft light-gray matrix

304 (Fig. 5a2). Inspection under a polarizing optical microscope (Fig. 5a3,4) reveals a texture
305 with euhedral to anhedral grains set in a chlorite- and opaque-rich matrix. Matrix minerals
306 are locally aligned to form a fluidal texture. Two types of grains are recognized: (1)
307 euhedral to subhedral grains with pseudo-hexagonal and prismatic shapes (Fig.5a4,5) and
308 (2) rounded fractured grains with clear appearance under plane polarized light (Fig. 5a3).
309 The euhedral to subhedral grains may be former phenocrysts now completely replaced by
310 secondary chlorite and carbonates, mainly dolomite and minor Mg-calcite, as determined
311 by energy-dispersive spectrometry in a SEM. These phenocrysts occur as single grains or
312 as clusters that locally gives the rock a glomeroporphyritic texture. The rounded fractured
313 grains are made of quartz (sample T75-30-3). The matrix is composed of euhedral to
314 subhedral microlites, now completely replaced by secondary low-Fe chlorite, and rounded
315 Ti-rich minerals. High-Fe chlorite fills the interstices among microlites. Sample T75-30-5 is
316 cut by at least two sets of veins. Earlier veins, maximum thickness 0.25 mm, are filled by
317 coarse grained Fe-bearing dolomite with irregular shapes. Late veins are wider, and are
318 filled by euhedral dolomite. Finally, sample T75-30-5 contains amygdale showing a
319 zonation, from rim to core of the amygdala, chlorite, opaque material and dolomite (Fig.
320 5a6).

321 **4. Discussion**

322 4.1 Environmental significance of the Aurelia and Augusto rocks and carbonate facies

323 Samples of rock analyzed from the Aurelia seamount preserve a porphyritic texture with
324 different types of phenocrysts set in a matrix with microlites that locally define a flow
325 texture. These features are compatible with an igneous nature of the samples. Their
326 primary mineralogy is now replaced by secondary phases such as low-Fe chlorite and
327 dolomite. Similarly, the matrix contains microlites now replaced mainly by low-Fe chlorite,
328 and Ti-rich phases that possibly represent remnants of primary Fe-Ti oxides that

329 underwent iron loss during low-temperature rock-water interaction. Plotting our data of Ti
330 and Zr, two elements usually interpreted as relatively immobile during low-T alteration
331 (Pearce, 2014), the rocks of the Aurelia Seamount fall in the calc-alkaline field (Fig. 5b).

332 From a carbonate/biostratigraphic viewpoint, samples from the Aurelia and Augusto
333 Seamounts consist of crusts cemented throughout their total thickness without textural
334 evolution from chalk to limestones. The crusts, with thickness between 15 to 30 mm, are
335 made of Mg-calcite biomicrite rich in planktonic foraminifera with a very subordinate
336 silicate component. The occurrence of *Globorotalia truncatulinoides* on the Aurelia
337 Seamount suggests for this sample an age not older than Early Pleistocene (Iaccarino et
338 al., 2007). This is also confirmed by the presence of *Pulleniatina obliquiloculata*, a warm
339 tropical-subtropical species, that although it occurred in the Atlantic basin in Early Pliocene
340 (Zankl, 1969; Bolli and Sanders, 1985; Iaccarino et al., 2007), it is never recorded in
341 Pliocene Mediterranean deposits. Moreover, according to Bolli and Sanders (1985), *P.*
342 *obliquiloculata* shows major frequency peaks during the Pleistocene–Holocene time
343 interval. This taxon would have entered the Mediterranean during the Pleistocene warmer
344 climatic stages (Conti et al., 2013) probably from the Atlantic occurring exclusively in the
345 western sector of the Mediterranean basin. An interesting feature is the occurrence within
346 the carbonate crust from the Augusto Seamount of isolated volcanic minerals (quartz and
347 feldspar) and of volcanic fragments, probably indicating a coeval magmatic activity or
348 alternatively a supply of volcanic material eroded from a nearby seamount.

349 The occurrence in many areas of the Mediterranean of Quaternary deep-water
350 cemented limestones with different grades of consolidation, from brittle to consolidated
351 chalk to cemented limestones, has been reported in literature (Alloué, 1990). The study of
352 the carbonate crusts and their relationships with the volcanic substrate, are important for
353 understanding the rapid formation of hardgrounds in ancient sedimentary sequences.

354 A number of studies have focused on the driving mechanisms for the early
355 lithification of the Quaternary deep-sea crusts (Emelyanov & Shimkus, 1986; McKenzie
356 and Bernoulli, 1982; Alloué 1987, 1990; Remia et al., 2004). Early lithification, occurring at
357 or below the seafloor, takes place under varying conditions: it may occur in sediment-
358 starved environments, it may depend on ascending interstitial carbonate-rich waters, or on
359 microbiological precipitation or it may be physiochemically controlled and related to inward
360 diffusion of sea-water solutions. Concerning the degree of saturation relative to calcite,
361 Mediterranean waters remained saturated at all depths also during the Pleistocene cold
362 phases (Alloué, 1987). Another significant factor controlling carbonate precipitation or
363 dissolution is the concentration of dissolved phosphates and organic matter (Morse, 1986).

364 The carbonate crusts taken into consideration in this study are predominantly made
365 of Mg-calcite with a very subordinate silicate fraction, mostly represented by mica, quartz
366 chlorite and montmorillonite, probably deriving from the weathered volcanic substrate. One
367 of the factors controlling early lithification is the purity of lime mud; less than 2% of
368 insoluble residue (especially clay minerals) favors cementation and recrystallization (Zankl,
369 1969). Nevertheless an excess of hydrothermal metals (i.e. Mn-Fe-oxyhydroxides) may
370 “fertilize” areas of normal biological productivity, resulting in massive phytoplankton
371 blooms (Coale et al., 1996; Larson and Erba, 1999; Corda and Palmiotto, 2015). The
372 microorganisms activity may have a significant influence in precipitating hydrothermal Mn-
373 Fe-oxyhydroxide (Dekov and Savelli, 2004); in addition, Mutti and Bernoulli (2003) stress
374 the relationship between phosphate mineralization, trophic resources and microbial micrite
375 precipitation. Based on our observations, we assume a significant role of the
376 microbiological precipitation of calcite in facilitating the early lithification of planktonic ooze.

377 Sources of magnesium are usually seawater and sometimes, fresh waters but could
378 also derive from weathered magmatic Fe-Mg rich rocks. When magnesium is delivered to

379 seawater, Mg-calcite can precipitate (Mackenzie and Andersson, 2013; Morse and
380 Mackenzie, 1990).

381 The limited thickness of the carbonate crusts points to very slow rates of
382 sedimentation and /or accumulation probably related to high hydrodynamics. The very thin
383 brownish film of Mn-Fe oxides, even if non-continuous, covering the volcanic substrate
384 hints at a period of water-rock exposure before the carbonate planktonic-rich mud began
385 to deposit. During this period the volcanic substrate underwent a phase of extensional
386 tectonics promoting intense fracturing, as testified by neptunian dykes partially mineralized
387 and successively filled by pelagic sediments. This substrate should be firstly colonized by
388 small rapidly-growing opportunistic organisms such as serpulids, favored by strong storm
389 activity, and covered by few millimeters of carbonate mud cemented early. Above this first
390 phase of sedimentation, accompanied by early diagenesis, bioturbation processes and
391 Mn-Fe mineralization, a new phase of sedimentation of carbonate planktonic-rich ooze
392 began, that was rapidly lithified and mineralized.

393 Ultimately our findings suggest that the pelagic sediments settled on the magmatic
394 substrates underwent an early lithification process induced by precipitation of Mg-calcite
395 within the pelagic carbonate matrix in areas of very slow sedimentation rates. The volcanic
396 substrates underwent a tectonic instability, testified by fractures and neptunian dykes
397 infilled by planktonic mudstones. Their morphostructural configuration as isolated highs,
398 suffering high hydrodynamic conditions, is here interpreted as responsible for low
399 sedimentation/accumulation rates, clustering of planktonic foraminifera and skeletal
400 fragmentation. The slow rates of deposition favored prolonged conditions of exposure at
401 the seawater-sediment interface of the pelagic and skeletal carbonates, enhancing the
402 diffusion of seawater-ions throughout the sediments and promoting chemical precipitation
403 and the consequent development of hardgrounds prone to be colonized by corals and

404 serpulids. In addition, the presence of phosphorous as evidenced by the SEM-EDS
405 analysis, suggests that the pelagic carbonates underwent early diagenetic lithification
406 phases under high-fertility conditions which, favoring an increase of microbiota
407 communities, promoted an increase of microbiological micrite precipitation. The
408 widespread Mn-Fe mineralizations covering both the carbonate deposits and the
409 encrusting/colonizing biota on the base of crust morphologies, textural evidence and
410 tectonic setting, can be related to hydrothermal processes.

411 4.2 Geodynamic significance of the Aurelia and Augusto Seamounts

412 We discuss here the significance of the Aurelia and Augusto seamounts in the
413 geodynamics of the central Tyrrhenian Back-Arc Basin, based on our results, on data from
414 literature, on the regional bathymetry map and the map of the distribution of the reduced to
415 the pole magnetic anomalies of the Southern Tyrrhenian (Figure 6a and b, respectively).

416 The Magnaghi basin (Fig. 6a) starts opening during the Tortonian/Messinian (Loreto
417 et al., 2020). Volcanism of the Magnaghi Volcano is characterized by basalts with an Na-
418 alkaline affinity, dated from 3.1 to 2.7 Ma (Late Pliocene; Serri et al., 2001), in line with the
419 subchron C2An.1n (3.040 to 2.581 Ma; Cande and Kent, 1995) shown in Fig. 6b.

420 The Vavilov basin (Fig. 6a) opened between the Late Miocene and the Early
421 Pliocene (the older basalts from the ODP 373 are 7.5 Ma old; Hsü et al., 1978) when their
422 composition is similar to mid-ocean ridges (MORB), as shown by the basalts sampled from
423 the ODP 655 on the Gortani Ridge (Fig. 6a), dated ~4 Ma (Kastens et al., 1988). The
424 beginning of the Vavilov Volcano activity is placed at 3 Ma, at the same time of the
425 spreading of the basin (Robin et al., 1987). The Vavilov lavas, very similar to those of the
426 Magnaghi Volcano, are formed by basalts ranging from tholeiitic to Na-alkaline (Peccerillo,
427 2017). The end of extension in the Vavilov basin allows the growth of the volcano, which
428 shows in Figure 6b a negative magnetic anomaly (C2r.2r; 2.581 to 2.150 Ma; Savelli and

429 Ligi, 2017). According to Parson et al. (1990), the change in chemical composition from
430 MORB to calc-alkaline marks the evolution of a back-arc basin from an early stage, where
431 a pure extensional tectonics produced an oceanic crust with MORB affinity, to a mature
432 stage of back arc spreading, where the oceanic crust has a calc-alkaline affinity. Based on
433 the age of the boundary between the older sediments and calc-alkaline rocks sampled in
434 the ODP 651 (Northern Vavilov basin; Kastens et al., 1988; Bonatti et al., 1990), we
435 assume that the extensional tectonics of the Vavilov plain continued until 2.6 Ma.

436 The Marsili basin (Fig. 6a) starts opening in the Early Pleistocene (basalts dated ~ 2
437 Ma from the OPD 650; Kastens et al., 1988); it shows a negative/inverse magnetic
438 anomaly falling in the chron C1r.2r (1.770 to 1.070 Ma; Fig. 6b). The Marsili volcano is
439 located in the center of the basin, formed by calc-alkaline rocks (Trua et al., 2002) not
440 older than 1.07 Ma (Cocchi et al., 2009), corresponding with the positive/normal magnetic
441 anomaly C1n (0.780 to 0.00 Ma; Cocchi et al., 2009; see Fig. 6b). The Marsili is
442 surrounded by several volcanic islands and seamounts (Fig. 6a): the Palinuro Volcanic
443 Complex, a E-W oriented volcanic structure formed by basaltic-andesite compositions
444 lavas dated 0.8-0.3 Ma (e.g., Colantoni et al., 1981; Cocchi et al., 2017); the Alcione, and
445 Lametini 1 and 2 seamounts, related to the geodynamic environment to the Aeolian arc
446 and younger than 1 Ma (Barberi et al., 1974; Beccaluva et al., 1985; Lupton et al., 2011);
447 the Aeolian Islands, consisting of calc-alkaline to shoshonitic lavas and pyro-clastics, with
448 minor potassic alkaline rocks (Peccerillo, 2005), originated by volcanism due to the “wet”
449 melting of a suprasubduction mantle wedge (Lupton et al., 2011); the Enarete, Eolo, Sisifo
450 and Tiro Seamounts, the oldest volcanoes of the Aeolian Islands Arc (Beccaluva 1982;
451 1985). All these volcanoes and seamounts show a normal/positive magnetic anomaly (i.e.
452 Bortoluzzi et al., 2010; Cocchi et al., 2017) that, as in Marsili, can be attributed to the C1n
453 (0.780 to 0.00 Ma), although some of them show a volcanism > 0.780 Ma, before the

454 formation of the Marsili volcano. For example, the Tiro and Sisifo Seamounts are formed
455 by calc-alkaline and high K₂O calcalkaline rocks dated ~1.5 Ma and from 1.3 Ma to 0.9,
456 respectively (Beccaluva et al., 1985); Enarete and Eolo, formed by basalts, dacites and
457 rhyolites, have been dated between 0.85-0.77 Ma (Beccaluva et al., 1982, 1985; Trua et
458 al., 2004).

459 Based on the geodynamic models of Carminati et al. (2010), we reconstructed a
460 cartoon showing the migration of the volcanic arc associated to the Ionian slab during the
461 last 3 Ma (Figure 7). In this cartoon, at 3 Ma, when the Magnaghi and Vavilov volcanoes
462 were active, we assume that Aurelia, Virgilio and the western part of Augusto seamount
463 were part of the active volcanic arc. We based on: 1) the calc-alkaline basement rocks of
464 the Aurelia (Ti/Z diagram data of Fig.5b), indicating a subduction-related volcanism; 2) the
465 calc-alkaline basement rocks of the western part of the Augusto (Colantoni et al.,1981),
466 testified also by the occurrence of volcanic fragments in our carbonate samples, and on
467 the strong positive magnetic anomaly (Fig. 6b and Cella, 1998); 3) the volcanic nature of
468 the Virgilio, considered a NNE-SSW oriented composite volcanic structure made by a
469 coalescence of a series of centres (Finetti et al., 1986); 4) the recognized planktonic
470 foraminifera assemblages of the Aurelia and Augusto carbonates, cannot be older than
471 Early Pleistocene, indicating a volcanic activity before 2.58 Ma.

472 Based on the bathymetry maps (Figs. 2 and 6a), the Augusto Seamount is
473 composed by several peaks forming a curved arc, located between 2400 and 1900 m
474 below sea level. This curved morphology resembles more the fossil Aeolian volcanic arc,
475 South of the Marsili, formed by the Seamounts Sisifo and Tiro, active between 1.5 and 1
476 Ma (Fig.7 - 1 Ma; Beccaluva et al.,1985), than the morphology of the modern Aeolian
477 volcanic arc (Fig.7 - 0 Ma). Considering the location of the Augusto, between the Aurelia
478 and the Augusto, and the Sisifo and Tiro, and based on the age of their volcanism, we

479 assume the Augusto Seamount as part of the Early/Middle Pleistocene Tyrrhenian
480 volcanic arc (Fig.7 - 2 Ma). The different trend of the Tyrrhenian volcanic arc between the
481 Late Pliocene (Fig. 7 - 3 Ma) and the Early Pleistocene (Fig. 7 – from 2 to 0 Ma) could
482 testify the change from eastward to southeastward of the Ionian slab retreat, due to
483 collision with the Apulia platform to the north and the Hyblean platform to the south, during
484 the Pliocene (Van Dijk et al., 2000). The geodynamic model by Corradino et al. (2022)
485 considers the area between Vavilov and Marsili as the present place of back-arc
486 extension, and the Marsili as part of a Pliocene volcanic arc. In contrast, our geological,
487 geochronological and petrological results show that the Aurelia and the Augusto
488 Seamounts were part of the active Tyrrhenian volcanic arc during the Late Pliocene-Early
489 Pleistocene, and that the Marsili is the present back-arc spreading center (positive/normal
490 magnetic anomaly C1n - 0.780 to 0.00 Ma; Fig. 6b).

491

492 4.3 The Vavilov-Marsili Transfer Zone

493 According to Macdonald et al. (1988) and Pagli et al. (2019), along the back-arc
494 basins, seafloor spreading is offset by transfer zones where strike-slip tectonics transfers
495 displacement between two similar non-coplanar structures. Transfer zones are striking
496 parallel to the regional direction of extension. They are local and passive fracture formed in
497 response to active faulting on faults which link with the transfer; an example is transfer
498 zone is the Central Lau Spreading Centre (CLSC) and the Eastern Lau Spreading Centre
499 (ELSC) in the Lau Back-arc Basin (SW Pacific Ocean; Parson and Wright, 1996). Also,
500 transfer zones could also be inherited from the overriding plate, as in the Northern Lau
501 Basin, where the upper plate is affected by strike-slip tectonics along older tectonic
502 lineaments (Palmiotto et al., 2022).

503 The central region of the Tyrrhenian Back-Arc Basin is characterized by a WNW-
504 ESE oriented basin, located between the Vavilov and the Marsili basins, perpendicular to
505 the NNE-SSW trend of the Vavilov and Marsili volcanoes (Fig. 6a). This basin shows low
506 values of magnetic anomalies (Fig. 6b) and, based on seismic refraction data (Recq et al.,
507 1984), it is characterized by a minimum value of crustal thickness (the velocity is 6 km/s at
508 only 5 km of depth). We show here part of a sparker profile (PM12; Fig. 6c and Supp. Fig.
509 5), acquired during the oceanographic expedition T71 (see the Fig.1a and the methods).
510 The profile PM12 is NE-SW oriented and crosses perpendicular the basin between Vavilov
511 and Marsili. An interpretation of the profile shows that the basin is covered by PQ
512 sediments and it shows in its center, from fix 32 to 37 (Fig. 6c and Supp. Fig. 5), a feature
513 we interpreted as a positive flower structure. This feature can be attributed to a
514 transcurrent fault that in the bathymetry map (Fig. 6a) can be followed from the Southern
515 Vavilov basin, where affects the Aurelia basement (see the sub-vertical fault in the profiles
516 PM4 and PM11 of Fig. 3 and Supp. Figs.3,4), to the Western Marsili basin. Furthermore,
517 based on the maps of the distribution of the reduced to the pole magnetic anomalies (Figs.
518 2c,d and 6b), the upper part of the Vavilov volcano and a small part of its eastern flank
519 show a positive magnetic anomaly which could be attributed to a recent volcanic event,
520 considering that the summit lavas have been dated between 0.37 and 0.09 Ma (C1n;
521 Robin et al., 1987; Savelli and Ligi, 2017). Based on those considerations, we interpreted
522 the Tyrrhenian as a BAB where two different segment of spreadings are active at the same
523 time and, the basin between the Vavilov and the Marsili, their “Transfer Zone” (Figs. 6 and
524 7).

525

526 **5. Conclusions**

527 We analyzed geophysical and geological data of two seamounts (Augusto and
528 Aurelia) located South of the Vavilov volcano. The Augusto is characterized by an arc-
529 shaped morphology, with several peaks located between 1950 and 2400 m below sea
530 level; the Aurelia shows an asymmetric perpendicular profile due sub-vertical faults
531 affecting its northern side, visible both from bathymetry and from the sparker profiles. The
532 distribution of the reduced to the pole magnetic anomalies shows positive values on the
533 Augusto, and low negative values on the Aurelia. Samples of rocks dredges from the
534 Seamounts show a magmatic nature of their basement (basalts with a calc-alkaline
535 affinity). Carbonate samples consist of thin crusts cemented early made of Mg-calcite
536 biomicrite rich in planktonic foraminifera, dated not older than Early Pleistocene. Based on
537 our results, we interpret the Augusto and Aurelia as part of the volcanic arc of the
538 Tyrrhenian BAB during the Late Pliocene–Early Pleistocene time.

539 **Acknowledgements**

540 Work supported by the Italian National Research Council (Consiglio Nazionale Ricerche).

541 We thank Enrico Bonatti for the revision of the English; Marco Ligi for constructive

542 comments that helped us to improve the manuscript; Marzia Rovere and Maria Filomena

543 Loreto for starting the creation of a digital seismic database of the old Sparker data at the

544 CNR-ISMAR of Bologna. We are also grateful to the Editor and to the Reviewers for their

545 constructive comments that helped improve the manuscript.

546

547 **References**

- 548 Allouc, J., 1987. Les paléocommunautés profondes sur fond rocheux du Pléistocène
549 méditerranéen. Description et essai d'interprétation paléogéologique. *Géobios* 20
550 (2), 241–263.
- 551 Allouc, J., 1990. Quaternary crusts on slopes of the Mediterranean Sea: A tentative
552 explanation for their genesis. *Mar. Geol.* 94, 205–238.
- 553 Barberi, F., Gasparini, P., Innocenti, F., Villari, L., 1973. Volcanism of the southern
554 Tyrrhenian Sea and its geodynamic implications. *J. Geophys. Res.* 78(23), 5221–5232.
- 555 Barberi, F., Bizouard, H., Capaldi, G., Ferrara, G., Gasparini, P., Innocenti, F., Joron, J.L.,
556 Lambret, B., Treuil, M., Allegre, C., 1978. Age and nature of basalts from the
557 Tyrrhenian Abyssal Plain. From Hsü, K., et al., 1978. Site 373: Tyrrhenian Basin. Initial
558 reports of the Deep Sea Drilling Project, 42(part 1), pp. 151–174, Washington, D.C.,
559 U.S. Government Printing Office.
- 560 Beccaluva, L., Gabbianelli, G., Lucchini, F., Rossi, P.L., Savelli, C., 1985. Petrology and
561 K/Ar ages of volcanics dredged from the Eolian seamounts: implications for
562 geodynamic evolution of the southern Tyrrhenian basin. *Earth Planet. Sci. Lett.* 74(2-
563 3), 187–208.
- 564 Beccaluva, L., Rossi, P.L., Serri, G., 1982. Neogene to Recent volcanism of the southern
565 Tyrrhenian-Sicilian area: Implications for the geodynamic evolution of the Calabrian
566 arc. *Earth Evol. Sci* 3, 222–238.
- 567 Bolli, H.M., Saunders, J.B., 1985. Oligocene to Holocene low latitude planktic foraminifera.
568 In: Bolli, H.M., Saunders, J.B., Perch-Nilsen, K. (Eds.), *Plankton Stratigraphy*.
569 Cambridge University Press, Cambridge, pp. 155–262.
- 570 Bonatti E., Seyler, M., Channell, J., Giraudeau, J., Mascle, G., 1990. Peridotites Drilled
571 From The Tyrrhenian Sea, Odp Leg 1071. In: Kastens, K.A., Mascle, J. et al.,

572 Proceedings of the Ocean Drilling Program, Scientific Results, Vol. 107, College
573 station, Texas.

574 Bortoluzzi, G., Carrara, G., Fabretti, P., Gamberi, F., Marani, M., Penitenti, D., Stanghellini,
575 G., Tonani, M., Zitellini, N., Bonazzi, C., Lippolis, S., Musacchio, M., Daviddi, A.,
576 Diroma, G., Ferrarini, A., Leotta, A., Gilod, D., Nikaronenkov, B., Efimov, V., Erofeev,
577 S., 1999. Swath bathymetry and geophysical survey of the Tyrrhenian sea report on
578 bathymetric, magnetic and gravimetric investigations during cruises TIR96 and TIR99.
579 IGM TECHNICAL REPORT N. 52, Bologna.
580 http://ricerca.ismar.cnr.it/CRUISE_REPORTS/1990-1999/GELENDZHIK_TIR96_99_REP

581 Bortoluzzi, G., Ligi, M., Romagnoli, C., Cocchi, L., Casalbore, D., Sgroi, T., Cuffaro, M.,
582 Caratori Tontini, F., D'Orlando, F., Ferrante, V., Remia, A., and Riminucci, F., 2010,
583 Interactions between volcanism and tectonics in the western Aeolian sector,
584 southern Tyrrhenian Sea. *Geophys. J. Int.* 183, 64-78.

585 Cande, S.C., and Kent, D.V., 1995. Revised Calibration of the Geomagnetic Polarity
586 Timescale for the Late Cretaceous and Cenozoic. *J. Geophys. Res. Solid Earth*,
587 100, 6093-6095.

588 Cann, J.R., 1970. Rb, Sr, Y, Zr and Nb in some ocean floor basaltic rocks. *Earth Planet.*
589 *Sci. Lett.* 10, 7-11.

590 Caratori Tontini, F., Bassett, D., De Ronde, C.E.J., Timm, C., Wysoczanski, R., 2019.
591 Early evolution of a young back-arc basin in the Havre Trough. *Nat. Geosci.*, 12,
592 856-862.

593 Carminati, E., Lustrino, M., Cuffaro, M., Doglioni, C., 2010. Tectonics, magmatism and
594 geodynamics of Italy: What we know and what we imagine. In: M. Beltrando, A.
595 Peccerillo, M. Mattei, S. Conticelli, and C. Doglioni (Eds.), *The Geology of Italy*, J.
596 *Virtual Explor.*, ISSN 1441-8142, Vol. 36.

597 Carminati, E., Wortel, M.J.R., Meijer, P.T., Sabadini, R., 1998. The two-stage opening of
598 the western–central Mediterranean basins: a forward modeling test to a new
599 evolutionary model. *Earth Planet. Sci. Lett* 160(3-4), 667–679

600 Cella, F., Fedi, M., Florio, G., Rapolla, A., 1998. Boundaries of magnetic anomaly sources
601 in the Tyrrhenian region. *Ann. Geophys.* 51(1), 1–23.

602 Coale, K.H., Fitzwater, S.E., Gordon, R.M., Johnson, K.S., Barber, R.T., 1996. Control of
603 community growth and export production by upwelled iron in the equatorial Pacific
604 Ocean. *Nature* 379, 621–624.

605 Cocchi, L., Passaro, S., Caratori Tontini, F., and Ventura, G., 2017, Volcanism in slab tear
606 faults is larger than in island-arcs and back-arcs, *Nature Communications* 8, 1451.

607 Cocchi, L., Caratori Tontini, F., Muccini, F., Marani, M. P., Bortoluzzi, G., Carmisciano, C.,
608 2009. Chronology of the transition from a spreading ridge to an accretional
609 seamount in the Marsili backarc basin (Tyrrhenian Sea). *Terra Nova* 21, 369 – 374.

610 Colantoni, P., Fabbri, A., Gallignani, P., Sartori, R., Rehault, J.P., 1981. Carta litologica e
611 stratigrafica dei mari italiani. Scale 1:500.000. Litografica Artistica Cartografica,
612 Firenze.

613 Conti, A., Bigi, S., Cuffaro, M., Doglioni, C., Scrocca, D., Muccini, F., Cocchi, L., Ligi, M.,
614 Bortoluzzi, G., 2017. Transfer zones in an oblique back-arc basin setting: Insights from
615 the Latium-Campania segmented margin (Tyrrhenian Sea). *Tectonics* 36(1), 78–107.

616 Conti, M.A., Girasoli, D.E., Frezza, V., Conte, A.M., Martorelli, E., Matteucci, R., Chiocci,
617 F.L., 2013. Repeated events of hardground formation and colonisation by endo-
618 epilithozoans on the sediment-starved Pontine continental slope (Tyrrhenian Sea,
619 Italy). *Mar. Geol.* 336, 184–197.

620 Corda, L., Palmiotto, C., 2015. Rhodalgol–foramol facies in equatorial carbonates: Insights
621 from Miocene tectonic islands of the central Atlantic. *Palaeogeogr. Palaeoclimatol.*
622 *Palaeoecol.* 428, 21–30.

623 Corradino, M., Balasz, A., Faccenna, C., and Pepe, F., 2022. Arc and forearc rifting in the
624 Tyrrhenian subduction system. *Scientific Reports* 12, 4728.

625 Della Vedova, B., Pellis, G., Foucher, J.P. Rehault, J.-P, 1984. Geothermal structure of the
626 Tyrrhenian Sea. *Mar. Geol.* 55, 271–289.

627 Dekov, V.M., Savelli, C., 2004. Hydrothermal activity in the SE Tyrrhenian Sea: an
628 overview of 30 years of research. *Mar. Geol.* 204, 161–185.

629 Doglioni, C., 1991. A proposal for the kinematic modelling of W-dipping subductions-
630 possible applications to the Tyrrhenian-Apennines system. *Terra Nova* 3, 423–434.

631 Doglioni, C., E. Gueguen, P. Harabaglia, Mongelli, F., 1999. On the origin of W-directed
632 subduction zones and applications to the western Mediterranean. *Geol. Soc. Spec.*
633 *Publ.* 156, 541–561.

634 Doglioni, C., Innocenti, F., Morellato, C., Procaccianti, D., Scrocca, D., 2004. On the
635 Tyrrhenian sea opening. *Mem. Descr. Carta Geol. d'It.* 44, 147–164.

636 Emelyanov, E.M., Shimkus, K.M., 1986. *Geochemistry and Sedimentology of the*
637 *Mediterranean sea. Sedimentology and Petroleum Geology.* Reidel, Dordrecht, 553.

638 Fabbri, A., Gallignani, P., Zitellini, N., 1981. Geologic evolution of the peri-Tyrrhenian
639 sedimentary basins. In: Wezel, F.C, “Sedimentary basins of Mediterranean
640 margins”, 101-26, C.R.N., Italian Project of Oceanography, Tecnoprint, Bologna,
641 1981.

642 Faccenna, C., Mattei, M., Funicello, R., Jolivet, L., 1997. Styles of back-arc extension in
643 the central Mediterranean. *Terra Nova* 9(3), 126–130.

644 Faccenna, C., Becker, T.W., Lucente, F.P., Jolivet, L., Rossetti, F., 2001. History of
645 subduction and back arc extension in the Central Mediterranean. *Geophys. J. Int.*
646 145(3), 809–820.

647 Faggion, O., Pinna, E., Savelli, C., Schreider, A.A., 1999. Geomagnetism and age study of
648 Tyrrhenian Seamounts. *Geophys. J. Int.* 123, 915–930.

649 Farran, M., 2008: IMAGE2SEGY: Una aplicación informática para la conversión de
650 imágenes de perfiles sísmicos a ficheros en formato SEG Y. *Geo- Temas* 10,
651 1215–1218.

652 Finetti, I.R., Del Ben, A., 1986. Geophysical study of the Tyrrhenian opening. *Boll. di*
653 *Geofis. Teor. ed Appl.* 28, 75–155.

654 Finetti, I. R., 2005. CROP project: deep seismic exploration of the central Mediterranean
655 and Italy. (Eds. By Finetti, I. R.), Elsevier, Vol. 1.

656 Florio, G., Passaro, S., de Alteriis, G., Cella, F., 2022. Magnetic Anomalies of the
657 Tyrrhenian Sea Revisited: A Processing Workflow for Enhancing the Resolution of
658 Aeromagnetic Data. *Geosciences* 2022, 12, 377.

659 Fretzdorff, S., Livermore, R. A., Devey, C. W., Leat, P. T., Stoffers, P., 2002. Petrogenesis
660 of Back-Arc East Scotia Ridge, South Atlantic Ocean. *Journal of Petrology*, 43, 1435 –
661 1467.

662 Fujiwara, T., Yamazaki, T., Joshima M., 2001. Bathymetry and magnetic anomalies in the
663 Havre Trough and southern Lau Basin: from rifting to spreading in back-arc basins.
664 *Earth Planet. Sci. Rev.*, 185, 253-264.

665 Hofmann, A.W., 1988. Chemical Differentiation of the Earth: The Relationship between
666 Mantle, Continental Crust, Oceanic Crust. *Earth Planet. Sci. Lett.* 90, 297-314.

667 Hsü, K., Montadert, L., Bernoulli, D., Bizon, G., Cita, M.B., Erickson, A., Fabrcius, F.,
668 Garrison, R.E., Kidd, R.B., Mèlerés, F., Müller, C., Wright, C.R., 1978. Site 373:

669 Tyrrhenian Basin. Initial reports of the Deep Sea Drilling Project 42(part 1), pp. 151-
670 174, Washington, D.C., U.S. Government Printing Office.

671 Hynes, A., Mott, J., 1985. On the causes of back-arc spreading. *Geology* 13, 387–389.

672 Iaccarino, S., Premoli Silva, I., Biolzi, M., Foresi, L.M., Lirer, F., Turco, E., Petrizzo, M.R.,
673 2007. Practical manual of Neogene Planktonic Foraminifera. International School on
674 Planktonic Foraminifera, 6th course, Perugia 19-23 February 2007, University of
675 Perugia, 1–181.

676 Kastens, K., Mascle, J., Auroux, C., Bonatti, E., Broglia, C., Channell, J., Curzi, P., Emeis,
677 K.-C., Glaçon, G., Hasegawa, S., Hieke, W., Mascle, G., McCoy, F., Mckenzie, J.,
678 Mendelson, J., Müller, C., Réhault, J.P., Robertson, A., Sartori, R., Sprovieri, R.,
679 Torii, M., 1988. ODP Leg 107 in the Tyrrhenian Sea: Insights into passive margin
680 and back-arc basin evolution. *Geol. Soc. Am. Bull.* 100(7), 1140–1156.

681 Kastens, K. A., Mascle, J., 1990. The geological evolution of the Tyrrhenian Sea: An
682 introduction to the scientific results of ODP Leg 107. In: *Proceedings of the Ocean*
683 *Drilling Program, Scientific Results, Vol. 107*, (Ed. by K. A. Kastens & J. Mascle, et
684 al.), pp. 3–26. Ocean Drilling Program, College station, Texas.

685 Larson, R.L., Erba, E., 1999. Onset of the mid-Cretaceous greenhouse in the Barremian–
686 Aptian: igneous events and the biological, sedimentary, and geochemical
687 responses. *Paleoceanography* 14, 663–678.

688 Leat, P.T., Larter, R.D., 2003. Intra-oceanic subduction systems: introduction. *Geological*
689 *Society, London, Special Publications*, 219, 1-17.

690 Livermore, R., Cunningham, A., Vanneste, L., Larter, R., 1997. Subduction influence on
691 magma supply at the East Scotia Ridge. *Earth Planet. Sci. Lett.* 1997, 150, 261-
692 275.

693 Loreto, M.F., Zitellini, N., Ranero, C., Palmiotto, C., Manel, P., 2020. Extensional tectonics
694 during the Tyrrhenian back-arc basin formation and a new morpho-tectonic map.
695 Basin Research 33, 138–158.

696 Lupton, J., De Ronde, C., Sprovieri, M., Baker, E.T., Bruno, P.P., Italiano, F., Walker, S.,
697 Faure, K., Leybourne, M., Britten, K., Greene, R., 2011. Active hydrothermal
698 discharge on the submarine Aeolian Arc. J. Geophys. Res. 116, 1–22.

699 Macdonald, K.C., Fox, P.J., Perram, L.J., Eisen, M.F., Haymon, R.M., Miller, S.P.,
700 Carbotte, S.M., Cormier, M.H., and Shor, A.N., 1988. A new view of the mid-ocean
701 ridge from the behaviour of ridge-axis discontinuities. Nature 335, 217–225.

702 Magni, V., J., Naliboff, M., Prada, C., Gaina, 2021. Ridge Jumps and Mantle Exhumation
703 in Back-Arc Basins. Geosciences 11, 475.

704 Malinverno, A., Ryan, W.B., 1986. Extension in the Tyrrhenian Sea and shortening in the
705 Apennines as result of arc migration driven by sinking of the lithosphere. Tectonics
706 5(2), 227–245.

707 Marani, M., Bonatti, E., Gamberi, F., 2004. From seafloor to deep mantle: architecture of
708 the Tyrrhenian back-arc basin. Mem. Descr. Carta Geol. D'It. 64, 1–194.

709 Marani, M., Gamberi, F., 2004. Structural framework of the Tyrrhenian Sea unveiled by
710 seafloor morphology. Mem. Descr. Carta Geol. d'It. 44, 97–108.

711 Martinez, F., Taylor, B., 2002. Mantle wedge control on back-arc crustal accretion. Nature
712 416, 417–420.

713 McKenzie, F.T., Bernoulli, D., 1982. Geochemical variations in Quaternary hardgrounds
714 from the Hellenic trench region and possible relationship to their tectonic setting.
715 Tectonophysics 86, 149-157.

716 Mackenzie, F.T., Andersson, A.J., 2013. The marine carbon system and ocean
717 acidification during Phanerozoic time. Geochem. Perspect. 2(1), 1–227.

718 Morse, J.W. 1986. The surface chemistry of calcium carbonate minerals in natural waters:
719 an overview. *Mar. Chem.* 20., 91–112.

720 Morse, J.W, McKenzie, FT., 1990. *Geochemistry of sedimentary carbonates.*
721 *Developments in Sedimentology* 48, Elsevier, 696.

722 Mutti M., Bernoulli D., 2003. Early marine lithification and hardground development on a
723 Miocene ramp (Maiella, Italy) key surfaces to track changes in trophic resources in
724 nontropical carbonate settings. *J. Sediment. Res.* 73, 296–308.

725 Pagli, C., Sang-Ho, Y., Ebinger, C., Keir, D., Wang, H., 2019. Strike-slip tectonics during
726 rift linkage. *Geology* 47, 31–34.

727 Palmiotto, C., Ficini, E., Loreto, M.F., Muccini, F., Cuffaro, M., 2022. Back-Arc Spreading
728 Centers and Superfast Subduction: The Case of the Northern Lau Basin (SW
729 Pacific Ocean). *Geosciences* 12, 50.

730 Palmiotto, C., Loreto, M.F., 2019. Regional scale morphological pattern of the Tyrrhenian
731 Sea: New insights from EMODnet bathymetry. *Geomorphology* 332, 88–99.

732 Parson, L.M., Pearce, J.A., Murton, B.J., Hodkinson, R.A., and the RRS Charles Darwin
733 Scientific Party, 1990. Role of ridge jumps and ridge propagation in the tectonic
734 evolution of the Lau back-arc basin, southwest Pacific. *Geology* 18, 470–473.

735 Parson, L.M., Wright, I.C., 1996. The Lau-Havre-Taupo back-arc basin: A southward-
736 propagating, multi-stage evolution from rifting to spreading. *Tectonophysics* 263, 1–
737 22.

738 Pearce, J.A., 2014. Immobile Element Fingerprinting of Ophiolites. *Elements* 10, 101-108.

739 Pearce, J., Cann, J., 1973. Tectonic Setting of Basic Volcanic Rocks determined using
740 Trace Element Analyses. *Earth Planet. Sci. Lett.* 19, 290–300.

741 Peccerillo, A., 2005. *Plio-quadernary volcanism in Italy*, vol. 365. Springer Verlag Berlin
742 Heidelberg.

743 Pensa, A., Pinton, A., Vita, L., Bonamico, A., De Benedetti, A.A., Giordano, G., 2019.
744 ATLAS of Italian Submarine Volcanic Structures. Mem. Descr. Carta Geol. d'It. 104,
745 77–183.

746 Prada, M., Sallarès, V., Ranero, C. R., Vendrell, M. G., Grevemeyer, I., Zitellini, N., De
747 Franco, R., 2014. Seismic structure of the Central Tyrrhenian basin: Geophysical
748 constraints on the nature of the main crustal domains. *J. Geophys. Res. Solid Earth*,
749 119(1), 52–70.

750 Prada, M., Ranero, C. R., Sallarès, V., Zitellini, N., & Grevemeyer, I., 2016. Mantle
751 exhumation and sequence of magmatic events in the Magnaghi-Vavilov Basin (Central
752 Tyrrhenian, Italy): New constraints from geological and geophysical observations.
753 *Tectonophysics* 689, 133–142.

754 Prada, M., Sallares, V., Ranero, C. R., Vendrell, M. G., Grevemeyer, I., Zitellini, N., De
755 Franco, R., 2018b. Spatial variations of magmatic crustal accretion during the opening
756 of the Tyrrhenian back-arc from wide-angle seismic velocity models and seismic
757 reflection images. *Basin Research* 30, 124–141.

758 Ranero, C.R., Sallarés, V., Zitellini, N., Grevemeyer, I., Guzman, M., Prada, M., Moeller,
759 S., De Franco, R., & The Medoc Cruise Party, 2012. The tectonic structure of the
760 Tyrrhenian Basin, a complex interaction among faulting and magmatism. *Rend. Online*
761 *Soc. Geol. It.* 21, 251–252.

762 Recq, M., Rehault J.P., Steinmetz L., Fabbri A., 1984. Amincissement de la crouete et
763 accretion au centre du bassin Tyrrhenien d'après la sismique refraction. *Mar. Geol.* 55,
764 411–428.

765 Rehault, J.P., Moussat, E., Fabbri, A., 1987. Structural evolution of the Tyrrhenian back-
766 arc basin. *Mar. Geol.* 74 (1-2), 123–150.

767 Remia A., Montagna P., Taviani M., 2004. Submarine diagenetic products on the
768 sediment-starved Gorgona slope, Tuscan Archipelago (Tyrrhenian Sea). *Chem.*
769 *Ecol.* 20 (1), 131–153.

770 Robin, C., Colantoni, P., Gennesseaux, M., Reehault, J.P., 1987. Vavilov seamount: a mild
771 alkaline Quaternary volcano in the Tyrrhenian basin. *Mar. Geol.* 78, 125–136.

772 Rosenbaum, G., Gasparon, M., Lucente, F.P., Peccerillo, A., Miller, M.S., 2008.
773 Kinematics of slab tear faults during subduction segmentation and implications for
774 Italian magmatism. *Tectonics* 27(2).

775 Rovere, M., Wurtz, M., 2015. Atlas of the Mediterranean seamounts and seamount-like
776 structures. IUCN, Gland, Switzerland and Málaga, Spain.

777 Sartori, R., 1986. Notes on the geology of the acoustic basement in the Tyrrhenian Sea.
778 *Mem. Soc. Geol. It.* 36, 99–108.

779 Sartori, R., 2003. The Tyrrhenian back-arc basin and subduction of the Ionian lithosphere.
780 *Episodes* 26(3), 217–221.

781 Savelli, C., 1988. Late Oligocene to Recent episodes of magmatism in and around the
782 Tyrrhenian Sea: implications for the processes of opening in a young inter-arc basin of
783 intra-orogenic (Mediterranean) type. *Tectonophysics* 146, 163–181.

784 Savelli, C., Ligi, M., 2017. An updated reconstruction of basaltic crust emplacement in
785 Tyrrhenian sea, Italy. *Scientific Reports* 7(1), 1–12.

786 Schellart, W. P., Freeman, J., Stegman, D. R., Moresi, L., May, D., 2007. Evolution and
787 diversity of subduction zones controlled by slab width. *Nature Letters*, 446, 308–311.

788 Schliffke, N., Van Hunen, J., Allen, M.B., Magni, V., Gueydan, F., 2022. Episodic back-arc
789 spreading centre jumps controlled by transform fault to overriding plate strength ratio.
790 *Nature Communications*, 13, 582.

791 Sdrolias, M., Muller, R.D., 2006. Controls on back-arc basin formation. *Geochem.*
792 *Geophys. Geosystems* 7 (4), 1–40.

793 Selli, R., Lucchini, F., Rossi, P.L., Savelli, C., Del Monte, M., 1977. Dati geologici,
794 petrochimici e radiometrici sui vulcani centro-tirrenici. *Giorn. Geol.* 42, 221–246.

795 Serri, G., Innocenti, F., Manetti, P., 2001. Magmatism from Mesozoic to Present:
796 Petrogenesis, time-space distribution and geodynamic implications. In: Vai, G.B.,
797 Martini, P.I., eds., *Anatomy of a Mountain: the Appenines and the Adjacent*
798 *Mediterranean Basins*, Dordrecht, the Netherland, Kluwer Academic Publishers,
799 pp.77–104.

800 Scrocca, D., Doglioni, C., Innocenti, F., Manetti, P., D'Offizi, S., 2003. CROP Atlas:
801 seismic reflection profiles of the Italian crust. *Mem. Descrit. Carta Geolo. d'It.* 62, 1–
802 193.

803 Trincardi, F., Zitellini, N., 1987. The rifting of the Tyrrhenian Basin. *Geo-Mar. Lett.* 7(1), 1–
804 6.

805 Trua, T., Serri, G., Marani, M., Renzulli, A., Gamberi, F., 2002. Volcanological and
806 petrological evolution of Marsili Seamount (southern Tyrrhenian Sea). *J. Volcanol.*
807 *Geotherm. Res.* 114 (3-4), 441–464.

808 Trua, T., Serri, G., Rossi, P.L., 2004. Coexistence of IAB-type and OIB-type magmas in
809 the southern Tyrrhenian back-arc basin: evidence from recent seafloor sampling and
810 geodynamic implications. *Mem. Descrit. Carta Geolo. d'It.* 44, 83–96.

811 Trua, T., Marani, M., Gamberi, F., 2018. Magma Plumbing System at a Young Back-Arc
812 Spreading Center: The Marsili Volcano, Southern Tyrrhenian Sea. *Geochem.*
813 *Geophys. Geosystems*, 19.

814 Uyeda, S., Kanamori, H., 1979. Back-arc opening and the mode of subduction. *J. Geophys.*
815 *Res.*, 84, 1049–1061.

- 816 Van Van Dijk, J.P., Bello, M., Brancaleoni, G.P., Toscano, C., 2000. A regional structural
817 model for the northern sector of the Calabrian Arc (southern Italy). *Tectonophysics* 324
818 (4), 267–320.
- 819 Ventura, G., Milano, G., Passaro, S., Sprovieri, M., 2013. The Marsili Ridge (Southern
820 Tyrrhenian Sea, Italy): An island-arc volcanic complex emplaced on a ‘relict’ back-arc
821 basin. *Earth Sci. Rev.*, 116, 85-94.
- 822 Weins, D. A., Kelley, K.A., Plank, T., 2006. Mantle temperature variations beneath back-
823 arc spreading centers inferred from seismology, petrology, and bathymetry. *Earth*
824 *Planet. Science Lett.*, 248, 30-42.
- 825 Wessel, P., Smith, W.H.F., 1998. New improved version of the Generic Mapping Tools
826 released. *EOS, Transaction of American Geophysical Union* 79, 579.
- 827 Wezel, F.C., 1982. The Tyrrhenian Sea: a Rifted Krikogenic-Swell Basin. *Mem. Soc. Geol.*
828 *It.* 24, 531–568.
- 829 Wilkinson, M.D., Dumontier, M., Aalbersberg, I.J., Appleton, G., 2016. The FAIR
830 Guiding Principles for scientific data management and stewardship. *Scientific*
831 *Data* 3, 160018.
- 832 Zankl, H., 1969. Structural and Textural evidence of early lithification in fine grained
833 carbonate rocks. *Sedimentology* 12, 241–256.
- 834 Zitellini, N., Trincardi, F., Marani, M., Fabbri, A., 1986. Neogenic tectonic of the Northern
835 Tyrrhenian Sea. *Giornale di Geologia* 48, 25–40.

836 **Captions of the Figures**

837 **Figure 1.** Geographic setting of the Mediterranean Sea (white star). A) Base colored
838 bathymetry map of the Tyrrhenian Back-Arc Basin (BAB). Black square is the area
839 shown in Fig. 2; black lines are isobaths (interval of 1000 m); the Tyrrhenian
840 Abyssal Plain (TAP), deeper than 3000 m, has been evidenced with the white area;
841 yellow, green and pink lines are the location of sparker lines acquired in the 1971,
842 1973 and 1975, respectively. Thicked lines indicate parts of the seismic profiles
843 interpreted in this paper. B) Base shaded bathymetry map of the Tyrrhenian BAB.
844 Black square is the area shown in Fig. 6; black line is the coast line; red lines are
845 the location of the magnetic lines acquired in the 1996 and 1999. Bathymetry has
846 been downloaded EMODnet portal ([http://portal.emodnet-bathymetry.eu/gebco-](http://portal.emodnet-bathymetry.eu/gebco-bathymetry-basemap)
847 [bathymetry-basemap](http://portal.emodnet-bathymetry.eu/gebco-bathymetry-basemap)) and gridded using GMT open software; bathymetric data
848 have been used to create 2D digital elevation model image using Global Mapper
849 Software.

850 **Figure 2.** Maps of the bathymetry and of the reduced to the pole magnetic anomalies of
851 the Southern Vavilov region. A) Shaded relief image of the bathymetry. Sun angle:
852 70°; Azimuth: 330°. Vertical Exaggeration: 10. Contour black lines are isobaths
853 every 100 m; green and pink lines indicate the location of the sparker lines shown in
854 Fig. 3; orange, yellow and green dots are the points of the dredges (75-30, 75-35
855 and 75-36, respectively). B) Slope shader relief map of the bathymetry (isobath
856 interval of 500 m). Red areas show the six peaks along the summit of the Augusto
857 Seamount. Sun angle: 70°; Azimuth: 330°. Vertical Exaggeration: 10. C) Shaded
858 relief image of the distribution of the reduced to the pole magnetic anomalies where
859 contour black lines indicate the lines with the same anomaly value (interval of 50
860 nT). D) Shaded relief image of the distribution of the reduced to the pole magnetic

861 anomalies where contour black lines are isobaths (interval of 100 m). 1. D'Ancona I
862 Seamount; 2. D'Ancona II Seamount; 3. Plinia Seamount; 4. Vavilov Seamount; 5.
863 Tibullo Seamount; 6. Aurelia Seamount; 7. Virgilio Seamount; 8. Augusto
864 Seamount; 9. Emilia Seamount.

865 **Figure 3.** Sparker profiles with their relative interpretation, maps of magnetic anomaly and
866 magnetic profiles extracted along the profiles. (A-A') Sparker Line PM3E; (B-B')
867 Sparker Line PM4; (C-C') Sparker Line PM11; (D-D') Sparker Line PM10E.

868 **Figure 4.** (a) Sample from dredge 75-30-3 (Aurelia Seamount). Macroscopic view of the
869 direct contact between the volcanic substrate and the overlying carbonate crust.
870 Neptunian dykes filled by carbonate mud are also visible; SEM photomicrograph of
871 the sample: the related EDAS spectrum B evidenced a predominantly carbonate
872 composition of the crust with a very subordinate clay-sized silicate fraction; the
873 black film marking the contact with the volcanic substrate is represented by Mn-Fe
874 oxides (spectrum A). (b) Black-coated corals (*Desmophyllum*) from dredge 75-35-5
875 (western Augusto Seamount), scale bar 2cm. (c) Thin section photomicrographs
876 from dredge 75-36-7A sample (eastern Augusto Seamount) showing isolated
877 volcanic minerals scattered within the planktonic-rich carbonate mud; quartz grains
878 are also evidenced by the SEM photomicrograph of the sample and the related
879 EDAS spectrum. (d) Thin section photomicrographs of the carbonate crusts: 1-2)
880 geopetal structures in pteropod-foraminifer wackestone, pteropod sections are
881 partially filled by foraminifer micrite and microspar at the top; 3) planktonic
882 foraminifera: *Pulleniatina obliquiloculata*, globigerinids, *Globorotalia truncatulinoides*
883 (dredge 75-30-3 sample), scale bar 500 μm ; 4) planktonic foraminifera: *Pulleniatina*
884 *obliquiloculata*, globigerinids (dredge 75-30-3 sample), scale bar 500 μm ; 5)

885 planktonic foraminifera: *Pulleniatina obliquiloculata*, globigerinids, *Globorotalia*
886 *inflata*, *Globigerinoides* spp. (dredge 75-36-7A sample), scale bar 1mm; 6) cloud of
887 planktonic foraminifera, pteropods shell, bioturbation evidences (dredge 75-36-7A
888 sample), scale bar 1mm. (e) Sample from dredge 75-36-7A. Thin section
889 photomicrograph showing a boring structure filled by planktonic-foraminifer mud;
890 SEM photomicrograph of the sample and the related EDAS spectra evidencing the
891 same composition of the carbonate mud outside and inside the cavity (A and B
892 spectra) and the Mn-Fe oxides-rich film coating the boring.

893 **Figure 5.** (a) 1-2) Low-magnification overview of the chosen samples. (3-4)
894 Photomicrographs (plane polarized light) showing altered phenocryst with euhedral
895 to subhedral shape. (5-6) Backscattered electron images with phase labelling based
896 on EDS microanalysis. Early igneous phenocrysts are now replaced by secondary
897 phases, mostly chlorite and dolomite. (b) Ti-Zr discrimination diagram (Cann, 1970;
898 Pearce and Cann, 1973) where the data of this study are compared to available
899 data from the Marsili Volcano (Pearce, 2014).

900 **Figure 6.** A) Shaded relief bathymetric image of the Southern Tyrrhenian Sea. Bathymetry
901 has been downloaded EMODnet portal ([http://portal.emodnet-bathymetry.eu/gebco-](http://portal.emodnet-bathymetry.eu/gebco-bathymetry-basemap)
902 [bathymetry-basemap](http://portal.emodnet-bathymetry.eu/gebco-bathymetry-basemap)) and gridded using GMT open software; bathymetric data
903 have been used to create 2D digital elevation model image using Global Mapper
904 Software. Sun angle: 70°; Azimuth: 330°. Vertical Exaggeration: 10. B) Map of the
905 distribution of the reduced to the pole magnetic anomalies in the Southern
906 Tyrrhenian Sea. Black contour lines are isobaths every 500 m. C) Sparker Profile
907 PM12 with interpretation.

908 **Figure 7.** Cartoon showing the formation and evolution of the volcanic arc related to the
909 Ionian subduction during the last 3 Ma. Geodynamic reconstruction is based on

910 the model published by Carminati et al. (2010). 3 Ma) Active volcanism of the
911 Magnaghi and Vavilov volcanoes; the active arc is formed by the Aurelia, the Virgilio
912 and the Western part of the Augusto Seamount. 2 Ma) Active volcanism of the
913 Magnaghi and Vavilov volcanoes; the active arc is formed by the Augusto
914 Seamount. 1 Ma) Active volcanism of the Marsili volcano; the active arc is formed
915 by the Sisifo and Tiro Seamounts. 0 Ma) Active volcanism of the Vavilov and Marsili
916 volcanoes; the active arc is formed by the Aeolian Islands and Seamounts.

917 **Supplementary Figure 1.** Seismic Sparker Profile PM3E not interpreted.

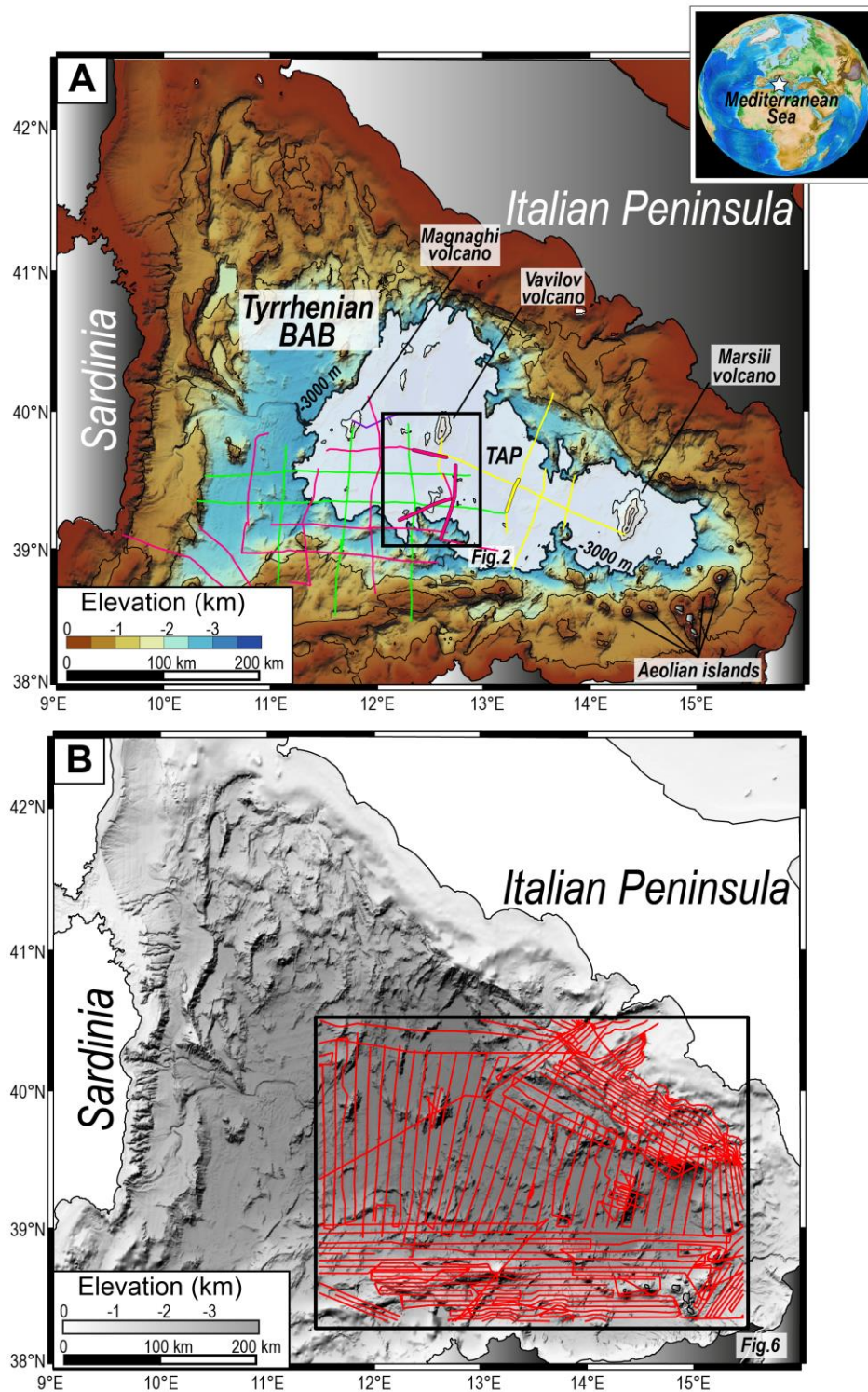
918 **Supplementary Figure 2.** Seismic Sparker Profile PM4 not interpreted.

919 **Supplementary Figure 3.** Seismic Sparker Profile PM11 not interpreted.

920 **Supplementary Figure 4.** Seismic Sparker Profile PM10E not interpreted.

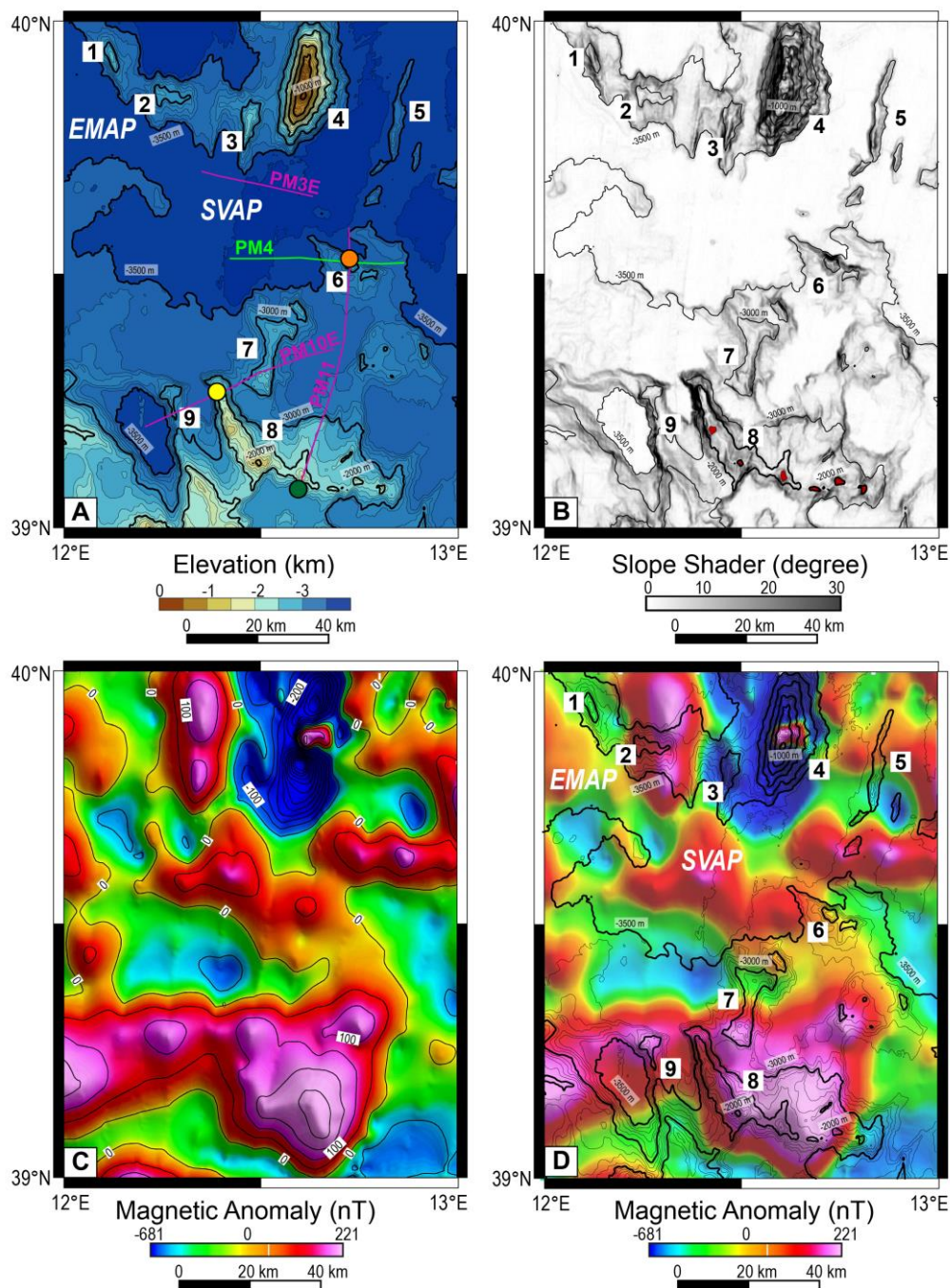
921 **Supplementary Figure 5.** Seismic Sparker Profile PM12 not interpreted.

922



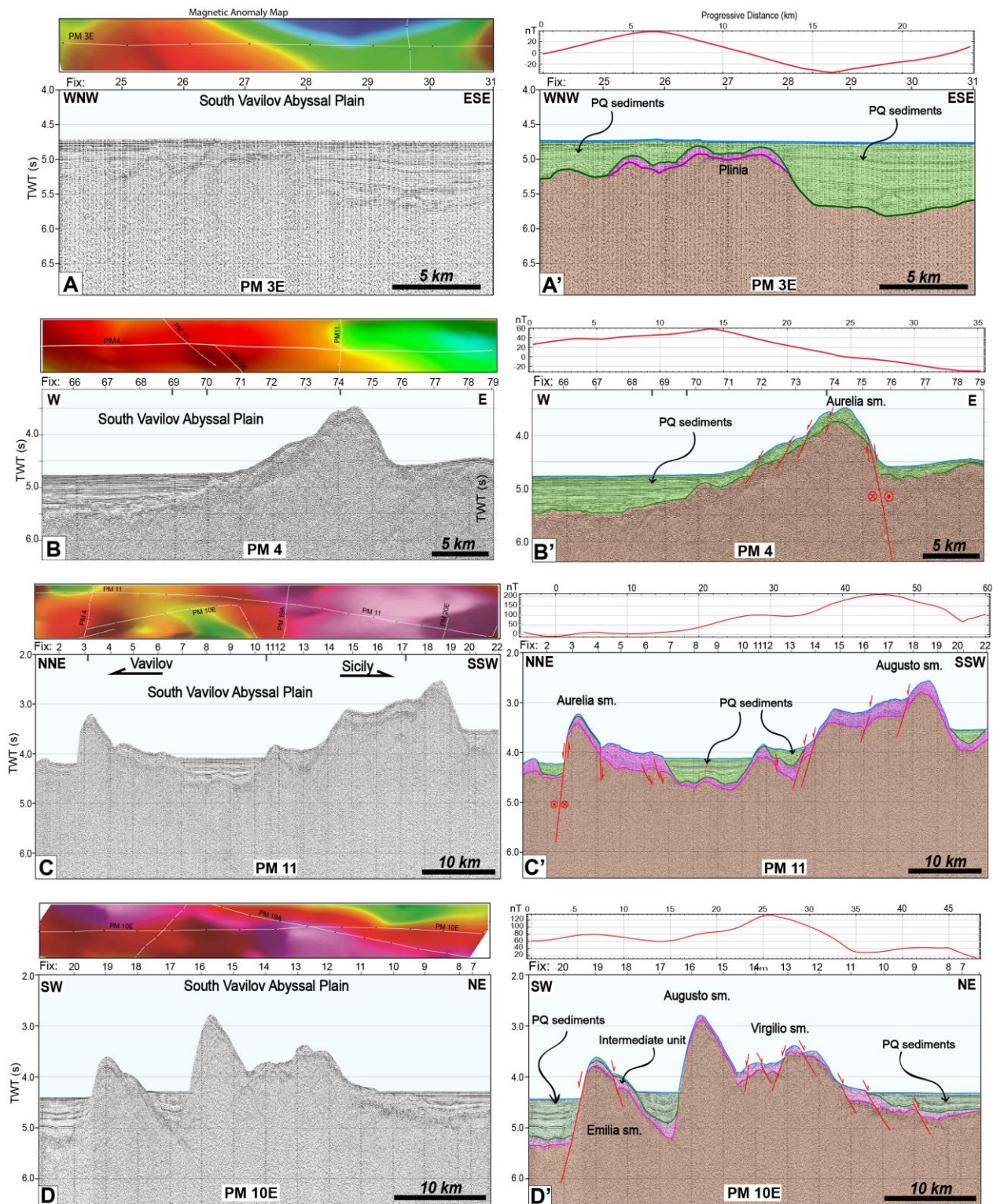
1

2 **Palmiotto et al_TECTO15884_Figure 1.** Geographic setting of the Mediterranean Sea (white star). A) Base
 3 colored bathymetry map of the Tyrrhenian Back-Arc Basin (BAB). Black square is the area shown in
 4 Fig. 2; black lines are isobaths (interval of 1000 m); the Tyrrhenian Abyssal Plain (TAP), deeper than
 5 3000 m, has been evidenced with the white area; yellow, green and pink lines are the location of
 6 sparker lines acquired in the 1971, 1973 and 1975, respectively. **Thicked lines indicate parts of the**
 7 **seismic profiles interpreted in this paper.** B) Base shaded bathymetry map of the Tyrrhenian BAB.
 8 Black square is the area shown in Fig. 6; black line is the coast line; red lines are the location of
 9 the magnetic lines acquired in the 1996 and 1999. Bathymetry has been downloaded EMODnet portal
 10 (<http://portal.emodnet-bathymetry.eu/gebco-bathymetry-basemap>) and gridded using GMT open
 11 software; bathymetric data have been used to create 2D digital elevation model image using Global
 12 Mapper Software.



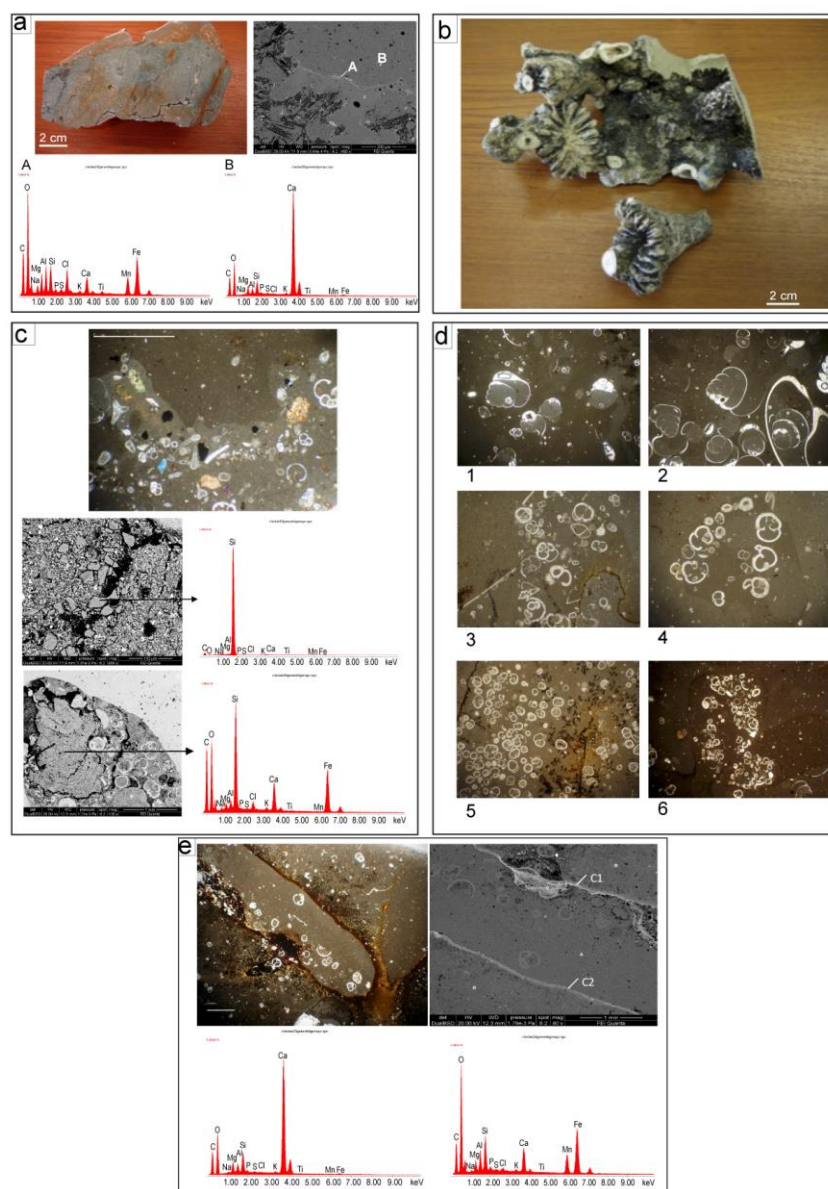
1

2 **Palmiotto et al_TECTO15884_Figure 2.** Maps of the bathymetry and of the reduced to the pole magnetic
 3 anomalies of the Southern Vavilov region. A) Shaded relief image of the bathymetry. Sun angle: 70°;
 4 Azimuth: 330°. Vertical Exaggeration: 10. Contour black lines are isobaths every 100 m; green and
 5 pink lines indicate the location of the sparker lines shown in Fig. 3; orange, yellow and green dots
 6 are the points of the dredges (75-30, 75-35 and 75-36, respectively). B) Slope shader relief map of
 7 the bathymetry (isobath interval of 500 m). **Red areas show the six peaks along the summit of the**
 8 **Augusto Seamount.** Sun angle: 70°; Azimuth: 330°. Vertical Exaggeration: 10. C) Shaded relief
 9 image of the distribution of the reduced to the pole magnetic anomalies where contour black lines
 10 indicate the lines with the same anomaly value (interval of 50 nT). D) Shaded relief image of the
 11 distribution of the reduced to the pole magnetic anomalies where contour black lines are isobaths
 12 (interval of 100 m). 1. D'Ancona I Seamount; 2. D'Ancona II Seamount; 3. Plinia Seamount; 4.
 13 Vavilov Seamount; 5. Tibullo Seamount; 6. Aurelia Seamount; 7. Virgilio Seamount; 8. Augusto
 14 Seamount; 9. Emilia Seamount.



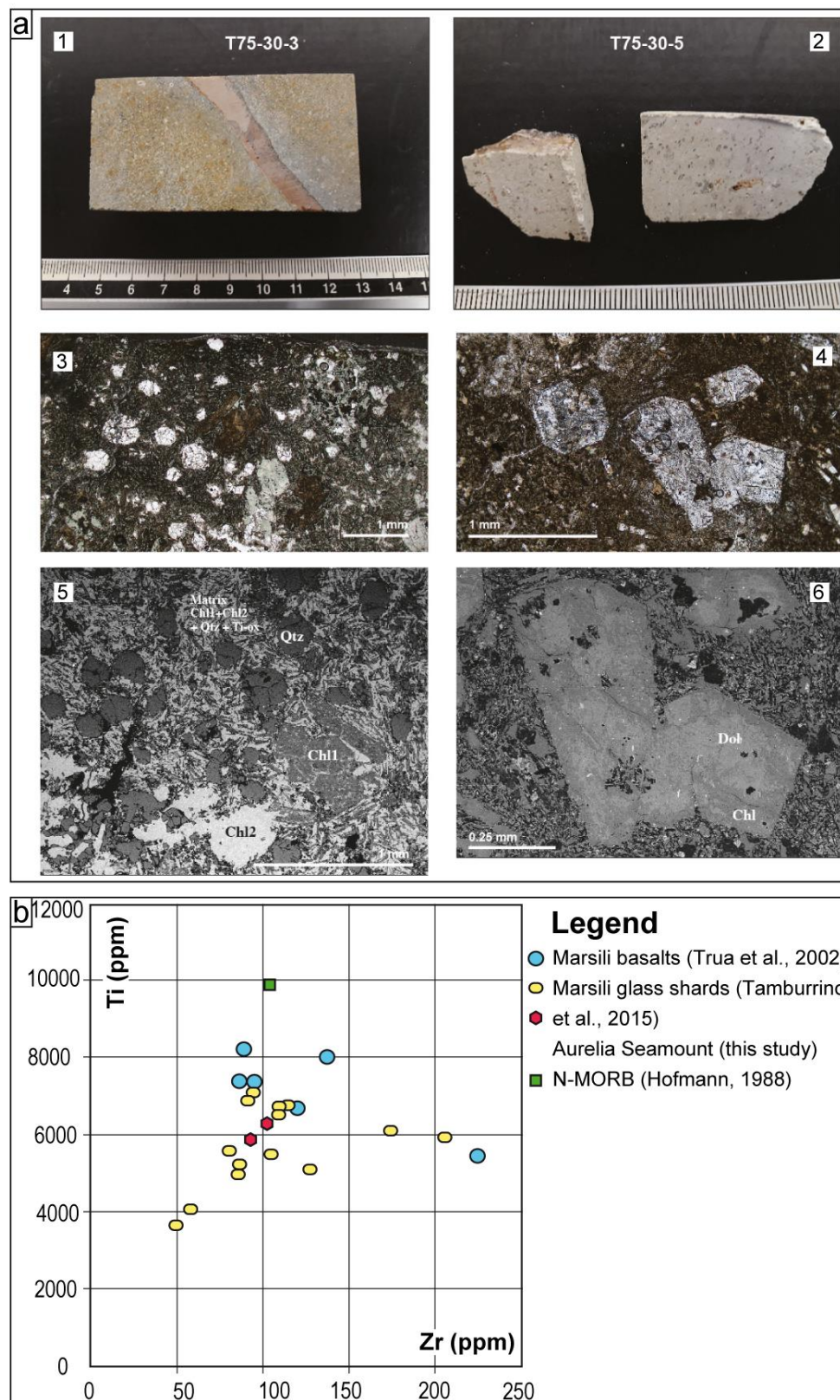
1

2 **Palmiotto et al_TECTO15884_Figure 3.** Sparker profiles with their relative interpretation, maps of magnetic
 3 anomaly and magnetic profiles extracted along the profiles. (A-A') Sparker Line PM3E; (B-B')
 4 Sparker Line PM4; (C-C') Sparker Line PM11; (D-D') Sparker Line PM10E.



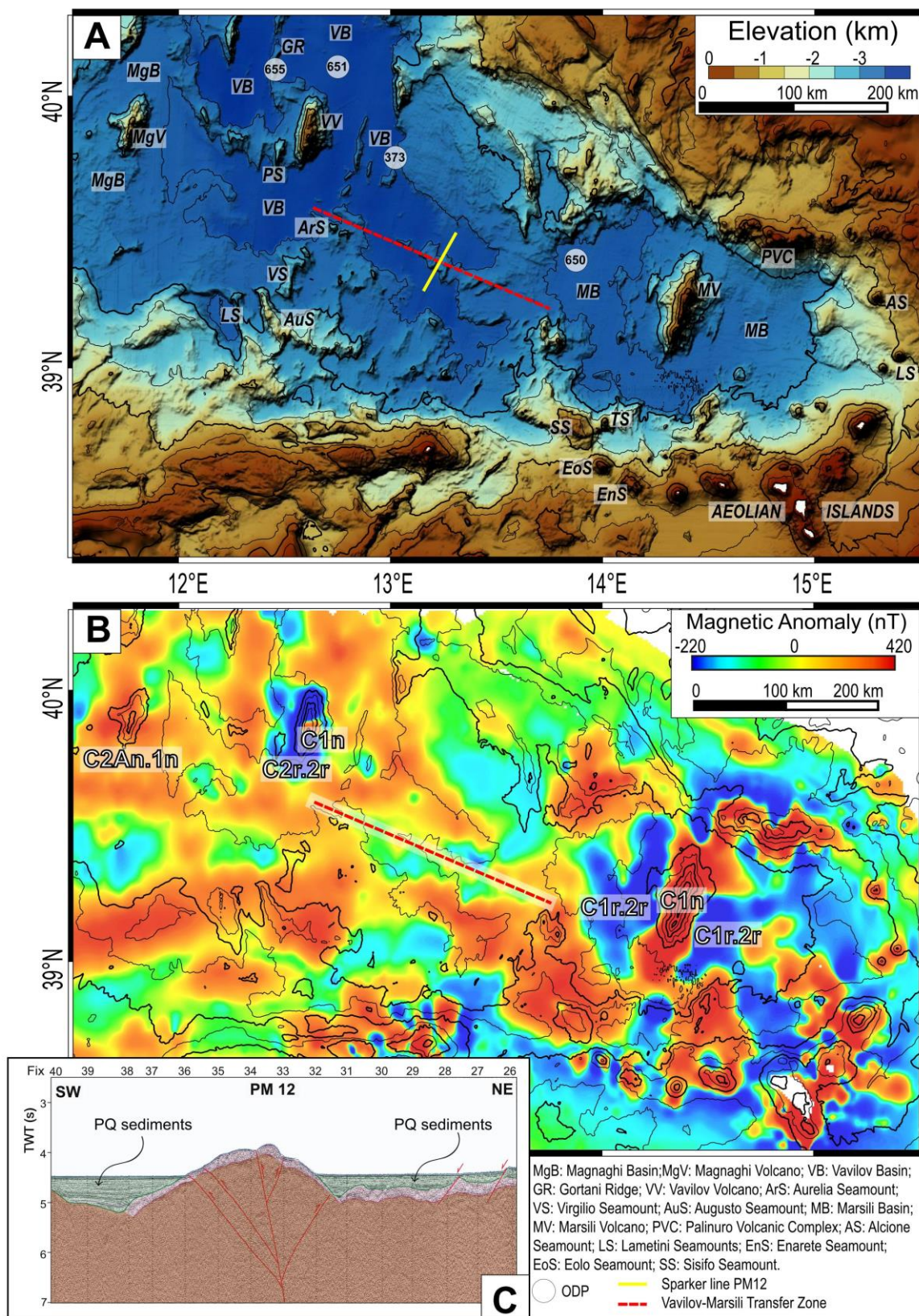
1

2 **Palmiotto et al_TECTO15884_Figure 4.** (a) Sample from dredge 75-30-3 (Aurelia Seamount). Macroscopic
 3 view of the direct contact between the volcanic substrate and the overlying carbonate crust.
 4 Neptunian dykes filled by carbonate mud are also visible; SEM photomicrograph of the sample: the
 5 related EDAS spectrum B evidenced a predominantly carbonate composition of the crust with a very
 6 subordinate clay-sized silicate fraction; the black film marking the contact with the volcanic substrate
 7 is represented by Mn-Fe oxides (spectrum A). (b) Black-coated corals (*Desmophyllum*) from dredge
 8 75-35-5 (western Augusto Seamount), scale bar 2cm. (c) Thin section photomicrographs from
 9 dredge 75-36-7A sample (eastern Augusto Seamount) showing isolated volcanic minerals scattered
 10 within the planktonic-rich carbonate mud; quartz grains are also evidenced by the SEM
 11 photomicrograph of the sample and the related EDAS spectrum. (d) Thin section photomicrographs
 12 of the carbonate crusts: 1-2) geopetal structures in pteriopod-foraminifer wackestone, pteropod
 13 sections are partially filled by foraminifer micrite and microspar at the top; 3) planktonic foraminifera:
 14 *Pulleniatina obliquiloculata*, globigerinids, *Globorotalia truncatulinoides* (dredge 75-30-3 sample),
 15 scale bar 500 μ m; 4) planktonic foraminifera: *Pulleniatina obliquiloculata*, globigerinids (dredge 75-
 16 30-3 sample), scale bar 500 μ m; 5) planktonic foraminifera: *Pulleniatina obliquiloculata*,
 17 globigerinids, *Globorotalia inflata*, *Globigerinoides* spp. (dredge 75-36-7A sample), scale bar 1mm;
 18 6) cloud of planktonic foraminifera, pteropods shell, bioturbation evidences (dredge 75-36-7A
 19 sample), scale bar 1mm. (e) Sample from dredge 75-36-7A. Thin section photomicrograph showing
 20 a boring structure filled by planktonic-foraminifer mud; SEM photomicrograph of the sample and the
 21 related EDAS spectra evidencing the same composition of the carbonate mud outside and inside the
 22 cavity (A and B spectra) and the Mn-Fe oxides-rich film coating the boring.



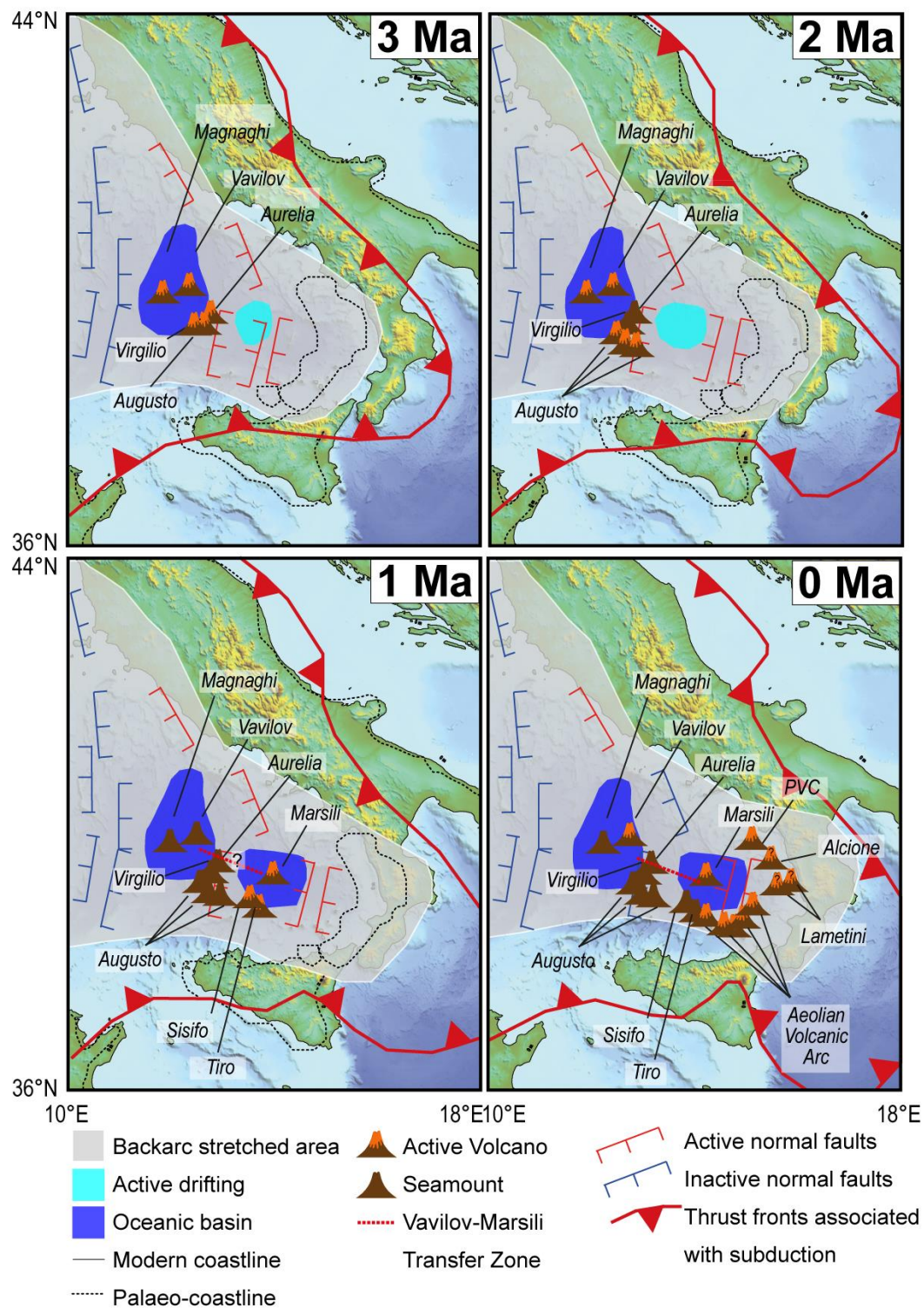
1

2 **Palmiotto et al_TECTO15884_Figure 5.** (a) 1-2) Low-magnification overview of the chosen samples. (3-4)
 3 Photomicrographs (plane polarized light) showing altered phenocryst with euhedral to subhedral
 4 shape. (5-6) Backscattered electron images with phase labelling based on EDS microanalysis. Early
 5 igneous phenocrysts are now replaced by secondary phases, mostly chlorite and dolomite. (b) Ti-Zr
 6 discrimination diagram (Cann, 1970; Pearce and Cann, 1973) where the data of this study are
 7 compared to available data from the Marsili Volcano (Pearce, 2014).



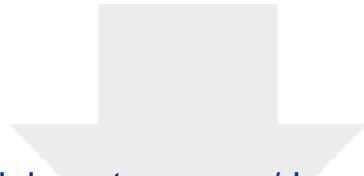
1

2 **Palmiotto et al_TECTO15884_Figure 6.** A) Shaded relief bathymetric image of the Southern Tyrrhenian
 3 Sea. Bathymetry has been downloaded EMODnet portal ([http://portal.emodnet-](http://portal.emodnet-bathymetry.eu/gebco-bathymetry-basemap)
 4 [bathymetry.eu/gebco-bathymetry-basemap](http://portal.emodnet-bathymetry.eu/gebco-bathymetry-basemap)) and gridded using GMT open software; bathymetric data
 5 have been used to create 2D digital elevation model image using Global Mapper Software. Sun
 6 angle: 70°; Azimuth: 330°. Vertical Exaggeration: 10. B) Map of the distribution of the reduced to the
 7 pole magnetic anomalies in the Southern Tyrrhenian Sea. Black contour lines are isobaths every 500
 8 m. C) Sparker Profile PM12 with interpretation.



1

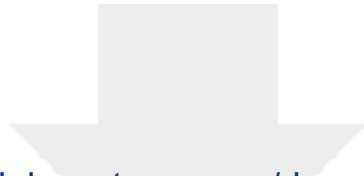
2 **Palmiotto et al_TECTO15884_Figure 7.** Cartoon showing the formation and evolution of the volcanic arc
 3 related to the Ionian subduction during the last 3 Ma. Geodynamic reconstruction is based on the
 4 model published by Carminati et al. (2010). 3 Ma) Active volcanism of the Magnaghi and Vavilov
 5 volcanoes; the active arc is formed by the Aurelia, the Virgilio and the Western part of the Augusto
 6 Seamount. 2 Ma) Active volcanism of the Magnaghi and Vavilov volcanoes; the active arc is formed
 7 by the Augusto Seamount. 1 Ma) Active volcanism of the Marsili volcano; the active arc is formed
 8 by the Sisifo and Tiro Seamounts. 0 Ma) Active volcanism of the Vavilov and Marsili volcanoes;
 9 the active arc is formed by the Aeolian Islands and Seamounts.



[Click here to access/download](#)

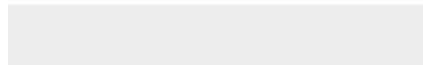
Supplementary material for online publication only
Palmiotto_et_al_TECTO15884_SuppFigure1.jpg

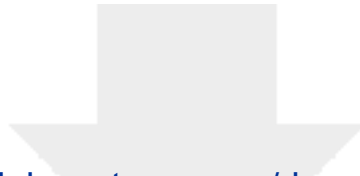




[Click here to access/download](#)

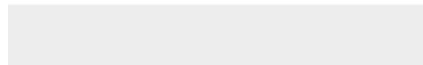
Supplementary material for online publication only
Palmiotto_et_al_TECTO15884_SuppFigure2.jpg

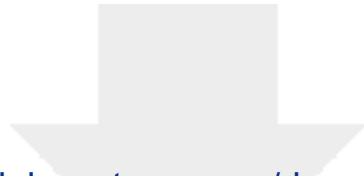




[Click here to access/download](#)

Supplementary material for online publication only
Palmiotto_et_al_TECTO15884_SuppFigure3.jpg

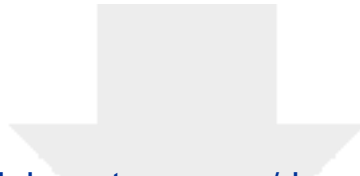




[Click here to access/download](#)

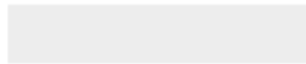
Supplementary material for online publication only
Palmiotto_et_al_TECTO15884_SuppFigure4.jpg





[Click here to access/download](#)

Supplementary material for online publication only
Palmiotto_et_al_TECTO15884_SuppFigure5.jpg



1 **New insights on the fossil arc of the Tyrrhenian Back-Arc Basin**
2 **(Mediterranean Sea)**

3
4 Camilla Palmiotto^{1*}, Roberto Braga², Laura Corda³, Letizia Di Bella³, Valentina Ferrante¹,
5 Maria Filomena Loreto¹ and Filippo Muccini^{4,5}

6 ¹ *Consiglio Nazionale delle Ricerche, Istituto di Scienze Marine, via Gobetti 101, 40129, Bologna, Italy.*

7 ² *Dipartimento di Scienze Biologiche, Geologiche e Ambientali, Università di Bologna, Piazza di Porta San*
8 *Donato 1, 40126, Bologna, Italy.*

9 ³ *Dipartimento di Scienze della Terra, Università "La Sapienza", Piazzale Aldo Moro 5, 00185, Roma, Italy.*

10 ⁴ *Istituto Nazionale di Geofisica e Vulcanologia, via di Vigna Murata 605, 00143, Roma, Italy.*

11 ⁵ *Consiglio Nazionale delle Ricerche, Istituto di Geologia Ambientale e Geoingegneria, 00185, Roma, Italy.*

12
13 *Corresponding author. Tel: +39 051 6398900

14 E-mail address: camilla.palmiotto@bo.ismar.cnr.it

15
16 **Credit Author Statement**

17 **Camilla Palmiotto:** Conceptualization; writing, reviewing and editing; morphological and
18 magnetic analysis; Figures creation. **Maria Filomena Loreto:** Seismic data interpretation
19 and writing. **Valentina Ferrante:** Seismic data curation. **Laura Corda:** Carbonate samples
20 interpretation and writing. **Letizia Di Bella:** Paleontological analysis and writing. **Roberto**
21 **Braga:** petrographycal analysis, writing, reviewing and editing. **Filippo Muccini:** Magnetic
22 data curation, reviewing and editing.

Declaration of interests

The authors declare that they have no known competing financial interests or personal relationships that could have appeared to influence the work reported in this paper.

The authors declare the following financial interests/personal relationships which may be considered as potential competing interests: